MD-03-SP107B4J

STATE HIGHWAY ADMINISTRATION RESEARCH REPORT

EXPERIMENTAL INVESTIGATIONS ON MECHANICAL BEHAVIOR OF UNSATURATED SUBGRADE SOIL WITH LIME STABILIZATION AND FIBER REINFORCEMENT

NATIONAL TRANSPORTATION CENTER
MORGAN STATE UNIVERSITY

SP107B4J
FINAL REPORT

November 2003

DISCLAIMER

The contents of this report reflect the views of the author who is responsible for the facts and the accuracy of the data presented herein. The contents do not necessarily reflect the official views or policies of the Maryland State Highway Administration. This report does not constitute a standard, specification, or regulation.

Experimental Investigations on Mechanical Behavior of Unsaturated Subgrade Soil with Lime Stabilization and Fiber Reinforcement

By Jiang Li, PhD., P.E.
Associate Professor
Room 220, MEB
Department of Civil Engineering
School of Engineering
Phone: 443.885.4202
Fax: 443.885.8218
Email: jli@eng.morgan.edu

Morgan State University
5200 Perring Parkway
Baltimore, MD 21251

November 2003

1. Report No.	2. Government Accession No.	3. Recipient's Catalog No.
MD-03-SP107B4J		

4. Title and Subtitle	5. Report Date
Experimental Investigations on Mechanical Behavior of Unsaturated Subgrade Soil with Lime Stabilization and Fiber Reinforce	**November 2003**
	6. Performing Organization Code
7. Author/s	8. Performing Organization Report No.
Dr. Jiang Li	
9. Performing Organization Name and Address	10. Work Unit No. (TRAIS)
Morgan State University **1700 E. Cold Spring Lane** **Baltimore, MD 21251-0001**	11. Contract or Grant No. **SP107B4J**
12. Sponsoring Organization Name and Address	13. Type of Report and Period Covered
Maryland State Highway Administration **Office of Policy and Research** **707 North Calvert Street** **Baltimore MD 21202**	**Final Report**
	14. Sponsoring Agency Code

15. Supplementary Notes

16. Abstract

In the present report, experimental investigations on mechanical behavior of unsaturated subgrade soil with fiber reinforcement and lime stabilization were conducted.

The soil samples were collected from the soil/aggregate laboratory at the Maryland State Highway Administration (MD-SHA), Maryland Department of Transportation. The experiments were carried out to investigate physical and mechanical properties of subgrade soil that was mixed with geofiber and lime. The reinforced and stabilized soil with fiber and lime is considered as a composite material.

Investigations in this study included two phases. In the first phase, the investigation was for static behavior of composite subgrade soil under the compressive shear loading. In the second phase, the investigation emphasized dynamic behavior of reinforced and stabilized soil under cyclic shear loading. In this research, three aspects of investigations are presented.

First, new constitutive models for static and dynamic loading were established for composite material. In the present report, elastic constitutive relationship was assumed to describe both the linear and nonlinear shear stress-strain relations of composite material. Static behavior was described with a nonlinear elastic model, and dynamic behavior was expressed with a linear elastic model. For the nonlinear model, elastic shear modulus was assumed to be a function of multiple variables such as shear strain, contents of fiber and lime, confining pressure, and the curing period of samples. In contrast, for the linear model, elastic modulus was not only defined as a function of confining pressure, contents of fiber and lime, and the aging period of samples but also repetitions of cyclic loading. For convenience of experimental investigation, the shear stress-strain relation in a three-dimensional stress space reduced to that in a quasi-triaxial stress space in which the conventional triaxial shear tests were conducted.

Second, experimental investigations and calibration of constitutive models were conducted.

Experimental data from laboratory tests were utilized to verify and justify the linear or nonlinear elastic model suggested in this report. Constitutive parameters of linear and nonlinear models were investigated and calibrated using experimental results from both static and dynamic triaxial shear tests. The linear regression method was adopted to find constitutive parameters. The constitutive relationship of the composite material made of soil, fiber and lime was established once constitutive parameters for the linear and nonlinear models were determined. The elastic shear moduli were investigated, for example, the initial shear and tangential moduli in the nonlinear elastic model under static loading, and the shear or resilient modulus in the linear model under cyclic loading. Moreover, for static loading, the Coulomb – Mohr's failure criterion was applied. The strength indices c and ϕ were studied for the composite soil with fiber and lime. A linear relation was introduced to describe parameters c and ϕ as a function of fiber and lime content, and the sample-curing period. The coefficients of the linear relation for parameters c and ϕ versus fiber and lime content, and sample aging time were found using the experimental data.

Finally, impacts of fiber and lime as well as other factors that affect mechanical behavior of the composite material were discussed. Impact factors on shear moduli were introduced for both the linear and nonlinear models. The impact factors for the nonlinear model under static loading were defined to exhibit effect of variables such as cell pressure, fiber and lime contents, and the sample-curing period on the initial modulus and soil strength, namely parameters 1/A and 1/B related to the shear modulus G. In contrast, the impact factors for the linear model under cyclic loading were introduced to show effect of the same variables (σ_0, m_F, m_L and t) plus the repetition of cyclic loading on resilient modulus and dynamic behavior of composite soils.

17. Key Words	18. Distribution Statement: No restrictions		
Constitutive Relationship, Nonlinearity, Shear Stress and Strain, Deviatoric Stress and Strain, Elastic Modulus, Resilient Modulus, Fiber Reinforcement, Lime Stabilization, Composite Material	**This document is available from the Research Division upon request.**		
9. Security Classification (of this report)	20. Security Classification (of this page)	21. No. Of Pages	22. Price
None	**None**	**97**	

Form DOT F 1700.7 (8-72) Reproduction of form and completed page is authorized.

TABLE OF CONTENTS

ABSTRACT

In the present report, experimental investigations on mechanical behavior of unsaturated subgrade soil with fiber reinforcement and lime stabilization were conducted.

The soil samples were collected from the soil/aggregate laboratory at the Maryland State Highway Administration (MD-SHA), Maryland Department of Transportation. The experiments were carried out to investigate physical and mechanical properties of subgrade soil that was mixed with geofiber and lime. The reinforced and stabilized soil with fiber and lime is considered as a composite material.

Investigations in this study included two phases. In the first phase, the investigation was for studies of static behavior of composite subgrade soil under the compressive shear loading. In the second phase, the investigation emphasized dynamic behavior of reinforced and stabilized soil under cyclic shear loading. In this research, three aspects of investigations were presented.

First, new constitutive models for static and dynamic loading were established for the composite material. In the present report, elastic constitutive relationship was assumed to describe both the linear and nonlinear shear stress-strain relations of the composite material. Static behavior was described with a nonlinear elastic model, and dynamic behavior was expressed with a linear elastic model. For the nonlinear model, elastic shear modulus was assumed to be a function of multiple variables such as shear strain, contents of fiber and lime, confining pressure, and the curing period of samples. In contrast, for the linear model, elastic modulus was not only defined as a function of confining pressure, contents of fiber and lime, and the aging period of samples but also repetitions of cyclic loading. For convenience of experimental investigation, the shear stress-strain relation in a three-dimensional stress space reduced to that in a quasi-triaxial stress space in which the conventional triaxial shear tests were conducted.

Second, experimental investigations and calibration of constitutive models were conducted. Experimental data from laboratory tests were utilized to verify and justify the linear or nonlinear elastic model suggested in this report. Constitutive parameters of linear and nonlinear models were investigated and calibrated using experimental results from both static and dynamic triaxial shear tests. The linear regression method was adopted to find constitutive parameters. The constitutive relationship of the composite material made of soil, fiber and lime was established once constitutive parameters for the linear and nonlinear models were determined. The elastic shear moduli were investigated, for example, the initial shear and tangential moduli in the nonlinear elastic model under static loading and the shear or resilient modulus in the linear model under cyclic loading. Moreover, for static loading, the Coulomb – Mohr's failure criterion was applied. The strength indices c and ϕ were studied for the composite soil with fiber and lime. A linear relation was introduced to describe parameters c and ϕ as a function of fiber and lime contents, and the sample-curing period. The coefficients of the linear relation for parameters c and ϕ versus fiber and lime contents, and the sample aging time were found using the experimental data.

Finally, impacts of fiber and lime as well as other factors that affect mechanical behavior of the composite material were discussed. Impact factors on shear moduli were introduced for both the linear and nonlinear models. The impact factors for the nonlinear model under static loading were defined to exhibit effect of variables such as cell pressure, fiber and lime contents, and the sample-curing period on the initial modulus and

soil strength, namely parameters 1/A and 1/B related to the shear modulus G. In contrast, the impact factors for the linear model under cyclic loading were introduced to show effect of the same variables (σ_0, m_F, m_L and t) plus the repetition of cyclic loading on resilient modulus and dynamic behavior of composite soils.

ACKNOWLEDGMENTS

This two-year research program was sponsored by the Maryland State Highway Administration (MD -SHA) and the National Transportation Center (NTC) at Morgan State University (MSU). The principal investigator (the P.I.) is grateful to both the MD-SHA and the NTC-MSU for their support in this research project.

INTRODUCTION

One of the top priorities of highway administrations is to increase productivity and decrease the rate of road wear [1]. Improvement of the nation's highways performance is normally focused on the quality of the roadway surface. Pavement performance will largely rely on the mechanical behavior of pavement and subgrade soil layers.

In order to increase the capacity of transportation of highway systems, it is recommended to use the higher payload of trucks to improve road productivity as the higher payload reduces both the total number of vehicles in operations and the cost of truck freight transport that is about $140 billon per annum (TPA, 1985). The higher payload, however, increases the rate of road deterioration due to a higher level of shear stress within pavement and subgrade layers. The higher level of shear stress induced by traffic loads not only affects performance of the road surface but also impacts interaction between pavement and subgrade soil layers. Therefore, it is important to investigate the composite subgrade soil with better mechanical properties that can improve road quality under the vehicle-induced shear force. In this present investigation, subgrade soil mixed with fiber and lime powder is utilized for shear testing because geofiber contributes extra tensile and shear resistance to reinforce subgrade soil, and lime provides additional binding and cohesive force to stabilize subgrade soil.

Geofiber is one of many geosynthetic products and is widely used in Geotechnical Engineering to improve engineering properties of materials. For example, soil material with fiber reinforcement improves material strength against tensile and shear stress so that risk of pavement cracking and rutting is lowered. The advantages of using the geofiber material reinforcement are many such as low cost, lightweight, convenient construction and transportation, strong anti-biologic erosion, high chemical stabilization, etc. If lime (CaO) is also added to composite subgrade soil, the effect of interlock, shear and tensile resistance can be enhanced. Although many investigators previously conducted research for soils reinforced with geofiber [2-12], little effort has been made for composite subgrade soil reinforced with both geofiber and lime powder. The present research centers on investigating mechanical behavior of subgrade soil mixed with fiber and lime in response to the both static and dynamic loads.

For static tests, there are three aspects. First, nine groups of triaxial shear tests have been conducted with three different groups of specimens that are sample soil mixed with fiber only and with both fiber and lime. The sample soil with different fiber and lime contents is cured for a period prior to triaxial shear tests. Second, a nonlinear elastic model is introduced to describe nonlinear elastic behavior of unsaturated subgrade soil with lime stabilization and fiber reinforcement. Third, constitutive parameters of this model are investigated and calibrated using experimental results from conventional triaxial shear tests. In contrast, dynamic tests are carried out for experimental investigations on cyclic behavior of the fiber-reinforced and lime-stabilized soil. The experimental investigations were conducted using dynamic triaxial apparatus. Test data and results from dynamic shear tests were collected and analyzed to determine how composite soil responds to cyclic loading and how mechanical properties of subgrade soil can be improved.

It should be pointed out that research findings and results from the present investigations not only can be utilized for design in roadbeds but also can be employed for other applications such as improvement of soft ground, stabilization of soil slops, and reinforcement of bridge footings, shallow and deep foundations in highway engineering.

CONSTITUTIVE RELATIONSHIP

The constitutive relationship of deformable material represents the physical law describing the relation between stress and strain. In the present report, the elastic constitutive relationship for the composite soil is introduced and studied.

Elastic Stress – Strain Relationship in a Three Dimensional Space

The elastic stress – strain relation can be linear and nonlinear, and is defined below [13]:

$$\sigma_{ij} = E_{ijkl}\varepsilon_{kl} \ , \qquad \text{(Eq.1)}$$

or can be expressed in terms of volume and shear stress-strain relations by:

$$\sigma_{ij} = \sigma_{kk}\delta_{ij} + \sigma^{D}_{ij} = 3\kappa\varepsilon_{kk}\delta_{ij} + 2G\varepsilon^{D}_{ij} \qquad \text{(Eq.2)}$$

where σ_{ij} = a stress tensor (kPa)
σ_{kk} = the trace of the stress tensor (kPa)
σ^{D}_{ij} = a shear stress tensor (kPa)
ε_{kl} = a strain tensor
ε_{kk} = the trace of the strain tensor when k = 1, 2 and 3 are repeated.
δ_{ij} = the Kronecker delta (δ_{ii} =1 when i = j; δ_{ij} = 0 when i ≠ j; i and j = 1, 2, and 3)
κ = bulk modulus, a parameter of elasticity (kPa)
G = shear modulus, a parameter of elasticity (kPa)
E_{ijkl} = the fourth order tensor of elasticity (kPa), and is defined by:

$$E_{ijkl} = (\kappa - 2G/3)\delta_{ij}\delta_{kl} + G(\delta_{il}\delta_{jk} + \delta_{ik}\delta_{jl}) \qquad \text{(Eq.3)}$$

The volume and shear stress-strain relations: $\sigma_{kk} = 3\kappa\varepsilon_{kk}$ and $\sigma^{D}_{ij} = 2G\varepsilon^{D}_{ij}$ in Eq.2 can be alternatively expressed in terms of stress and strain invariants [14]:

$$I_1 = 3\kappa J_1 \text{ and } \sqrt{I_2^D} = 2G\sqrt{J_2^D} \qquad \text{(Eq.4a, 4b)}$$

where $I_1 = \sigma_{kk} = (\sigma_{11} + \sigma_{22} + \sigma_{33})$, the first invariant of a stress tensor (kPa)
$J_1 = \varepsilon_{kk} = (\varepsilon_{11} + \varepsilon_{22} + \varepsilon_{33})$, the first invariant of a strain tensor

$I^D_2 = \sigma^D_{ij}\sigma^D_{ij}/2$, the second invariant of a deviatoric stress tensor (kPa).

$J^D_2 = \varepsilon^D_{ij}\varepsilon^D_{ij}/2$, the second invariant of a deviatoric strain tensor.

The elastic stress-strain relation for isotropic, homogenous and isothermal material can be described using any two out of the following five elastic parameters, namely, parameter λ, bulk modulus κ, shear modulus G, Poisson's ratio ν, and Young's modulus E. It should be pointed out that throughout this report, stresses, if not specified, are effective stresses rather than total stresses.

Elastic Stress – Strain Relationship in a Quasi Three Dimensional Space

For convenience of experimental investigations, stress and strain in the three-dimensional space needs to reduce to a quasi-triaxial space in which the conventional triaxial shear tests are conducted. For instance, in the principal quasi-triaxial stress space, $\sigma_1 \neq \sigma_2 = \sigma_3$, $\varepsilon_1 \neq \varepsilon_2 = \varepsilon_3$, and the stress-strain relations in Eq.4a and 4b reduce to:

$$\sigma_1 + 2\sigma_3 = 3\kappa(\varepsilon_1 + 2\varepsilon_3) \qquad \text{(Eq.4c)}$$

$$\sigma_1 - \sigma_3 = 2G(\varepsilon_1 - \varepsilon_3) \qquad \text{(Eq.4d)}$$

where $(\sigma_1-\sigma_3)$ is difference of the major and minor principal stresses σ_1 and σ_3; $(\varepsilon_1- \varepsilon_3)$ is difference of the major and minor principal strains ε_1 and ε_3. For conventional triaxial shear tests, Eq.4d can be further simplified to:

$$\sigma_1 - \sigma_3 = 2G\varepsilon_1 \qquad \text{(Eq.4e)}$$

Eq.4e represents the axial deviatoric stress-strain relation that was studied and verified via shear tests using the conventional triaxial apparatus in laboratory. It should be pointed out that in Eqs.4c and 4d, both the bulk and shear moduli κ and G are functions of multiple variables that are to be discussed in the next section. The variables related to strain, stress, or rates of strain and stress may have significantly impacts on shear modulus G, and cause the nonlinearity of stress-strain relationship in Eq.4e. In contrast, the variables associated with the materials such as fiber, lime, etc. may also affect shear modulus G but may not play a role in causing the nonlinearity of stress-stain relationship. The present investigation emphasizes the shear stress-strain relation shown in Eq.4e. Both the linear and nonlinear shear stress-strain relations are introduced and discussed in the next section.

The Linear Elastic Stress – Strain Relation

In this report, a linear elastic model is introduced for the dynamic stress-strain relation. This suggests that all strain is instantaneously and totally recoverable upon the removal of the loaded stress. Stress increases proportionally or linearly with increase of strain. The elastic modulus in the linear model is not a function of strain though it can be a function of other variables related to the composite material. In this report, for example, bulk and shear moduli are defined by:

$$\kappa = \kappa(I_1, m_f, m_l, N, t) \qquad \text{(Eq.5)}$$

$$G = G(I_1, m_f, m_l, N, t) \qquad \text{(Eq.6)}$$

where $I_1 = \sigma_{kk}$, the first invariant of stress (kPa).
N = repetitions of cyclic loading (N is an integer and $N \geq 1$).
t = the curing period of specimens prior to shear tests (day)
m_F = fiber content (%)
m_L = lime content (%)

Fiber and lime contents m_F and m_L within prepared soil specimens are defined by $W_F/(W_S + W_L)$ and W_L/W_S respectively. W_F, W_L and W_S stand for weights of fiber, lime powder and dry soil.

In research of dynamic behavior under cyclic loading, investigating shear modulus G in Eq.6 is focused if the shear stress-strain relation in Eq.4e is applied. The shear modulus G in Eq.6 is assumed to be a product of multiples power functions of five variables [14], and is given in the following form:

$$G(I_1, m_F, m_L, N, t) = c_0 (I_1 / p_0)^{c_1} (1 + m_F)^{c_2} (1 + m_L)^{c_3} (N)^{c_4} (t / t_1)^{c_5} \qquad \text{(Eq.7)}$$

where p_0 = unit atmospheric pressure (kPa)
t_1 = one day (day)
c_i ($i = 0 \ldots 5$) = constitutive coefficients that are dimensionless except for c_0 (kPa)

The terms p_0 and t_1 in Eq.7 are introduced to make ratios σ_0/p_0 and t/t_1 dimensionless. Substituting Eq.7 into Eq.4b gives the linear shear stress-strain relation written in terms of invariants of shear stress and strain tensors in the three dimensional stress space:

$$\sqrt{I_2^D} = c_0 (I_1/p_0)^{c_1} (1 + m_F)^{c_2} (1 + m_L)^{c_3} (N)^{c_4} (t/t_1)^{c_5} \sqrt{J_2^D} \qquad \text{(Eq.8a)}$$

If the quasi-triaxial stress space is applied for experimental investigations, then according to Eq.4e, Eq.8a reduces to:

$$\sigma_1 - \sigma_3 = c_0(\sigma_0 / p_0)^{c_1}(1+m_F)^{c_2}(1+m_L)^{c_3}(N)^{c_4}(t/t_1)^{c_5}\varepsilon_1 \qquad \text{(Eq.8b)}$$

where σ_0 simplified from I_1 is confining or cell pressure (kPa), and the coefficient 2 in Eq.4e is dropped and included in the parameter c_0 in Eq.8b

One may note that in Eq.7 shear modulus G of elasticity is not a function of shear strain. Therefore, when testing conditions and material parameters (i.e., σ_0, N, t, m_F and m_L) are given, G becomes a constant and the relation (σ_1- σ_3) versus ε_1 in Eq.8b is the linear elastic relation. For different values of variables σ_0, N, t, m_F and m_L, the relation (σ_1- σ_3) versus ε_1 in Eq.8b represents a family of the linear elastic relations. However, if the shear modulus G of elasticity is a function of the axial shear strain or stress, then the shear stress-strain relation becomes nonlinear. In the next section, the nonlinear elastic model describing the stress-strain relation under static loads will be introduced and discussed.

The Nonlinear Elastic Stress – Strain Relation

For the static investigations, a nonlinear elastic model is suggested to express the stress-strain relation of subgrade soil. Soil as one of many engineering materials exhibits evident nonlinear mechanical behavior particularly when soil deformation is large. For the nonlinear elastic model, elastic parameters κ and G are a function of variables such as strain, strain rate, time and other variables. For example, the bulk modulus κ and shear modulus G can be defined as a function of the first and the second deviatoric invariants of strain tensors J_1 and J^D_1 that are related to volume and shear strains individually:

$$\kappa = \kappa(I_1, J_1, m_F, m_L, t) \qquad \text{(Eq.9)}$$

$$G = G(I_1, J_2^D, m_F, m_L, t) \qquad \text{(Eq.10)}$$

Comparing to the linear model in Eqs.5 and 6, one may notice that in Eqs.9 and 10 both bulk and shear moduli are functions of strain tensor invariants J_1 and J^D_2 but not cyclic loading repetition N. The strain invariants J_1 and J^D_2 are related to volume and shear strains respectively. Therefore, for the nonlinear stress–strain model, elastic stress dose not change linearly with elastic strain. As mentioned previously, research of the shear stress-strain relation in Eq.4e is emphasized. Moreover, the shear modulus G in Eq.10 is defined in the following expression [15]:

$$G = 1/(A + B\sqrt{J_2^D}) \qquad \text{(Eq.11)}$$

where A and B (1/kPa) are constitutive parameters, and defined by the following expressions in the quasi-triaxial space:

$$A = a_0(\sigma_0/p_0)^{a_1}(1+m_F)^{a_2}(1+m_L)^{a_3}(t/t_1)^{a_4} \quad \text{(Eq.12a)}$$

$$B = b_0(\sigma_0/p_0)^{b_1}(1+m_F)^{b_2}(1+m_L)^{b_3}(t/t_1)^{b_4} \quad \text{(Eq.12b)}$$

where a_i and b_i ($i = 1\ldots4$) are constitutive parameters and are to be determined using the experimental data from the static triaxial shear tests. Bearing Eqs.12a and 12b in mind and inserting Eq.11 into Eq.4b yield the shear stress-strain relation in terms of invariants of stress and strain tensors:

$$\sqrt{I_2^D} = \frac{\sqrt{J_2^D}}{[a_0(\frac{I_1}{p_0})^{a_1}(1+m_F)^{a_2}(1+m_L)^{a_3}(\frac{t}{t_1})^{a_4}]+[b_0(\frac{I_1}{p_0})^{b_1}(1+m_F)^{b_2}(1+m_L)^{b_3}(\frac{t}{t_1})^{b_4}]\sqrt{J_2^D}} \quad \text{(Eq.13)}$$

which can further reduce to a simplified form in the quasi triaxial stress space according to Eq.4e:

$$\sigma_1 - \sigma_3 = \frac{\varepsilon_1}{[a_0(\frac{\sigma_0}{p_0})^{a_1}(1+m_F)^{a_2}(1+m_L)^{a_3}(\frac{t}{t_1})^{a_4}]+[b_0(\frac{\sigma_0}{p_0})^{b_1}(1+m_F)^{b_2}(1+m_L)^{b_3}(\frac{t}{t_1})^{b_4}]\varepsilon_1} \quad \text{(Eq.14)}$$

where the coefficient 2 in Eq.4e, similar to the linear model, is dropped and included in the parameters a_0 and b_0 in Eq.14 for convenience of discussion.

If material parameters m_L and m_F equal zero (i.e., sample soil without fiber and lime), then Eq.14 reduces to the nonlinear model presented by Duncan *et al.* [16]. If the impact of confining pressure on the stress-strain relation is not considered, then Eq.14 further is simplified to the nonlinear hyperbolic model first introduced by Konder [17]. In the present investigation, the expression Eq.14, the generalized hyperbolic elastic stress–strain model for the composite subgrade soil, is introduced to describe the nonlinear behavior of the composite soil under static loading.

In order to understand the hyperbolic relation given by Eq.14, it is worthy to discuss the physical meaning of parameters defined in Eq.14. For constant parameters A and B defined in Eqs.12a and 12b, one can rewrite Eq.14 by the following simple form:

$$\sigma_1 - \sigma_3 = G\varepsilon_1 = (\frac{1}{A + B\varepsilon_1})\varepsilon_1 \qquad \text{(Eq.15)}$$

In fact, from the stress-strain relation shown in Figure 1, parameters A and B are respectively the reciprocal of the initial tangent modulus G_i (1/kPa) [= $(\sigma_1-\sigma_3)/\varepsilon_1|_{\varepsilon\to 0}$ =1/A] and the reciprocal of the asymptotic or ultimate value of the stress difference $(\sigma_1-\sigma_3)_{ult}$ [=$(\sigma_1-\sigma_3)|_{\varepsilon\to\infty}$ = 1/B] (see Figure 2).

From Eq.15, the following linear relation between 1/G [=$\varepsilon_1/(\sigma_1-\sigma_3)$] and the axial strain ε_1 should be addressed as it is useful when the constitutive parameters are to be determined from the experimental data, namely:

$$1/G = \varepsilon_1/(\sigma_1 - \sigma_3) = A + B\varepsilon_1 \qquad \text{(Eq.16)}$$

Apparently, parameters A and B shown in Figure 2 represent the intercept and the slope of a straight line. If experimental results from the static triaxial compressive tests support the relation shown in Eq.16, then the nonlinear model in Eq.15 is justified and verified as well.

Accordingly, the tangential modulus G_t (= $d(\sigma_1-\sigma_3)/d\varepsilon_1$) can be derived by taking derivative of Eq.15 with respect to the axial strain ε_1:

$$G_t = \frac{\partial(\sigma_1 - \sigma_3)}{\partial\varepsilon_1} = \frac{A}{(A + B\varepsilon_1)^2} \qquad \text{(Eq.17)}$$

The physical meaning of the tangential modulus G_t is also shown in Figure 1. As parameters A and B in Eq. 12a and 12 b are functions of multiple variables (i.e., σ_0, t, m_F and m_L), Eq.17, therefore, represents a family of curves. This is true for the relations in Eqs.15 and 16 as well. The constitutive parameters in both the linear and nonlinear models are to be calibrated from the experimental investigations in the next section.

EXPERIMENTAL INVESTIGATIONS

Specimen Preparation

Materials applied and tested

Sample soils for tests were taken from the Soil/Aggregate Laboratory at the Geotechnical Exploration Division at the Maryland State Highway Administration (SHA). These subgrade soils were originally collected from road construction sites in Howard Country, Maryland and had the following physical properties: the wet unit weight γ_{dry} = 17 kN/m^3 (95 lb./ft^3); plastic limit PL = 5%; the soil classification (AASHTO) is A4.

Lime powder used for specimen preparations was manufactured by the Lhoist Group Company. The lime powder is made of chemical hydrated lime with high calcium. The employed lime powder comprises Calcium Oxide (>71.5%) and Magnesium Oxide (about 1.0%). 100 percent of lime powder particles can pass through No. 20 U. S. standard sieve and 93% through No. 100 US. standard sieve. The product of lime powder meets the standards of American Water Works Association (AWWA B202 – 93) for the hydrated lime.

Geofiber used for specimen preparation was manufactured by Synthetic Industries Inc. The fiber is made of polypropylene, a chemically stable and inert polymer. The fibers mixed with sample soil are flexible, black and discrete strands about 3.5 cm (about 1.5 in) in length.

Specimens for both static and dynamic shear tests were prepared with fiber contents m_F = 0%, 0.2% and 0.5% and lime contents m_L = 0%, 2% and 5% by weight, respectively.

The procedure for specimen preparation

Sample preparation for conventional triaxial shear tests follows the procedure suggested by Synthetic Industries Inc.:

1. Soil Processing. Process soils through a #4 sieve; then thoroughly mix sample. Split sample into appropriate batches, not to exceed 10 lbs. (4.5 kg.)
2. Soil Conditioning. Place soil sample in mixing bowl. Start mixer and slowly add the required moisture to bring the sample up to approximately 80% of optimum moisture. Mix the soil sample until water is well distributed throughout the batch, based on visual observation. Remove moist soil and seal in plastic bag for 24 hours to allow specimen to hydrate thoroughly.
3. Mixing Procedure. Mixer bowl should not be filled more than one-half full for mixing. Therefore, weigh up to 10 lbs. (4.5 kg.) of soil into the mixer bowel. Add enough water to bring this batch to optimum moisture content. Uniformly spread the soil batch in 5 equal depth lifts in the mixer bowl, adding the fibers on each lift as described below. Uniformly spread ¼ of the total fiber content for the batch over the first lift of soil. Place the second lift of soil over the first layer of fibers. Continue this soil-fiber sequence until all the soil and fibers have been added. There will be 5 lifts of soil and 4 lifts of fibers, so the 5th lift of soil will cover the 4th lift of fibers and

no fibers will be visible at the surface prior to mixing. Mix the batch while at the same time, adding the remaining water. The water must be added slowly so that a continuous stream is supplied to the batch. Placing all the water too soon or intermittent adding of the water will result in a poor-mixing operation. The entire batch should have received an initial mixing operation by the time the final water is added. Mix until the mixture appears uniform. Remove the soil from the mixer bowl, place the mixture into bags and seal. Let the mixture hydrate for at least 24 hours prior to preparation of test specimens.

4. Sample Remold. The remolded mixture sample is compacted using a compaction mold (7.12 cm D x 14.2 cm H). Compact a specimen in five layers. Weigh 1,500 g mixture sample and separate it into five, so each layer has an equal amount of mixture. Each layer is compacted with 15 blows using a 2.5 kg. rammer. Trim both upper and lower surfaces. Remove the mold, keep the sample in a plastic bag to avoid loss of water content and place the specimen in a water bath until it is ready for the triaxial test. The specimen is cylindrical with a dimension of 6.86 cm (2.8 inch) in diameter and 13.72 cm (5.6 inch) in height.
5. Sample curing. Before shear tests, three aging periods (7, 14 and 28 days) are respectively used to cure the specimens with lime powder. During the curing periods, room humidity and temperature are controlled to minimize the moisture loss of the prepared specimens that are put in the sealed plastic bags.

Equipment and Test Conditions

The device and testing conditions for static tests

Experimental investigations for static shear tests were conducted using the triaxial shear apparatus manufactured by GEOCOMP Corp. The static triaxial apparatus has a strain-control system. The strain rate of compressive shear tests was 0.6% per minute. The axial mono-increase loading exerted on top of a specimen was controlled at a constant strain rate till the specimen failure occurs. Testing data such as axial stress and strain were collected through transducers by a data acquisition system. The value of the strength or the stress at failure was determined by taking either the peak stress value or the stress value at the axial strain = 15%. The shearing tests followed the AASHTO code T297 (or ASTM D4767) with the consolidation-undrained (CU) condition. Confining or cell pressures applied for triaxial shear tests were 50, 100, 150, or 200 kPa, respectively. The shear tests were conducted for specimens with different curing periods, different contents of fiber and lime. Specimens are prepared with m_L = 0%, 2% and 5% and m_F = 0%, 0.2% and 0.5%. The group number of tested specimens and experimental conditions applied to triaxial static shear tests were listed in Tables 1 and 2.

The device and testing conditions for dynamic tests

Experimental investigations for dynamic tests were conducted using a dynamic triaxial compressive shear test apparatus (RMT-1000). The RMT1000 system is the stress control shear device, and is manufactured by Structured Behavior Engineering Laboratory, Inc. Similar to static shear tests, cyclic shear tests were conducted under different testing conditions (e.g., different cyclic repetitions and confining pressures) for several groups of specimens having three curing periods, and two contents of fiber and

lime. The specimens are the same as those prepared for static shear tests, namely three lime contents (m_L = 0%, 2% and 5%) and three fiber contents (m_F = 0%, 0.2%, and 0.5%) except four confining or cell pressures for dynamic triaxial shear tests are 21, 50, 100 or 150 kPa, respectively. Cyclic repetitions for loading N are 50, 100 and 500. The axial cyclic loading waveform has a half-sine form. Shear tests are carried out by following the AASHTO code T292-91 with the CU condition. The axial load and deformation of the specimen, etc. are measured during the loading procedure. The tested specimen named and experimental conditions applied to triaxial cyclic shear tests are listed in Tables 3–9. The specimen n Tables 3 - 9 are named by the following way: 21, A, B and C in the first one or two letter represent the cell pressures 21, 50, 100 or 150 kPa respectively; the following two letters 07, 14 and 28 stands for the curing periods; then the next two letters indicate fiber and lime contents (e.g., 52 stands for m_F = 0.5 % and m_L = 2 %) and the last three letter are for the cyclic repetition N (i.e., 50, 100 or 150). The sample number 21145250, for example, denotes the specimen with σ_0 = 21 kPa, t = 14, m_F = 0.5%, m_L = 2% and N = 50. Similarly, the sample number A0755100 stands for σ_0 = 50 kPa, t = 7 days, m_F = 0.5%, m_L = 5% and N = 100.

Test Results and Data Analysis

Mechanical behavior in response to static loading

Research in this section is focused on investigating impacts of fiber and lime on the stress-strain relations as well as strength of composite soil under static loading. As mentioned in the early section, the stress-strain relation in response to the triaxial shear force is studied using the nonlinear elastic model introduced in Eq.15. This nonlinear model has two functions A and B. Each of functions A and B with constitutive parameters (a_i and b_i, i = 0…4) is defined as a product of four power functions for variables m_F, m_L, σ_0 and t. The constitutive parameters are to be determined by applying the experimental data from the compressive shearing tests that are discussed in details below.

Results of static compressive shear tests

Various results from more than thirty-six shear tests are collected, processed and presented through Figure 3 to Figure 19. Based on shear tests, effects of multiple variables on mechanical behavior of composite soil are analyzed and discussed respectively as follows:

1. Impacts of cell pressure and fiber content on the stress-strain relation without lime.

Relations ($\sigma_1 - \sigma_3$) versus ε_1 (the deviatoric stress versus the axial strain) are presented in Figures 3a, 3b and 3c for cell pressure σ_0 = 50, 100, 150 and 200 kPa. Each figure corresponds to fiber contents m_F = 0%, 0.2% and 0.5% and m_L = 0% (i.e., the specimens without lime). The impact of cell pressure and fiber content on the stress-strain relation is evident. For example, the family curves in each figure indicate effect of cell pressure on the stress-strain relation as stress increases with increase of confining pressure for any given strain. Furthermore, the effect of fiber content m_F on the strength of composite

subgrade soil can be observed by picking up one curve from each figure with the same cell pressure. If the relations $(\sigma_1 - \sigma_3)$ versus. ε_1 with cell pressure $\sigma_0 = 50$ kPa are chosen from Figures 3a, 3b and 3c, for instance, the axial stress values $(\sigma_1 - \sigma_3)$ at the axial strain ε_1 = 5% are 90, 120, and 150 kPa which respectively correspond to m_F = 0%, 0.2% and 0.5 %. The fiber impact on soil strength is also demonstrated in Figures 9a, 9b and 9c for the later discussion. As the tested specimens in this group have no lime content, for the given cell pressure shear strength increases due to the fiber reinforcement

In all three figures, the relations of $(\sigma_1 - \sigma_3)$ versus ε_1 are nonlinear. The axial deviatoric stress $(\sigma_1 - \sigma_3)$ nonlinearly changes with the axial strain ε_1. Moreover, based on the testing data the relations $1/G = \varepsilon_1/(\sigma_1 - \sigma_3)$ versus ε_1 with the same testing conditions are drawn in Figures 6a, 6b and 6c that correspond to Figures 3a, 3b and 3c individually. Test curves in Figures 6a, 6b and 6c illustrate that the relation $\varepsilon_1/(\sigma_1 - \sigma_3)$ versus ε_1 is linear, and that parameters A and B as assumed in Eqs.12 and 13 are functions of variables m_F, m_L and σ_0 since the slope B and intersection A of the straight lines shown in Figures 6a, 6b and 6c change with variables. This also suggests that the assumption of the nonlinear model in Eq.15 can be confirmed by the testing results because the linear relation Eq.16 with parameters A and B is an alternative expression of the hyperbolic relation Eq.15.

2. Impacts of cell pressure and sample-curing time on the stress-strain relation with both fiber and lime.

Nonlinear relations $(\sigma_1 - \sigma_3)$ versus ε_1 are shown in Figures 4a, 4b and 4c for cell pressures σ_0 = 50, 100, and 150 kPa and fiber contents m_F = 0.2% and lime content m_L = 5%. For each figure, the curing period t is 7, 14 and 28 days individually. For given m_F = 0.2% and m_L = 5%, impacts of cell pressure and the specimen-curing periods on the stress-strain relation are noticeable. Namely, with increase of cell pressure the axial stress increases at any given axial strain ε_1. Effect of specimen curing time on the stress-strain relation can be observed by selecting one curve with given cell pressure from each diagram from Figures 4a, 4b and 4c. For instance, choosing the curve with cell pressure σ_0 = 50 kPa from the family curves in Figures 4a, 4b and 4c finds that stress values at the axial strain ε_1 = 5% are individually 480, 600, and 800 kPa and correspond to t = 7, 14 and 28 days. More explicit exhibition of effect of the specimen-aging period on the stress-strain relation is shown and discussed in the later section.

Similarly, relations between $(\sigma_1 - \sigma_3)$ and ε_1 shown in Figures 4a, 4b and 4c are nonlinear, and the axial deviatoric stress $(\sigma_1 - \sigma_3)$ increases with increase of axial strain ε_1. The linear expressions $1/G = \varepsilon_1/(\sigma_1 - \sigma_3)$ versus ε_1 from the samples in the same group are plotted in Figures 7a, 7b and 7c that are associated with Figures 4a, 4b and 4c respectively. The linear relations between $1/G = \varepsilon_1/(\sigma_1 - \sigma_3)$ versus ε_1 in Figures 7a, 7b and 7c support the nonlinear relation in Eq.16 in which parameters A and B are not only functions of m_F, m_L and σ_0 but also functions of the sample-curing period t.

3. Impacts of cell pressure and the sample-curing time on the stress-strain relation with both fiber and lime.

Nonlinear relations $(\sigma_1 - \sigma_3)$ versus ε_1 shown in Figures 5a, 5b and 5c are similar to those shown in Figures 4a, and 4c except for $m_F = 0.5\%$ rather than 0.2%. For the given $m_F = 0.5\%$ and $m_L = 5\%$, impacts of cell pressure and the specimen-curing periods on the stress-strain relation are obvious. Namely, with increase of cell pressure σ_0 the axial stress $(\sigma_1 - \sigma_3)$ increases at any given axial strain ε_1. The effect of the specimen-curing time on the stress-strain relation can be observed by selecting one curve with given cell pressure from each figures. For instance, picking the curve with cell pressure $\sigma_0 = 50$ kPa from the family curves in Figures 5a, 5b and 5c finds that the stress values at the axial strain $\varepsilon_1 = 5\%$ are 600, 800, and 1000 kPa and correspond to t = 7, 14 and 28 days individually. This suggests that soil shear strength increases with the specimen-aging time so that elastic shear modulus G is a function of the sample-curing period t as assumed in Eq.10. The axial deviatoric stress $(\sigma_1 - \sigma_3)$ nonlinearly increases with the axial strain ε_1 as well. The linear expression $1/G = \varepsilon_1/(\sigma_1 - \sigma_3)$ versus ε_1 plotted in Figures 8a, 8b and 8c are related to Figures 5a, 5b and 5c. Again, from Figures 8a, 8b and 8c, the linear relation between $1/G = \varepsilon_1/(\sigma_1 - \sigma_3)$ and ε_1 confirms the nonlinear model in Eq.16, and the expressions for parameters A(m_F, m_L, σ_0 and t) and B(m_F, m_L, σ_0 and t) in Eqs.12a and 12b.

4. Impacts of cell pressure and fiber on the stress-strain relation without lime ($m_L = 0\%$).

Family curves of relations $(\sigma_1 - \sigma_3)$ vs. ε_1 in Figures 9a, 9b and 9c are in response to fiber contents $m_F = 0\%$, 0.2% and 0.5 % and lime content $m_L = 0\%$ (i.e., specimens without lime stabilization). The stress-strain relations for three family curves are plotted in Figures 9a, 9b and 9c for cell pressures $\sigma_0 = 50$, 100, and 150 kPa individually. Figures 9a, 9b and 9c demonstrate impacts of fiber reinforcement ($m_F = 0\%$, 0.2% and 0.5 %) on soil strength. Each stress-strain relation in the family curves in Figures 9a, 9b and 9c increases with the fiber content. For each stress-strain relation, the axial deviatoric stress $(\sigma_1 - \sigma_3)$ increases nonlinearly with increase of axial strain ε_1. This supports the assumption that the elastic shear modulus G (related to parameters A and B) is a function of fiber content m_F as defined by Eq.10. The linear expressions $1/G = \varepsilon_1/(\sigma_1 - \sigma_3)$ versus ε_1 related Figures 9a, 9b and 9c are plotted in Figures 12a, 12b and 12c. As mentioned in the previous discussion, the linear expression in Figures 12a, 12b and 12c allows one to determine parameters A and B conveniently. At the same time, based on the test data, the linear relation between $1/G = \varepsilon_1/(\sigma_1 - \sigma_3)$ and ε_1 justifies the nonlinear model in Eq.14 and the linear expression in Eq.16.

5. Impacts of the sample curing period and cell pressure on the stress-strain relation with given fiber and lime

The family curves of relations $(\sigma_1 - \sigma_3)$ vs. ε_1 in Figures 10a, 10b, 10c and 10d are in response to three sample-curing periods (t = 7, 14, and 28 days). The four figures with $m_F = 0.5\%$ and $m_L = 5\%$ are correspondingly plotted with cell pressures $\sigma_0 = 50$, 100, 150, and 200 kPa. Figures 10a, 10b, 10c and 10d are alternative illustrations of Figures

4a, 4b and 4c, and exhibit impacts of the sample-curing periods (t = 7, 14 and 28 days) on the stress-strain relations. Each stress-strain curve of the family curves in Figures 10a, 10b, 10c and 10d nonlinearly increases with the sample-curing time. For each stress-strain relation, the axial deviatoric stress $(\sigma_1 - \sigma_3)$ increases nonlinearly with axial strain ε_1. This verifies that soil shear strength increases with the specimen-aging time, and elastic shear modulus G is a function of the sample-curing period t introduced in Eq.10. In fact, one also can draw the linear relation between $\varepsilon_1/(\sigma_1 - \sigma_3)$ and ε_1 for the different sample-curing periods to determine parameters A and B.

6. Impacts of the sample-curing periods and cell pressure on the stress-strain relation with given contents of fiber and lime.

The family curves for relations $(\sigma_1 - \sigma_3)$ versus ε_1 in Figures 11a, 11b and 11c are drawn with three different sample-curing periods (t = 7, 14, and 28 days). Three figure with m_F = 0.2%, m_L = 5% are individually plotted with cell pressure σ_0 = 50, 100, and 150 kPa. The same attempt is made to demonstrate impacts of the sample-curing periods (t = 7, 14 and 28 days) on the stress-strain relations. Each stress-strain relation in the family curves shown in Figures 11a, 11b and 11c increases with the sample-curing time. For each stress-strain relation, the axial deviatoric stress $(\sigma_1 - \sigma_3)$ increases nonlinearly with increase of the axial strain ε_1. This validates the elastic shear modulus G in Eq.10 as a function of the sample-curing period t in this group with specific conditions.

7. Impacts of fiber content and cell pressure on the stress-strain relation with lime.

More curves in Figures 13a, 13b and 13c with the parameter m_F are illustrated for impacts of fiber content, cell pressures and the curing periods on the stress-strain relation. For instance, Figures 13a1, 13a2 and 13a3 indicate the fiber effect (m_F = 0.2% and 0.5%) on the stress-strain relation $(\sigma_1 - \sigma_3)$ vs. ε_1 with increased cell pressure σ_0 = 50, 100, or 150 kPa, lime content m_L = 5% and the curing period t = 7days. In contrast, Figures 13b1, 13b2 and 13b3 are plotted to demonstrate the fiber effect on the axial stress-train relations with the same conditions except for the curing period t = 14 days. Figures 13b1, 13b2 and 13b3 are also to illustrate the fiber effect on the axial stress-train relations with the curing period t = 28 days instead. Similar to the previous discussion, the axial stress in Figures 13a, 13b and 13c increases with increase of fiber content at any given axial strain. The stress-strain relations in Figures 13a and 13b and 13c are nonlinear and suggest the elastic modulus is the function of the axial strain. For purpose of comparison, Figures 14a, 14b and 14c corresponding to Figures 13 a, 13b and 13c are plotted to show the linearity between $\varepsilon_1/(\sigma_1 - \sigma_3)$ and ε_1 so that the functions A and B and related parameters in the nonlinear model can be determined.

8. Impacts of fiber reinforcement on soil strength without lime stabilization.

Figures 15a, 15b and 15c show effect of fiber reinforcement (m_F = 0.0, 0.2, and 0.5%) on the Column-Mohr's failure line with m_L = 0% and at ε_{1f} = 15% where ε_{1f} is the axial strain at failure. The relations of cohesion c and friction angle ϕ versus fiber content m_F found from Figures 15a, 15b and 15c are linear and drawn in Figures 18a and 19a respectively. From Figures 18a and 19a, the fiber reinforcement plays a significant role

in strength of composite soil because the strength parameter c and ϕ show linear relations with fiber content m_F.

9. Impacts of the sample-curing periods on the soil strength with lime stabilization.

Figures 16a, 16b and 16c show the effect of the sample-curing time t (7, 14 and 28 days) on the Column-Mohr's failure line with m_F = 0.2%, m_L = 5% and ε_{1f} = 15%. From Figures 16a, 16b and 16c, the relations of cohesion c and friction angle ϕ versus the aging time t are drawn in Figures 18b and 19b respectively. From Figures 18b and 19b, strength indices c and ϕ increase linearly with the curing period t. Impact of sample curing periods on the soil strength can also be found with the identical conditions except for m_F = 0.5% from Figures 17a, 17b and 17c in which effect of the sample-curing time t on the Column-Mohr's failure line is obvious (m_L = 5% and ε_{1f}= 15%). In the same way, Figures 18c and 19c indicate that strength indices c and ϕ linearly increase with the sample-aging time (m_F = 0.5% and m_L = 5%). In future sections, impacts of fiber and lime reinforcement will be discussed in details.

In brief, experimental results from the static triaxial shear tests verify the nonlinear stress-strain model in Eq.15 and shear modulus G in Eq.16 with various combinations of four variables σ_0, m_F, m_L and t having different values, indicate effects of the four variables on soil static behavior such as the stress-strain relation and soil failure, provide the necessary information for calibration of the ten constitutive coefficients, and finally suggest the linear relation of the strength parameters c and ϕ have linear relations with m_F, m_L and t (i.e., Eqs.28c and 28d)

Parameter calibration for the nonlinear model

To establish the nonlinear model suggested in either Eq.14 or Eq.15, the constitutive parameters introduced in Eqs.14 need to be determined. For convenience of calibrating constitutive parameters a_i and b_i (i = 0 …4) in Eq.14, one needs to rewrite Eqs.12a and12b in the following logarithmic forms:

$$\mathrm{LogA} = \mathrm{Log}a_0 + a_1\mathrm{Log}(\sigma_0/p_0) + a_2\mathrm{Log}(1+m_F) + a_3\mathrm{Log}(1+m_L) + a_4\mathrm{Log}(t/t_1) \quad \text{(Eq.18a)}$$

$$\mathrm{LogB} = \mathrm{Log}b_0 + b_1\mathrm{Log}(\sigma_0/p_0) + b_2\mathrm{Log}(1+m_F) + b_3\mathrm{Log}(1+m_L) + b_4\mathrm{Log}(t/t_1) \quad \text{(Eq.18b)}$$

Eqs.18a and 18b can alternatively be written in a more explicit linear expression with multiple variables:

$$Y = d_0 + d_1X_1 + d_2X_2 \ldots + d_kX_k = d_0 + \sum_{i=1}^{k} d_i X_i \quad \text{(Eq.19)}$$

where Y = Log A or Log B; d_i = a_i or b_i (i = 0…4); and X_i (i = 1…4) represents Log(σ_0/p_0), Log($1+m_F$), Log ($1+m_L$), or Log(t/t_1). To utilize Eq.19 for the linear regression with multiple variables, the values of variables (m_F, m_L, t and σ_0) and functions A and B in Figures 12 and 14 are converted to logarithmic values and are applied to Eq.19. The logarithmic values of A and B from nine groups of tested samples are listed in Tables 10a, 10b and 10c. A program coded in FORTRAN for the linear regression of multiple variables is adopted to calibrate the constitutive parameters a_i and b_i (i = 0…. 4). The parameters a_i and b_i are found and shown in Table 11a. The functions A and B in Eq.12 or Eq.13, therefore, can be expressed by:

$$A = 0.15(\sigma_0/p_0)^{-0.38}(1+m_F)^{-54.29}(1+m_L)^{-10.76}(t/t_1)^{-0.42} \quad \text{(Eq.20a)}$$

$$B = 0.01(\sigma_0/p_0)^{-0.17}(1+m_F)^{-167.25}(1+m_L)^{-25.81}(t/t_1)^{-0.21} \quad \text{(Eq.20b)}$$

Accordingly, the shear modulus of elasticity in Eq.11 and the stress-strain relation in Eq.14 becomes:

$$G = \frac{1}{A(\sigma_0, m_F, m_L, t) + B(\sigma_0, m_F, m_L, t)\varepsilon_1} = \frac{1}{0.15\sigma_0^{-0.38}(1+m_F)^{-54.29}(1+m_L)^{-10.76}t^{-0.42} + 0.01\sigma_0^{-0.17}(1+m_F)^{-167.3}(1+m_L)^{-25.8}t^{-0.21}\varepsilon_1}$$

(Eq.21a)

$$\sigma_1 - \sigma_3 = \frac{\varepsilon_1}{A(\sigma_0, m_F, m_L, t) + B(\sigma_0, m_F, m_L, t)\varepsilon_1} = \frac{\varepsilon_1}{0.15\sigma_0^{-0.38}(1+m_F)^{-54.29}(1+m_L)^{-10.76}t^{-0.42} + 0.01\sigma_0^{-0.17}(1+m_F)^{-167.3}(1+m_L)^{-25.8}t^{-0.21}\varepsilon_1}$$

(Eq.21b)

Eq.21b represents the established nonlinear elastic model that describes the shear stress-strain relation, and can be applied to designs of roadbeds, soil slopes, bridge foundations, etc. when the same composite materials are used.

Tangential shear modulus G_t of the composite material under static loading

Tangential modulus plays an important role in engineering analysis and design. The tangential modulus in Eq.17 can be found to be a function of multiple variables (m_F, m_L, t, σ_0, and ε_1) by applying expressions A and B in Eqs.20a and 20b to the tangential shear modules G_t in Eq.17 in the following expression:

$$G_t = \frac{G_i}{\left[1 + 0.07\left(\frac{\sigma_0}{p_0}\right)^{0.21}(1+m_F)^{-112.96}(1+m_L)^{-15.05}\left(\frac{t}{t_1}\right)^{0.21}\varepsilon_1\right]^2} \quad \text{(Eq.22)}$$

where G_i is the initial shear modulus and equals 1/A in Eq.20a. Eq.22 provides an important mathematical expression of the nonlinear tangential modulus G_t that is fundamental input for the analytical and numerical simulation and modeling in stress analysis within roadbeds, soil slopes, shallow and deep foundations.

Impact factors I_{Ai} and I_{Bi} for parameters A and B in the nonlinear model

In order to describe effects of cell pressure, fiber, lime and the sample-curing periods on static behavior of composite soil such as shear stress-strain relations, initial and tangential moduli, soil strength, etc, impact factors I_A and I_B are introduced. I_A and I_B are both functions of σ_0, m_F, m_L, and t, and describe the impacts on the functions A and B that are further related to the initial shear modulus and soil strength. Based on the calibrated results in Table 11a, the impact factors I_A and I_B are respectively defined as follows [14 -15]:

1. The impact factors of confining pressure:

$$I_{A\sigma} = A(\sigma_0, m_F, m_L, t)/\ A(1.0, m_F, m_L, t) = \sigma_0^{-0.38} \quad \text{(Eq.23a)}$$

$$I_{B\sigma} = B(\sigma_0, m_F, m_L, t)/\ B(1.0, m_F, m_L, t) = \sigma_0^{-0.17} \quad \text{(Eq.23b)}$$

2. The impact factors of fiber reinforcement:

$$I_{AF} = A(\sigma_0, m_F, m_L, t)/A(\sigma_0, 0, m_L, t) = (1+m_F)^{-54.29} \quad \text{(Eq.24a)}$$

$$I_{BF} = B(\sigma_0, m_F, m_L, t)/B(\sigma_0, 0, m_L, t) \ = \ (1+m_F)^{-167.25} \quad \text{(Eq.24b)}$$

3. The impact factors of lime stabilization:

$$I_{AL} = A(\sigma_0, m_F, m_L, t)/A(\sigma_0, m_F, 0, 1) \ = \ (1+m_L)^{-10.76} \quad \text{(Eq.25a)}$$

$$I_{BL} = B(\sigma_0, m_F, m_L, t)/B(\sigma_0, m_F, 0, 1) = \ \ (1+m_L)^{-25.81} \quad \text{(Eq.25b)}$$

4. The impact factors of the sample curing period:

$$I_{At} = A(\sigma_0, m_F, m_L, t)/ A(\sigma_0, m_F, m_L, 1) = t^{-0.42} \quad \text{(Eq.26a)}$$

$$I_{Bt} = B(\sigma_0, m_F, m_L, t)/ B(\sigma_0, m_F, m_L, 1) = t^{-0.21} \quad \text{(Eq.26b)}$$

where I_{ij} stands for impact factors. The subscript i (= A or B) is related to functions A and B, and the subscript j denotes the four variables (= σ_0, m_F, m_L or t). The impact factors defined above are relevant to functions A and B that affect shear modulus G in Eq.16. One may note that the impact factor of a variable equals to the power function of the same variable. This is because the assumption of the product of multiple power functions for A and B in Eqs.12a and 12b suggests no couple effect between variables σ_0, m_F, m_L, and t. This assumption is made for convenience of investigations.

Failure of composite material under static shear stress

If the Coulomb-Mohr's failure criteria is applied to the composite materials in the quasi-triaxial space, on a failure surface shear stress τ has a linear relation with normal stress σ:

$$\tau = c + \sigma \tan \phi \quad \text{(Eq.27)}$$

where c and ϕ denote soil cohesion (kPa) and internal frication angle (degree), and the terms τ and σ (kPa) are the shear and normal stresses on the failure plane.

As strength indices c and ϕ are functions of m_F, m_L and t according to the test results, the equation Eq.27 represents a family of failure lines. If the axial deviatoric strain at failure is taken as 15% (i.e., ε_{1f} = 15%), the relation $\tau - \sigma$ shown in Eq.27 further is drawn in Figures 15, 16 and 17 to determine the strength indices c and ϕ. The parameters c and ϕ with different variable values are found and listed in Table 12a in which the test data indicates that strength parameters c and ϕ are not constant but a function of fiber and lime contents, and the specimen-aging period [i.e., $c(m_F, m_L, t)$ and $\phi(m_F, m_L, t)$]. The results plotted in Figures 18 and 19 imply that the strength parameters c and ϕ may individually have the linear relation with m_F, m_L, or t. Therefore, parameters c and ϕ versus variable m_F, m_L, and t are assumed to have such linear relations:

$$\phi = k_0 + k_1 m_F + k_2 m_L + k_3 t \quad \text{(Eq28a)}$$

$$c = n_0 + n_1 m_F + n_2 m_L + n_3 t \quad \text{(Eq28b)}$$

where k_i and n_i (i = 0…3) are constants. To determine the coefficients in Eqs.28a and 28b, first find k_0 = 12.3 (degree) and n_0 = 58.91 (kPa) from Figures 18a and 19a in which the tested soil samples do not contain lime, then determine k_3 = 0.4 (degree/day) and n_3 = 0.26 (kPa/day) from Figures 18c and 19c, and finally, by solving two sets of linear equations, find k_1=20.83 (degree) and k_2 = 6.65 (degree) from Figures 18b and 18c, and n_1 = 69.87 (kPa) and n_2 = 25.14 (kPa) from Figures 19b and 19c. Consequentially, Eq28a and 28b become:

$$\phi = 12.31 + 20.83\, m_F + 6.657\, m_L + 0.4\, t \qquad \text{(Eq28c)}$$

$$c = 58.91 + 69.87\, m_F + 25.14\, m_L + 0.26\, t \qquad \text{(Eq28d)}$$

The coefficients k_i and n_i in Eq.28a and 28b are listed in Table 12c. As the values k_1 = 16.68 (kPa) and n_1 = 66.39 (kPa) can also be found from Figures 18a and 19a, these two figures are given in Table12c as well. One can also take an average values of k_1 = 14.5 (kPa) and n_1 = 68.13 (kPa) for the practical purpose. The parameters c and ϕ in Eqs.28c and 28d reduce to constants [i.e., ϕ = 12.31 (degree) and c = 58.91 (kPa)] if the shear tests conducted for the sample soil without fiber and lime.

If Eq.28c and 28d are applied to Eq.27, the linear relation τ versus σ on the failure plane in Eq.27 becomes a function of variables m_F, m_L, and t, and represents a family of failure lines with changing variables m_F, m_L, and t. The strength indices c and ϕ in Eq.28c and 28d are key parameters in engineering design, especially useful for applications or projects associated with design of roadbed, highway slopes, bridge footings and foundations where fiber reinforced and lime stabilized soils are utilized.

Mechanical behavior in response to dynamic loading

In this section, mechanical behavior of composite soils under cyclic loading is studied, including stress-strain relationship, shear or resilient modulus, and important factors that may affect soil mechanical properties. As assumed in the early section, to describe the cyclic stress-strain relation of fiber-reinforced and lime stabilized soil, the linear elastic model in Eq.8a or Eq.8b is adopted. The linear model is different from the nonlinear elastic model presented in Eq.14. In the nonlinear elastic model, parameters A and B are functions of fiber and lime contents, cell pressure and the sample-curing period. In contrast, shear modulus G in the linear model is not only the function of variables m_F, m_L, σ_0, and t but also the function of loading repetition N. The nonlinear elastic model is introduced for static shear tests, and shear modulus G is defined as a function of A and B [i.e., $G = 1/(A+B\varepsilon_1)$] with a total of ten constitutive parameters a_i and b_i (i = 0…4). The linear model, however, is introduced for cyclic loading, and the elastic shear modulus G in Eq.7 having six constitutive parameters c_i (i = 0…5). The constitutive parameters c_i are to be determined using the experimental data from the periodic shear tests. The experimental results from dynamic tests are to be discussed in the following sections.

Results of cyclic shear tests

Mechanical behavior of composite soil in response to dynamic shear loading is analyzed and presented through Figure 20 to Figure 36. In a total of seventeen figures, cyclic stress-strain relations are drawn in three groups according to different sample-curing periods. Figures 20 - 25, for instance, are plotted for t = 7 days, Figures 26 - 30 for t = 14 days and Figures 31 – 36 for t = 28 days. In each group, cyclic stress-strain relations change with different cell pressures, fiber and lime contents and loading repetitions. Figure 37 is used for illustration of variable impacts on the elastic shear modulus G. In Figures 38 and 40, the relations of shear modulus or resilient modulus Mr versus the mean principal stress σ_m [= $(\sigma_1 + \sigma_2 + \sigma_3)/3$] are plotted along with the five different variables. To distinguish the dynamic tests from the static ones, throughout Figures 20 to 36, notations σ_d and ε_d are employed to denote $(\sigma_1 - \sigma_3)$ and strain ε_1 that are previously used in the section of static tests. The subscript d represents dynamic tests. The notations CF, mF, mL, N and t used for legends in figures represent cell pressure, fiber content, lime content, loading repetition and the sample-curing period.

Based on the testing curves shown in Figures 20 – 36, effects of multiple variables on dynamic behavior of composite soil are respectively discussed as follows:

1. Impact of cell pressure on the cyclic stress-strain relation.

Relations of σ_d versus ε_d [i.e., $(\sigma_1 - \sigma_3)$ versus strain ε_1] are presented in Figures 20 – 36 with different cell pressure σ_0 (= 21, 50, 100, 150 kPa). Effect of cell pressures on the periodic stress-strain relation is significant. For example, the slope of each stress-strain line in the family curves within any diagram noticeably changes with cell pressure. In other words, for a given periodic strain ε_d within any diagram, the axial cyclic shear stress increases with increase of cell pressure when other variables such as m_F, m_L t, and N are given. This is true throughout Figures 20 to 36. Furthermore, in all seventeen figures, the relations of σ_d versus ε_d are linear. Namely, the axial cyclic stress σ_d linearly changes with the axial cyclic strain ε_d though the elastic modulus is a function of σ_0, m_F, m_L, t, and N as assumed in Eq.7. The linear relation between periodic stress and strain supports the assumption of the linear model introduced in Eq.8b. This allows one to find the six constitutive parameter c_i (i = 0…5) using the linear model in Eqs.7 or 8b. Readings of slope values from each stress-strain line from Figures 20 to 36 are listed in Tables 13 - 16 for the calibration of constitutive parameters. The data analysis in Figure 37a shows that the average values of the shear modulus G change with cell pressure σ_0 in a power function $G = 35{,}000\sigma_0^{0.11}$ (kPa). This fact is consistent with the relation introduced in Eq.7 in which changes in G with cell pressure is described by the power function when other variables are given. This also suggests that the axial cyclic stress σ_d increases in a power function for the given ε_d because of an alternative relation $\sigma_d = 35{,}000\sigma_0^{0.11}\,\varepsilon_d$ (kPa) based on Eq.8b. Increasing cell pressure enhances soil shear strength by providing extra normal and frictional resistance between granular particles.

2. Impact of fiber contents on the periodic stress-strain relation.

Though from the testing results show in Figures 20 – 36 effect of fiber content on the relation between σ_d and ε_d is not as evident as that of cell pressure discussed in the

previous section, one, however, can find how fiber reinforcement affects the stress-strain relation by examining Figure 37b. In Figure 37b, the average values of shear modulus G for the linear elastic stress-strain relation can be expressed by the formula $G = 56{,}800 m_F^{0.01}$ (kPa). Similarly, from Eq.8b, this formula can be rewritten by $\sigma_d = 56{,}800 m_F^{0.01} \varepsilon_d$ that implies that the average values of σ_d also change with m_F as a power function if ε_d and other variables are given. This is because the fiber content in soil samples plays a role in mechanical reinforcement and property improvement by increasing the inter lock and shear resistance within soil skeletal structure.

3. Impact of lime contents on the periodic stress-strain relation.

The testing results in Figures 20 – 36 demonstrate the noticeable impact of lime content on the relation between σ_d and ε_d. By comparing three pairs of figures with m_L= 2 and 5%, m_F = 0.5%, namely Figures 23a and 25a (t = 7 days), Figures 29a and 30a (t = 14 days), and Figures 35a and 36a (t = 28 days), one can find that the average values of σ_d at strain ε_d = 0.1% from m_L= 2% to 5% increase approximately by 4%, 14% and 50% when t = 7, 14 and 28 days. The effect of lime content on the stress-strain relation can be found from Figure 37c in which the average values of shear modulus G change with m_L can be described by the relation $G = 55{,}900 m_L^{0.012}$. This relation justifies the assumption in Eq.8b in which if ε_d and other variables are given, the relation between σ_d and m_L can be described by the power function $\sigma_d = 55{,}900 m_L^{0.012} \varepsilon_d$. The lime content in soil samples improves soil shear resistance by contributing the extra binding force between the granular particles so that the microstructure of the soil skeleton can be stabilized.

4. Impact of curing periods on the periodic stress-strain relation.

From the plotted diagrams in Figures 20 –36 one can find the obvious impact of the sample-curing period on the relations between σ_d and ε_d. For example, in Figures 21a, 28a and 33a, the average values of σ_d at strain ε_d = 0.1% are respectively about 68, 71 and 75 kPa when t = 7, 14 and 28 days, m_F = 0.2% and m_L= 5%. Namely, σ_d increases about 4-5 % when the sample-curing period is doubled from 7 days to 14, then to 28 days. The effect of sample curing period on the stress-strain relation can be further perceived from Figure 37e in which the shear modulus $G = 49{,}000\ t^{0.054}$ confirms the power function assumed in Eq.7. In other words, similar to Eq.8b, changes in σ_d can be also expressed in the power function $\sigma_d = 49{,}000\ t^{0.054} \varepsilon_d$ when ε_d and other variables are known. Increase of the sample-curing period allows the chemical stabilization to develop extra shear resistance between granular particles so that the mechanical property of composite soil can be improved.

5. Impact of the loading repetition on the periodic stress-strain relation.

Checking Figures 20 – 36 can examine effect of loading repletion N on dynamic behavior of the composite soil. For instance, in Figures 20a, 20b and 20c (ε_d. = 0.1%, m_F = 0.2% and m_L= 2%, t =7days) the average values of σ_d for the cyclic loading repetition N = 50, 100 and 500 are 75, 68 and 62 kPa respectively. Similarly, in Figures 21a, 21b and 21c (ε_d. = 0.1%, m_F = 0.2%, m_L = 5%, and t =7days), the average values of σ_d are

approximately 70, 65 and 59 kPa. Namely, the axial shear stress decrease as the loading repetition N increases. The effect of fiber content on the stress-strain relation can be noticed from Figure 37b in which the average values of shear modulus G change with loading repletion N in a form: $G = 77{,}600N^{-0.066}$. When compared to other variables, this expression implies that the cyclic shear stress σ_d decreases with N as an inversed power function with the given ε_d and other variables. This is because the repeated loading induces the cyclic shear stress that causes the structural damage to deformable soil skeleton.

6. Impact of loading repetition and the mean principal stress on the resilient modulus.

Figures 38 – 40 are plotted for the relation Mr versus σ_m along with different variables to exhibit effects of N and σ_m on the shear modulus or the resilient modulus. The impact of changing loading repetition and mean principal stress on the resilient modulus is significant. For instance, in each figure, the resilient modulus increases with increase of the mean principal stress σ_m, and decrease with increase of the loading repetition N at a given σ_m. This means the composite material is "hardened" with increase of the mean principal stress, but "softened" with increase of the cyclic loading repetition due to shearing damage to the soil skeletal structure.

In brief, experimental results from dynamics shear tests support the linear model in Eq.7, justify the resilient modulus in Eq.8b with various values of the five variables σ_0, m_F, m_L, t, and N, and finally present the test data for calibration of the constitutive parameter under cyclic loading.

Parameter calibration for the linear model

To establish the linear model suggested in either Eq.8a or Eq.8b, six constitutive parameters introduced in Eq.7 need to be determined. For convenience of calibrating constitutive parameters c_i ($i = 0 \ldots 5$) in Eq.7, one can rewrite Eq.7 in the logarithmic form:

$$\text{Log}G = \text{Log}c_0 + c_1\text{Log}(\sigma_0/p_0) + c_2\text{Log}(1+m_F) + c_3\text{Log}(1+m_L) + c_4\text{Log}N + c_5\text{Log}(t/t_1) \qquad \text{(Eq.29)}$$

If comparing Eq.29 to Eq.19, one may note $Y = \text{Log } G$, $d_i = c_i$ ($i = 0 \ldots 5$), and X_i ($i = 0 \ldots 5$) respectively denotes the five terms in Eq.29, specifically, $\text{Log}(\sigma_0/p_0)$, $\text{Log}(1 + m_F)$, $\text{Log}(1 + m_L)$, Log(N) and $\text{Log}(t/t_1)$.

Following the same way for calibrating parameters a_i and b_i, the parameters c_i in Eq.29 can be found using the linear regression. The parameters c_i ($i = 0 \ldots 5$) can also be calibrated using the multiple-step graphical methods. The values of elastic shear modulus G read from the slope value of the stress-strain lines in Figures 20 – 36 are converted into logarithmic values and listed along with other variable values (i.e., the values of σ_0, m_F, m_L, N and t) in Tables 13, 14, 15 and 16. If the parameters c_i in Table 11c are applied to Eq.8b, the linear elastic relation between σ_d and ε_d becomes:

$$\sigma_d = 41897(\sigma_0/p_0)^{0.11}(1+m_F)^{0.01}(1+m_L)^{0.012}(N)^{-0.066}(t/t_1)^{0.054}\varepsilon_d \quad \text{(Eq.30)}$$

Eq.30 represents the established linear elastic model for description of the dynamic stress-strain relationship. The linear elastic model in Eq.30 can be applied not only to design of roadbeds subjected to the traffic-induced cyclic loading, but also to design of highway slopes or foundations subjected to earthquake-induced cyclic loading if the same composite materials are employed.

Resilient modulus Mr of the composite material under cyclic loading

Resilient modulus plays an import role in engineering design. The resilient modulus is inherently the shear modulus. For the linear model, from Eq.7 or Eq.30, the resilient modulus is:

$$M_r = \sigma_d / \varepsilon_d = 41897(\sigma_0/p_0)^{0.11}(1+m_F)^{0.01}(1+m_L)^{0.012}(N)^{-0.066}(t/t_1)^{0.054} \quad \text{(Eq.31)}$$

As mentioned in the early section, the relations of resilient modulus Mr versus the mean principal stress σ_m are illustrated along with other variable in Figures 38-40. The mean principal stress σ_m equals the cell pressure σ_0 plus one-third of the axial cyclic stress σ_{cyclic}, namely, $\sigma_m = \sigma_0 + \sigma_{cyclic}/3$. It is more efficient to apply Eq.31 to project design than to apply the graphical method to diagrams to interpolate or extrapolate values of Mr.

Impact factors I_{Gi} on shear modulus G in the linear model

In order to describe effects of cell pressure, fiber and lime contents, and the sample-curing periods on the mechanical behavior of composite soil such as shear stress-strain relations, initial and tangential modulus, soil strength, etc, the impact factors I_{Gi} of σ_0, m_F, m_L, and t for the resilient modulus Mr are respectively defined and found from the experimental results as follows [14 -15]:

$$I_{G\sigma} = G(\sigma_0, m_F, m_L, t, N)/ G(1, m_F, m_L, t, N) = \sigma_0^{0.11} \quad \text{(Eq.32a)}$$

$$I_{GF} = G(\sigma_0, m_F, m_L, t, N)/G(\sigma_0, 0, m_L, t, N) = (1 + m_F)^{0.01} \quad \text{(Eq.32b)}$$

$$I_{GL} = A(\sigma_0, m_F, m_L, t)/A(\sigma_0, m_F, 0, 1) = (1 + m_L)^{0.012} \quad \text{(Eq.32c)}$$

$$I_{GN} = B(\sigma_0, m_F, m_L, t)/ B(\sigma_0, m_F, m_L, t, 1) = N^{-0.066} \quad \text{(Eq.32d)}$$

$$I_{Gt} = A(\sigma_0, m_F, m_L, t, N)/ A(\sigma_0, m_F, m_L, 1, N) = t^{0.054}, \quad \text{(Eq.32e)}$$

where I_{Gi} stands for the impact factor of the shear modulus G. The subscript i denotes the four variables (σ_0, m_F, m_L N or t). Similar to the static investigation, the impact factor of a variable on dynamic behavior equals the power function of the same variable based on the same reason. Again, for convenience of parameter calibration, the assumption of no couple effect between variables σ_0, m_F, m_L, N and t is made. The impact factors introduced in this section is directly associated with the shear modulus. The impact factors not only describe effects on the cyclic stress and shear modulus due to the same variable but also indicate sensitivity of σ_d and G to different variables. For example, Eq.32a shows how G responds to cell pressure and also exhibits different sensitivity to cell pressure and sample-curing period. The shear modulus G from cyclic shear test may be more sensitive to the cell pressure than to the sample-curing time t due to the difference between the two coefficients of the power functions (i.e., $c_1 = 0.1 > c_5 = 0.054$).

Failure of composite material under cyclic shear stress

The study on failure of composite material under cyclic loading is not significantly important, as elastic deformation under cyclic loading is small when compared that under to static loading. This is especially true for unsaturated subgrade soils. From Figure 20 to Figure 36, for instance, the axial recoverable strain ε_d under the axial cyclic stress σ_d is less than 0.3%. From static triaxial shear tests the stress-strain relation is approximately linear when the axial strain is less than 2%. It should be pointed out that when composite material is subjected to cyclic loading, viscous behavior could play a role in the stress-strain relation [17-18]. For a long term of repeated shear loading on soil, the failure due to material fatigue could occur as well. The soil's viscous and fatigue characteristics are related to soil rehological behavior that is beyond the scope of this investigation.

SUMMARIES AND CONCLUSIONS

Experimental investigations were conducted for fiber-reinforced and lime-stabilized subgrade soil using conventional static and dynamic triaxial apparatus. The investigations are summarized along with conclusions drawn from the test results as below:

1. Establishment of constitutive models.

Two new constitutive models for composite material have been introduced. In this report, the composite material is the subgrade soil reinforced with geofiber and stabilized with lime. What sets the two models apart from those introduced by previous investigators is that these two models are used to describe static and dynamic behavior with consideration of effects of fiber and lime contents and other related factors. For the static case, a nonlinear elastic model is introduced in Eq.21b as a hyperbolic function, and to simulate the nonlinear static behavior for the composite material. The shear modulus G in the nonlinear model is related to the axial strain and two parameters A and B that are further defined as a function of cell pressure, fiber and lime contents, and the sample-curing period [i.e., $G = 1/(A(\sigma_0, m_F, m_L \text{ and } t) + B(\sigma_0, m_F, m_L \text{ and } t)\varepsilon_1)$ in Eq.16]. For the dynamic case, a linear model established in Eq.21b or Eq.30 is suggested to express the cyclic stress-strain relation. The elastic modulus G in the linear model is assumed to be a function of five variables such as cell pressure, fiber and lime contents, the sample-curing period and loading repetitions, namely $G = G(\sigma_0, m_F, m_L, t \text{ and } N)$ in Eq.8b or Eq.31. Both shear moduli in the linear and nonlinear models are assumed to be a product of multiple power functions of variables (i.e., σ_0, m_F, m_L, t and N). The introduced linear and nonlinear models are further verified and justified using the experimental data from conventional triaxial shear tests under static and cyclic loading.

2. Experimental investigation for static and dynamic tests.

The same procedure for sample preparation is applied for static and dynamic shear tests. During the preparing procedure, soil samples are carefully mixed with different fiber contents (m_F = 0, 0.2 and 0.5%) and lime contents (m_L = 0, 2 and 5 %) and cured with different aging periods (7, 14 and 28 days) prior to static and dynamic shear tests. A total of nine groups of specimens are used for static compressive tests using the conventional triaxial apparatus. A total of sixty-two groups of specimens are employed for cyclic shear test using the dynamic triaxial apparatus. The results from static shear tests are presented in Figures 3 – 19, and from dynamic shear tests in Figures 20 – 40. For static tests, the results plotted in Figures 6-8, 12 and 14a-14c support the linear relation 1/G versus ε_1 defined in Eq.15. This further validates and justifies the hyperbolic nonlinear model in Eq.16 in response to static shear loading. Similarly, results from dynamic tests also confirm the linear relation between the axial cyclic stress and strain in Eq.8b.

3. Calibration of constitutive parameters.

Based on the experimental data from triaxial shear tests subjected to both static and dynamic loading, constitutive parameters are calibrated using the linear regression for

multiple variables. To do so, first, the expressions of the product of multiple power functions in Eqs.12a, 12b and 7 for A, B and G need to be converted into the linear expressions Eqs.18a, 18b and 29 in logarithmic forms. Then, conduct analysis of linear regression along with the shear test data to determine constitutive parameters. For the static model, ten parameters a_i and b_i (i = 0…4) are found and expressed in Eqs.20a and 20b and given in Tables 9a, 9b and 9c. For the dynamic model, the six coefficients c_i (i = 0 …5) are determined, applied to Eq. 30, and listed in Tables.11 -15. The calibrated constitutive parameters establish the linear model in Eq.30 and the nonlinear elastic model in 21b. Both the linear and nonlinear elastic models can be applied to predict strain or deformation of composite materials under static and dynamic forces. External forces may induce static or dynamic shear stress. For instance, static loads may generate the static shear stress, and traffic loads or earthquakes may produce the cyclic shear stress within roadbeds, soil slopes, and foundations.

4. Failure criterion for composite material and strength indices.

The Coulomb-Mohr's failure criterion is adopted for composite material under the static triaxial shear force. Linear relations of strength parameters c and ϕ versus m_F, m_L and t are established in the present investigation. As strength indices c and ϕ are not constant for composite material, based on the test data, a linear relation between strength indices and variables m_F, m_L and t is suggested. The test data shown in Figures 15 - 17 implies that cohesion c and internal friction angle ϕ are both the function of fiber and lime contents and the sample-curing period. From the results shown in Figures 18 and 19, and Tables 12a and 12b, the cohesion c and internal friction angle ϕ linearly change with m_F, m_L and t. Eight coefficients k_i, and n_i (i = 0…3) in the linear equations in Eqs.28a and 28b are determined and given in Table 12c. As the strength parameters c and ϕ of composite material are fundamental parameters, the relation Eqs.28e and 28d plays a practical role in applications to highway engineering, especially when corrections of the strength parameters c and ϕ need to be made for the composite materials applied to road subgrade, slope stabilization, and foundation reinforcement. The research of dynamic strength is not included in this investigation. Study of failure due to material fatigue under repeated loading is related to rehological behavior of the composite material and is beyond the scope of this report.

5. Impact of variables on the stress-strain relation and impact factors.

Impacts of five variables (σ_0, m_F, m_L t, and N) on the shear stress-strain relation are presented and discussed with the experimental results. For static shear tests, the axial deviatoric stress increases with increase of cell pressure, fiber and lime contents, and sample curing periods for the given axial strain. For dynamic shear tests, the cyclic shear stress also increases with increase of cell pressure, fiber and lime contents and sample curing periods, but decreases with increase of cyclic loading repetitions. To analyze effects of the five variables on mechanical behavior quantitatively, the impact factors I_A, I_B and I_G are defined. The impact factors I_A and I_B in Eqs.23-26 are used to count effect of each variable on the parameters A and B that are respectively related to the initial modulus and soil strength from static shear tests. Both parameters A and B affect the shear modulus G. Correspondingly, the impact factors I_{Gi} through Eqs.32a-32e are

employed to show effects of variables σ_0, m_F, m_L t, and N on shear modulus and cyclic shear stress from periodic shear tests. Except for using the defined formulas of the impact factors, quantitative analysis of static and dynamic behavior in response to variables σ_0, m_F, m_L, t, and N can also be conducted by interpolating or extrapolating the experimental data in Figures 3-14 from static tests and in Figures 20-36 form dynamic tests.

6. Study of tangential and resilient moduli.

Expression of tangential modulus G_t in static investigations is derived from the nonlinear hyperbolic stress-strain relationship in Eq.17. The physical meaning of the tangential modulus G_t is illustrated in Figure 2. The tangential modules G_t is an essential input parameter in analytic and numerical simulation, modeling, and computation for shear stress analysis, therefore, the tangential modulus G_t in Eq.31 is useful in design of roadbeds, slops and foundations associated with application of fiber–reinforced and lime-stabilized soils. Furthermore, the shear or the resilient modulus Mr in Eq.31 is based on cyclic shear tests, and is also a fundamental parameter in roadbed design as well as other applications in highway engineering, especially when the cyclic shear stress induced by traffics, sea wave, or earthquakes is considered. Both Eqs.17 and 31 are new expressions because both G_t and Mr are not constant any more but functions of multiple factors such as σ_0, m_F, m_L, t, and N. One can conduct the quantitative analysis of elastic moduli either using Eqs. 17 and 31 under static and dynamic loading or applying the graphical approach directly to the testing curves or results presented in the diagrams.

In brief, the findings and results from the present investigations can be used for analytical simulation, numerical modeling and computation in research of composite materials, applied to studies and predictions in stress and strain fields for material behavior in response to static or dynamic forces induced by traffic loads or other loads such as earthquakes, and more importantly employed to engineering design of roadbeds, soil lopes, footings and foundations etc where composite soils are applied.

NOMENCLATURE

a_i	constitutive parameters (i = 0…4), kg/m-sec^2
b_i	constitutive parameters (i = 0…4), kg/m-sec^2
c	cohesion, kg/m-sec^2
c_i	constitutive parameters (i = 0….5), kg/m-sec^2
d_i	parameters (i = 0….k) in a linear expression
A	a function defined for nonlinear model, kg/m-sec^2
B	a function defined for the nonlinear model, kg/m-sec^2
E_{ijkl}	a fourth order tensor of elasticity, kg/m – sec^2
G	the shear modulus, kg/m - sec^2
G_i	the initial shear modulus, kg/m - sec^2
G_t	the tangential modulus, kg/m - sec^2
I_{ij}	the impact factors (i= A or B and j = σ_0, m_L, m_F and t)
I_1	the first invariant of stress, kg/m - sec^2
I_2^D	the second invariant of stress tensor, kg/m - sec^2
J_2^D	the second deviatoric invariant of train tensor
k_i	constants (i = 0…3)
m_L	the lime content, %
m_F	the fiber content, %
Mr	the resilient modulus, kg/m - sec^2
n_i	constants (i = 0…3)
N	the number of repetition
p_0	unit atmosphere pressure (= 1.0 kPa), kg/m - sec^2
t	the sample-curing time, day
t_1	one day sample curing time, day
W_i	the weight of fiber, lime or soil (i = F for fiber, L for lime or S for soil)
δ_{ij}	the Kronecker delta
ε_f	the axial strain at failure
ε_i	the principal strain (i = 1… 3)
ε_1	the deviatoric axial strain
ε_{ij}^D	the deviatoric infinitesimal strain tensor
ϕ	the internal friction angle, degree
γ_W	the unit weight of water, kg/m^2 - sec^2
κ	the nonlinear bulk elasticity, kg/m-sec^2
$(\sigma_1 - \sigma_3)_f$	the axial deviatoric stress at failure, kg/m-sec^2
σ_{ij}^D	the deviatoric stress, kg/m-sec^2
σ_i	the principal stress (i = 1…3), kg/m - sec2
d/dt	the total derivative with respect to time t, 1/sec
∇	the derivative operator for gradient, divergence, and curl, 1/m
$\partial/\partial t$	the partial derivative with respect to time, 1/sec
^{o}	the degree of an internal friction angle.

Superscripts

D	deviatoric

Subscripts

A	related to the function A
B	related to the function B
F	fiber
G	the shear modulus
i	the initial state at the axial strain = 0
L	lime
N	the repetition of cyclic loading
t	the sample-curing time

REFERENCES

1. Transportation Research Board, New Trucks for Greater Productivity and Less Road Ware, Special Report 227, 1990.
2. Anthoine, A., Mixed Modeling of Reinforced Soils within the Framework of the Yield Design Theory, *Journal of Composite and Geotechnics,* 7(1&2), 67 – 82, 1989
3. Cubrinovski, M. et al., State Concept and Modified Elastoplasticity for Sand Modeling, *Journal of Soils and Foundations*, Vol. 38, No. 4, 213-225, Japanese Geotechnical Society, 1998
4. Fan J. and Yang Q., Composite Materials Modulus Calculated by Random Fiber Distribution Method, *Journal of Composite Materials,* Vol. 15, 1998
5. Fowler, J., Theoretical Design Consideration for Fabric Reinforced Embankments, Proc. 2d Intl. Geotextiles, St. Paul, MN:IFAI, 665 – 676, 1982
6. Jarrett, P.W., and McGown, A., Application of Polymeric Reinforcement in Soil Retaining Structures, Proceeding, Royal Military College, Kingston, Ontario, 35 – 56, 1988
7. Kataoka, Y. and Taya, M., Analysis of Mechanical Behavior of a Short Fiber Composite Using Micromechanics Based Model, *JSME International Journal*, Series A, Vol. 43, No. 1, 46 – 52, 2000.
8. Kang, G. Z. and Gao, Q., Stress Distribution and Deformation Characteristics of Matrix in Short Fiber Reinforced Metal Matrix Composites, *Journal of Composite Material*, Vol.17, No. 2, 20 – 24, 2000
9. Michalowski, R. L., and Zhao, A., Failure Criteria for Homogenized Reinforced Soils and Application in Limit Analysis of Slopes, Proc., Geosynthetics 93, Vol. 1., Industrial Fabrics Association Int., St. Paul. Minn., 443 – 453, 1993
10. Radoslaw, L., Michalowski, R. L., and Zhao, A., Continuum versus Structural Approach to Stability of Reinforced soil, *Journal of Geotechnical Engineering*, Vol. 121, No. 2, 152 – 162, 1995
11. Radoslaw, L., Michalowski, R. L., and Zhao, A., Failure of Fiber – Reinforced Granular Soils, *Journal of Geotechnical Engineering*, 226 – 233, 1996
12. Santoni, R. L. et al., Engineering Properties of Sand – Fiber Mixtures for Road Construction, *Journal of Geotechnical and Geoenvironmental Engineering*, Vol. 127, No. 3, 2001
13. Malvern, L. E., *Introduction to the Mechanics of a Continuous Medium*, Prentice-Hall, Englewood Cliffs, NJ, 1969.
14. J. Li, and D. Ding. Nonlinear Elastic Behavior of Fiber-Reinforced Soil under Cyclic Loading, *Journal of Soil Dynamics and Earthquake Engineering*, Vol. 22, No. 9-12, pp 977 – 983, 2002.
15. J. Li, and L. J. Zhang. Nonlinear Elastic Behavior for Soil Reinforced with Fiber and Lime, in the Proceedings of the 12th Pan-American Conference on Soil Mechanics and Geotechnical Engineering (eds., P.J. Culligan, H. H. Einstein, and A. J. Whittle), Vol.1, pp. 610-618, Germany: VGE, 2003.
16. J. M. Duncan and C. Y. Chang. Nonlinear Analysis of Stress and Strain in Soils. *Journal of Soil Mechanics and Foundations Division*, ASCE, 96(SM5): pp1625-1654, 1970.

17. R. L. Konder. Hyperbolic Stress-Strain Response: Cohesive Soil, *Journal of Soil Mechanics and Foundation Division,* ASCE, 89(SM1), 1963.
18. J. Li. Nonlinear Viscosity of Subgrade Soils under Cyclic Loading, in the Proceedings of the Geo-Denver 2000, ASCE, pp119-128, 2000.
19. J. Li. Experimental Investigations of Nonlinear Viscous Soils, in Proceedings of the Fourth International Conference on Constitutive Laws for Engineering Materials: Experiment, Theory, Computation and Applications, pp359-362, 1999.

THE LIST OF FIGURES

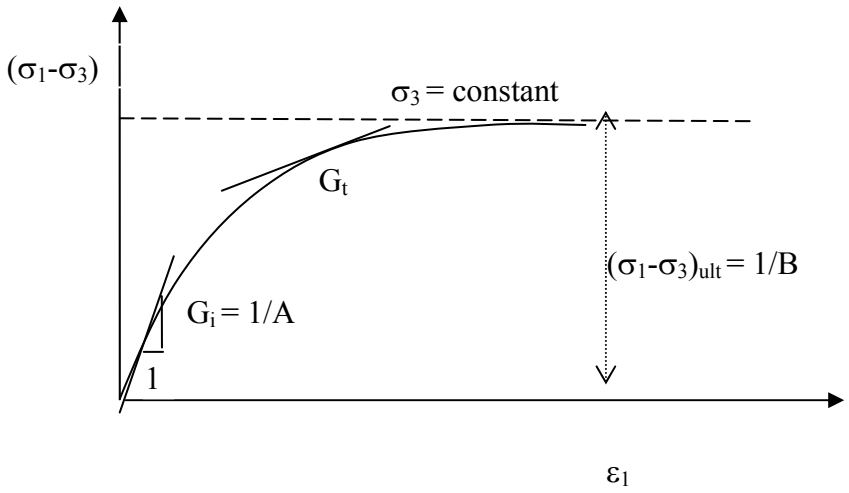

Fig. 1. Hyperbolic stress-strain relationship

Figure 2 The linear relation used to determine A and B

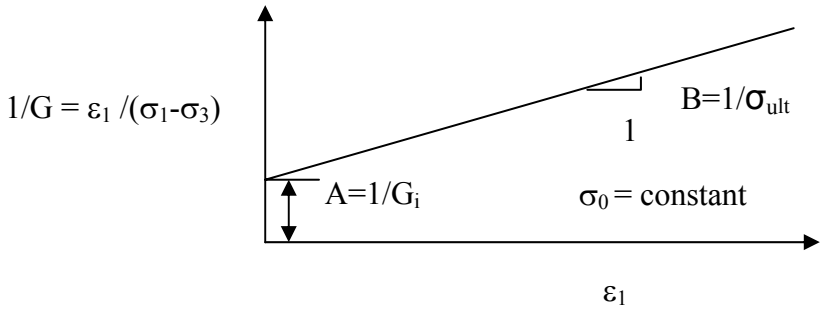

Fig. 2 A linear relation used to determine A and B

Figure 3 ($\sigma_1 - \sigma_3$) vs. ε_1 with m_L = 0%, and different m_F and σ_0

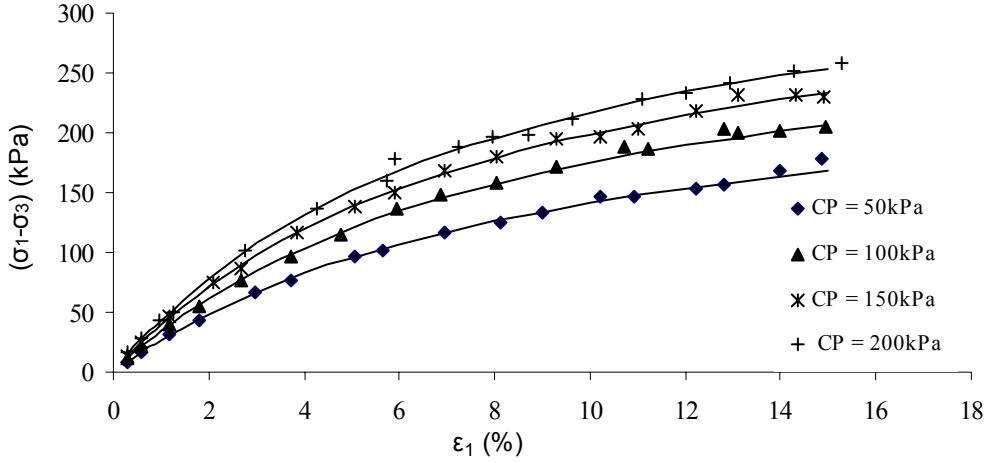

Fig.3a (σ_1 - σ_3) vs. ε_1 for m_F=0% and m_L=0%

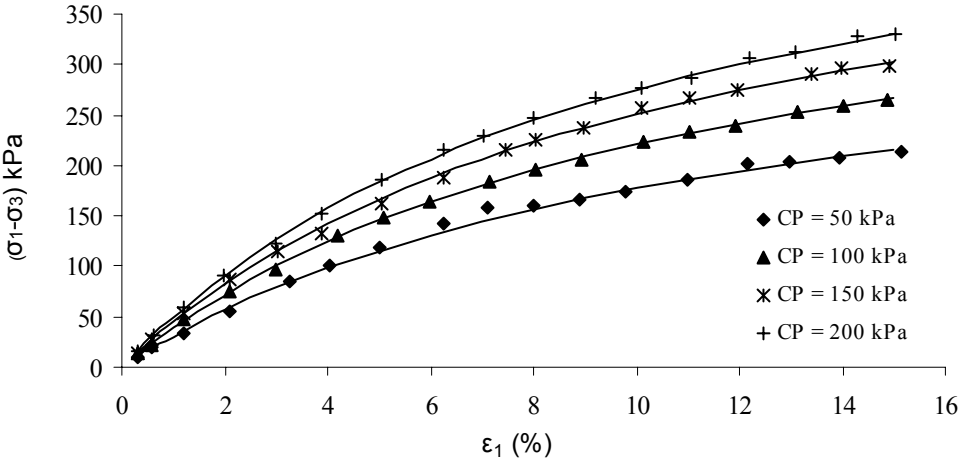

Fig.3b (σ_1 - σ_3) vs. ε_1 for m_F=0.2% and m_L=0%

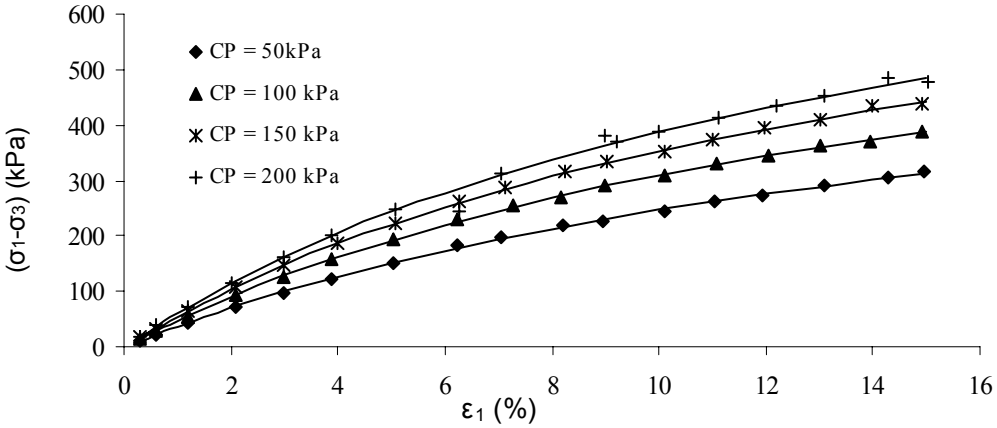

Fig.3c (σ_1 - σ_3) vs. ε_1 for m_F=0.5% and m_L=0%

Figure 4 ($\sigma_1 - \sigma_3$) vs. ε_1 with m_F = 0.2%, m_L = 5% and different σ_0 and t

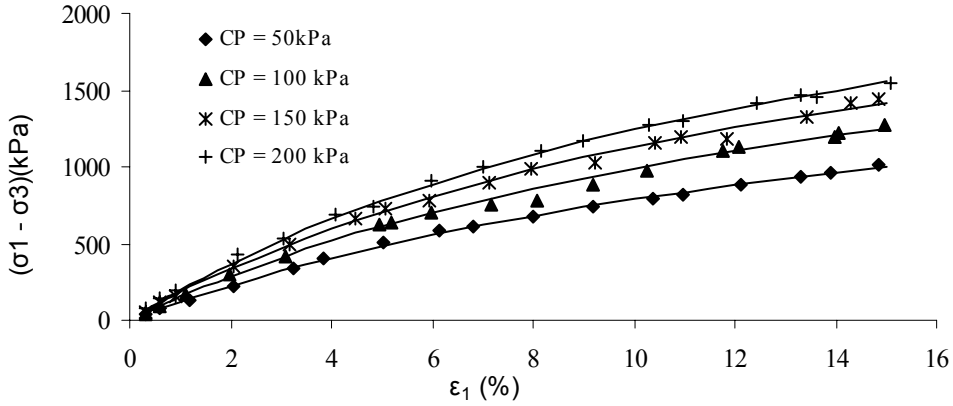

Fig.4.a ($\sigma_1 - \sigma_3$) vs. ε_1 for m_F=0.2%, m_L=5% and t=7days

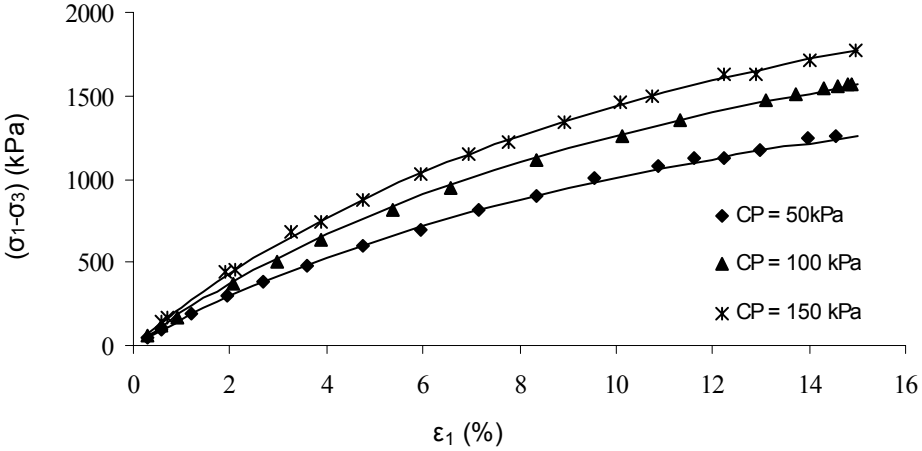

Fig.4.b ($\sigma_1 - \sigma_3$) vs. ε_1 for m_F=0.2%, m_L=5% and t=14days

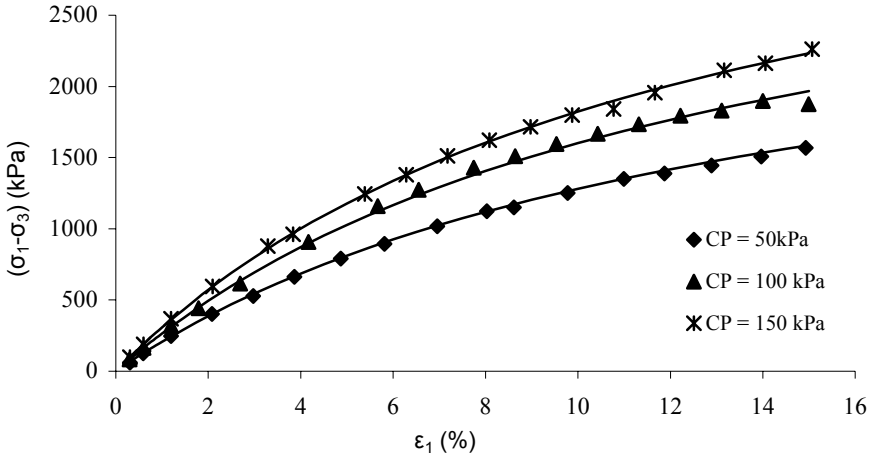

Fig.4.c ($\sigma_1 - \sigma_3$) vs. ε_1 for m_F=0.2%, m_L=5% and t=28days

Figure 5 ($\sigma_1 - \sigma_3$) vs. ε_1 with m_F = 0.5%, m_L = 5% and different σ_0 and t

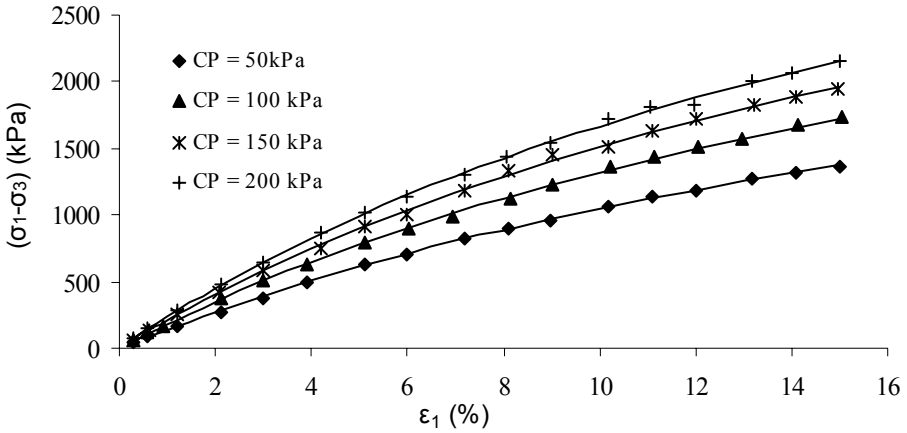

Fig.5.a (σ_1 - σ_3) vs. ε_1 for m_f=0.5%, m_l=5% and t=7days

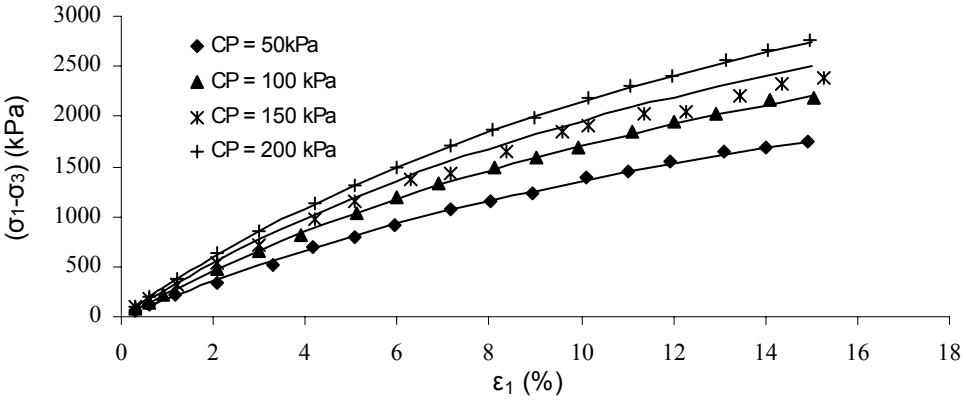

Fig.5.b (σ_1 - σ_3) vs. ε_1 for m_F=0.5%, m_L=5% and t=14days

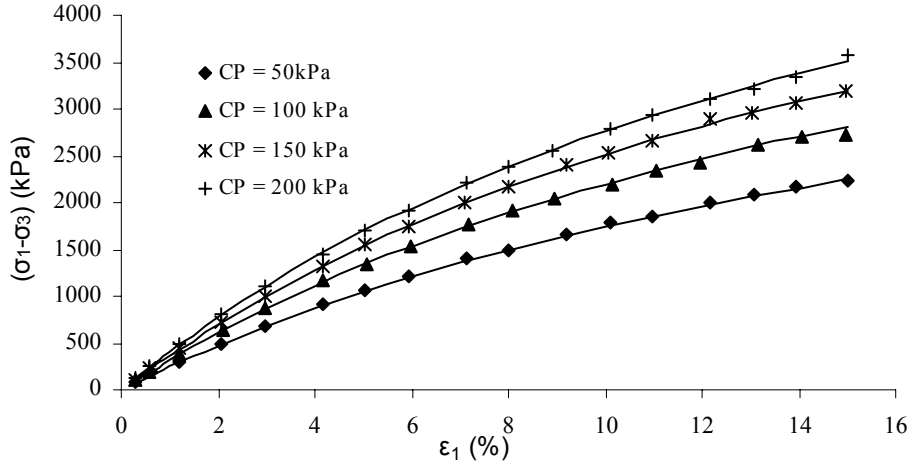

Fig5.c (σ_1 - σ_3) vs. ε_1 for m_F=0.5%, m_L=5% and t=28days

Figure 6 $\varepsilon_1/(\sigma_1 - \sigma_3)$ **vs.** ε_1 **with** m_L **= 0% and different** m_F **and** σ_0

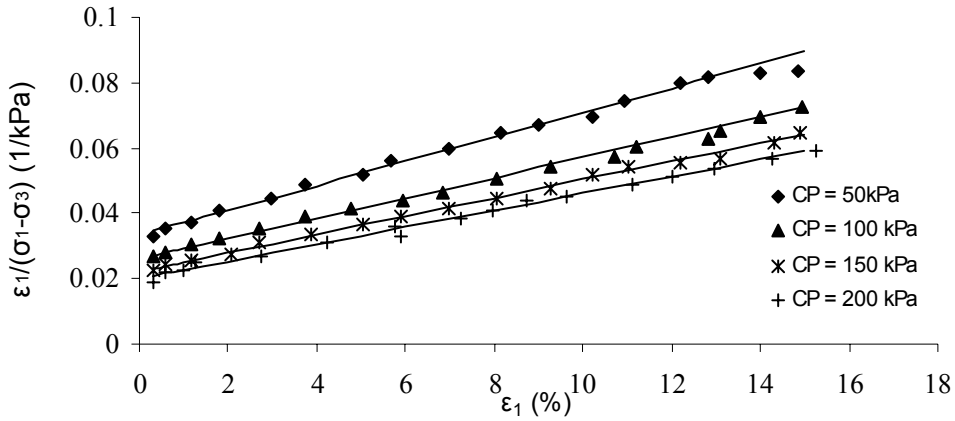

Fig.6.a $\varepsilon_1/(\sigma_1-\sigma_3)$ vs. ε_1 for m_F=0% and m_L=0%)

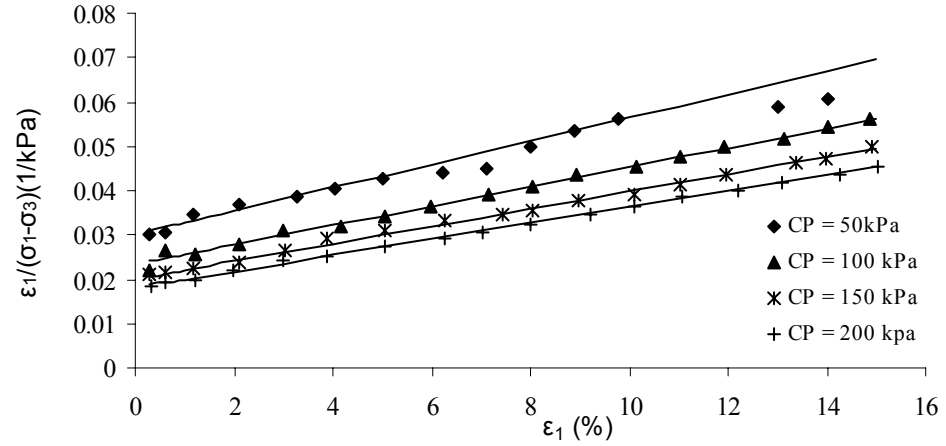

Fig.6.b $\varepsilon_1/(\sigma_1-\sigma_3)$ vs. ε_1 for m_F=0.2% and m_L=0%

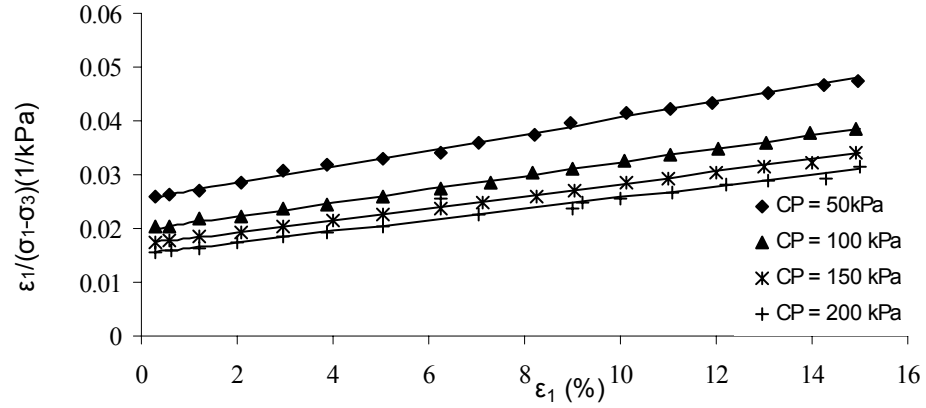

Fig.6.c $\varepsilon_1/(\sigma_1-\sigma_3)$ vs. ε_1 for m_F=0.5% and m_L=0%)

Figure 7 $\varepsilon_1/(\sigma_1 - \sigma_3)$ **vs.** ε_1 **with** m_F **= 0.2%,** m_L **= 5% and different** σ_0 **and t**

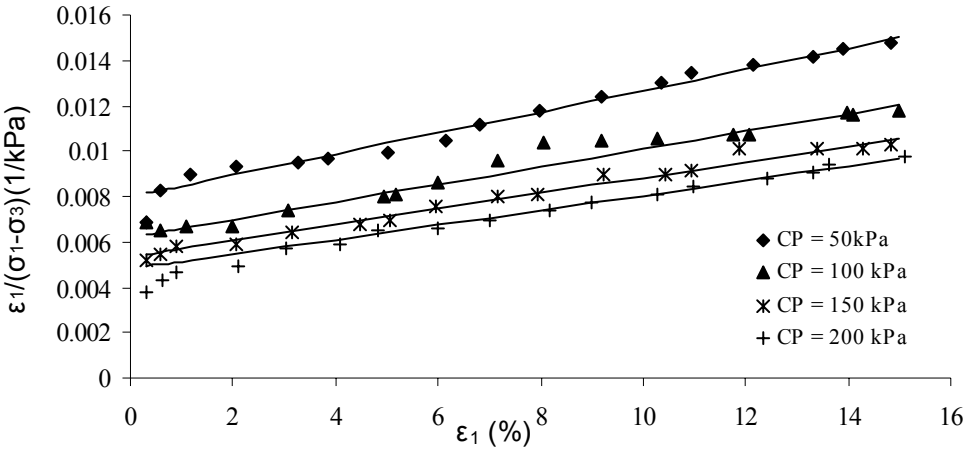

Fig.7.a $\varepsilon_1/(\sigma_1-\sigma_3)$ vs. ε_1 for m_F=0.2%, m_L=5% and t=7days

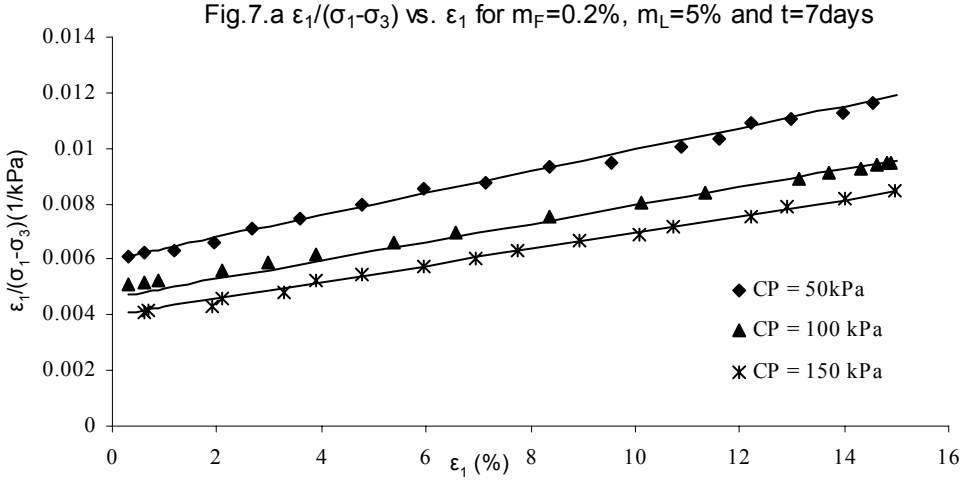

Fig.7.b $\varepsilon_1/(\sigma_1-\sigma_3)$ vs. ε_1 for m_F=0.2%, m_L=5% and t=14days

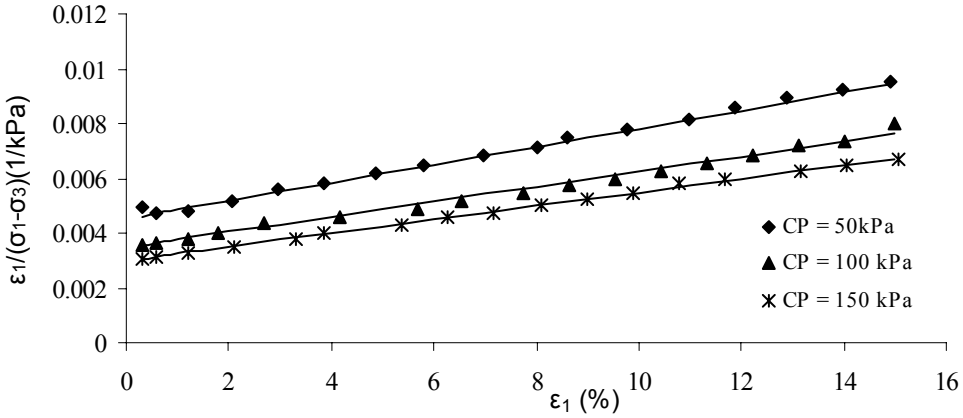

Fig.7.c $\varepsilon_1/(\sigma_1-\sigma_3)$ vs. ε_1 for m_F=0.2%, m_L=5% and t=28days

Figure 8 $\varepsilon_1/(\sigma_1 - \sigma_3)$ **vs.** ε_1 **with** m_F **= 0.5%,** m_L **= 5% and different** σ_0 **and t**

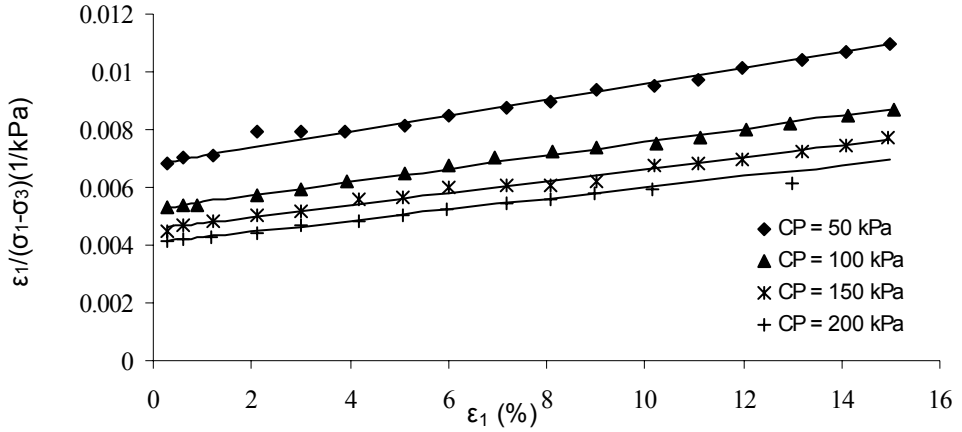

Fig.8.a $\varepsilon_1/(\sigma_1-\sigma_3)$ vs. ε_1 for m_F=0.5%, m_L=5% and t=7days

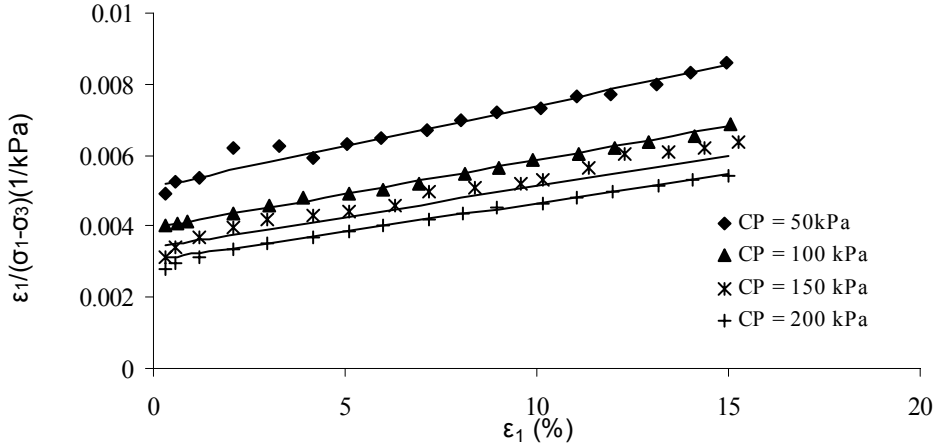

Fig.8.b $\varepsilon_1/(\sigma_1-\sigma_3)$ vs. ε_1 for m_F=0.5%, m_L=5% and t=14days

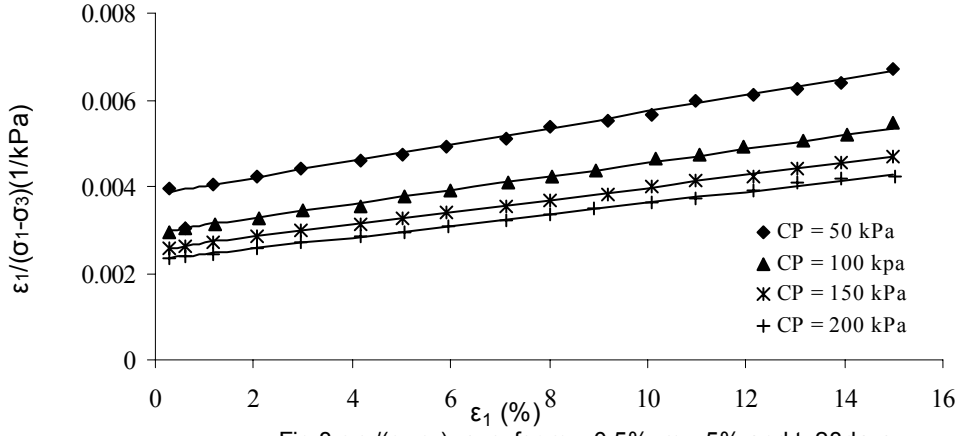

Fig.8.c $\varepsilon_1/(\sigma_1-\sigma_3)$ vs. ε_1 for m_F=0.5%, m_L=5% and t=28days

Figure 9 ($\sigma_1 - \sigma_3$) vs. ε_1 with m_L = 0%, and different m_F and σ_0

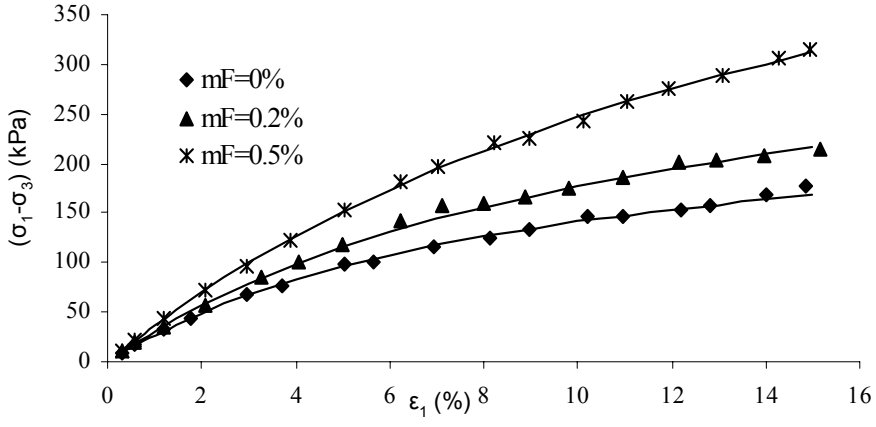

Fig.9.a (σ_1-σ_3) vs. ε_1 for m_L=0% and σ_0=50kPa

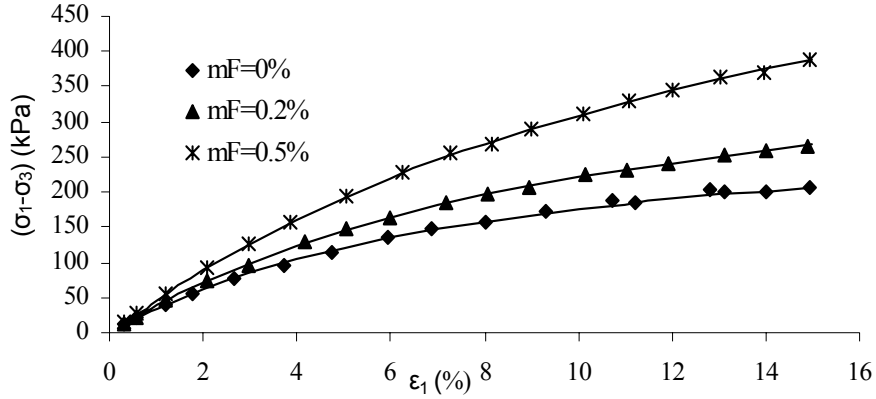

Fig.9.b (σ_1-σ_3) vs. ε_1 for m_L=0% and σ_0=100kPa

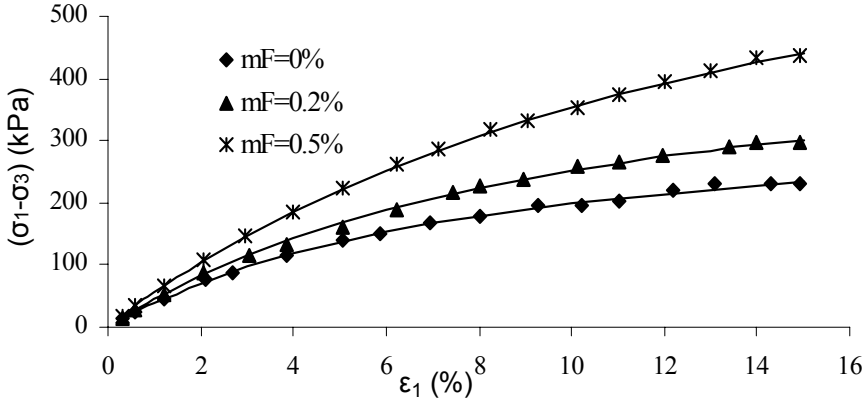

Fig.9.c (σ_1-σ_3) vs. ε_1 for m_L=0% and σ_0=150kPa

Figure 10 ($\sigma_1 - \sigma_3$) vs. ε_1 with m_F = 0.2%, m_L = 5%, and different σ_0 and t

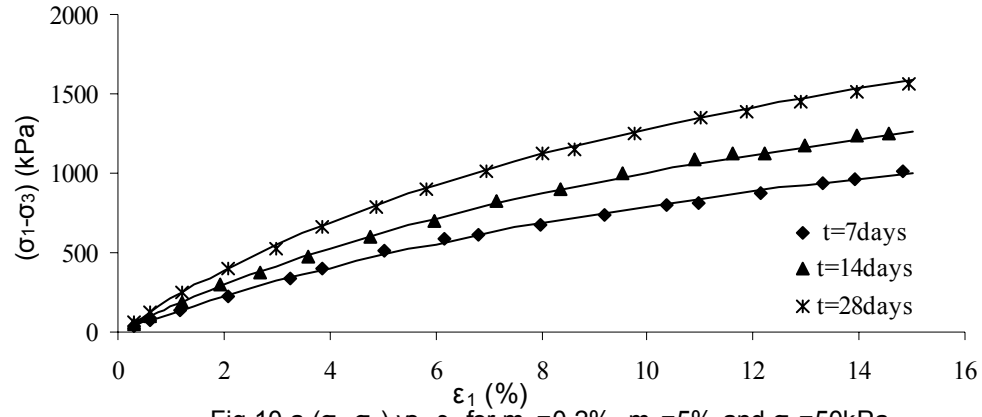

Fig.10.a (σ_1-σ_3) vs. ε_1 for m_F=0.2%, m_L=5% and σ_0=50kPa

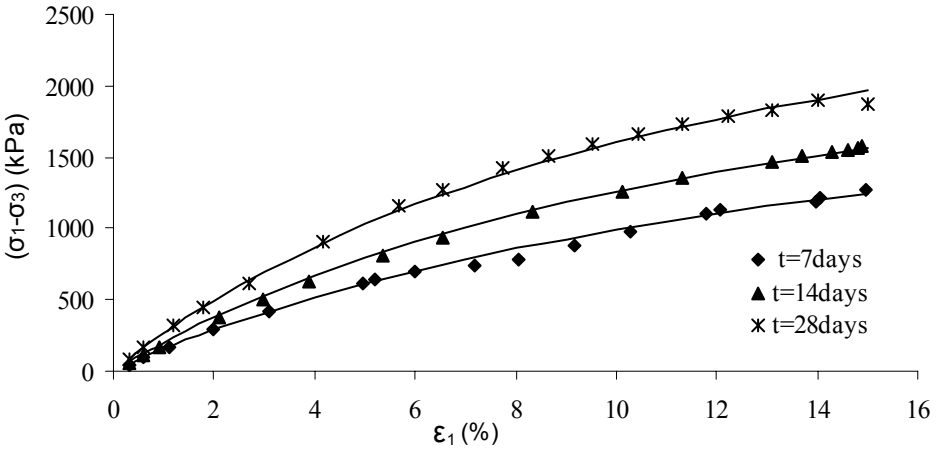

Fig.10.b (σ1-σ3) vs. ε1 for m_F=0.2%, m_L=5% and σ_0=100kPa

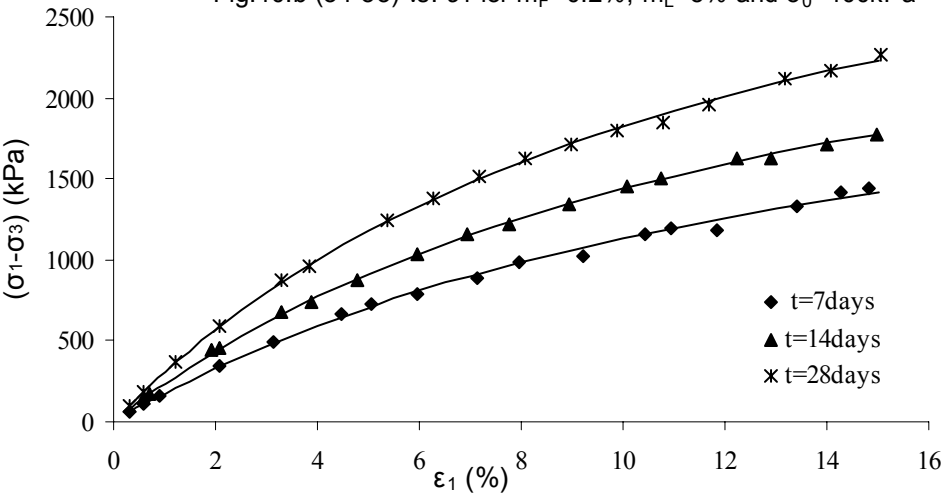

Fig.10.c (σ_1-σ_3) vs. ε_1 for m_F=0.2%, m_L=5% and σ_0=150kPa

Figure 11 ($\sigma_1 - \sigma_3$) vs. ε_1 with m_F = 0.5%, m_L = 5%, and different σ_0 and t

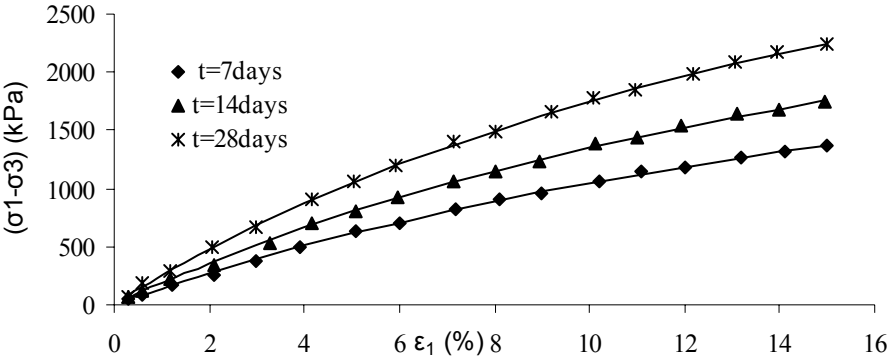

Fig.11.a (σ_1-σ_3) vs. ε_1 for m_F=0.5%, m_L=5% and σ_0=50kPa

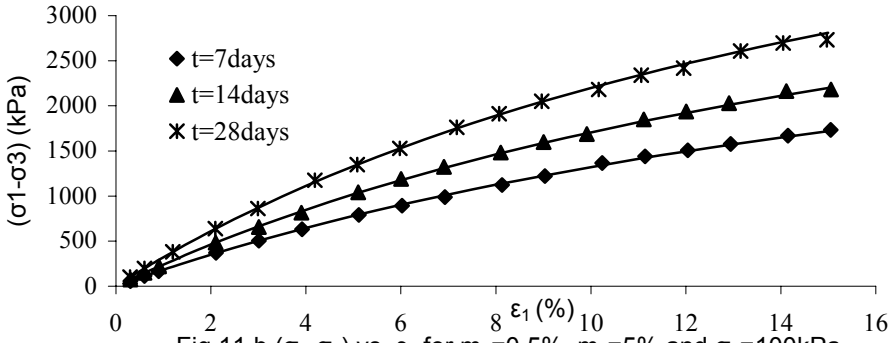

Fig.11.b (σ_1-σ_3) vs. ε_1 for m_F=0.5%, m_L=5% and σ_0=100kPa

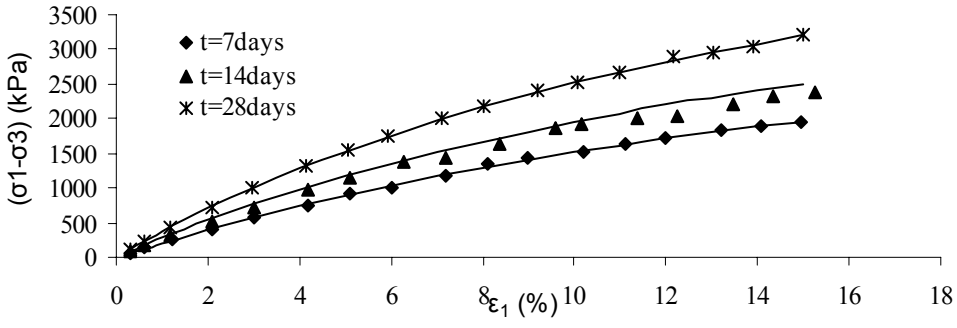

Fig.11.c (σ_1-σ_3) vs. ε_1 for m_F=0.5%, m_L=5% and σ_0=150kPa

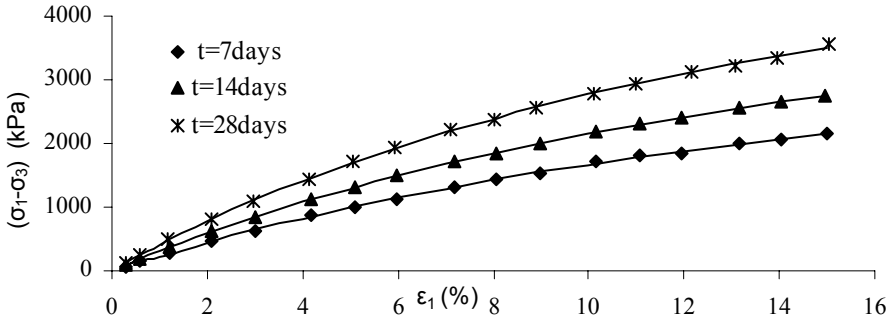

Fig.11.d (σ_1-σ_3) vs. ε_1 for m_F=0.5%, m_L=5% and σ_0=200kPa

Figure 12 $\varepsilon_1/(\sigma_1-\sigma_3)$ vs. ε_1 with $m_L = 0\%$, and different m_F and σ_0

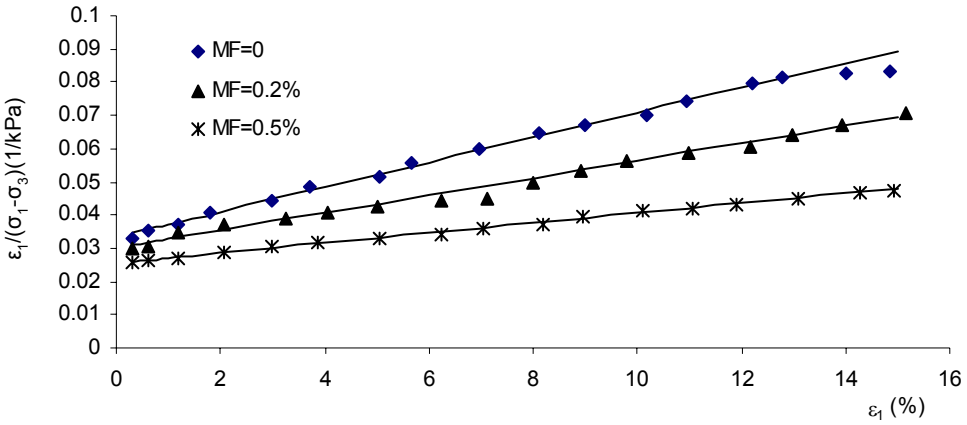

Fig12.a. $\varepsilon_1/(\sigma_1-\sigma_3)$ vs. ε_1 with different m_F, m_L=0 and σ_0=50kPa

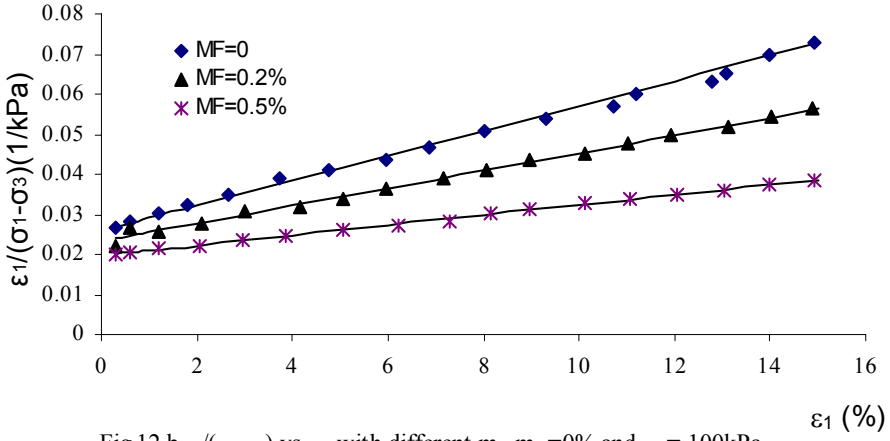

Fig.12.b $\varepsilon_1/(\sigma_1-\sigma_3)$ vs. ε_1 with different m_F, m_L=0% and σ_0 = 100kPa

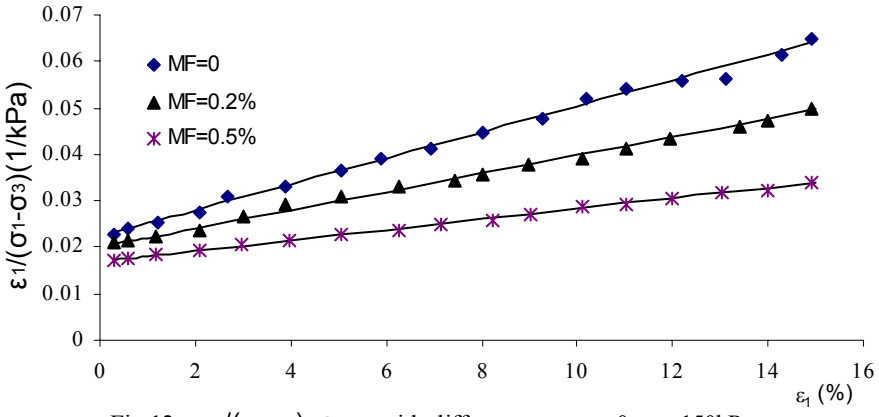

Fig.12.c $\varepsilon_1/(\sigma_1-\sigma_3)$ vs. ε_1 with different m_F, m_L= 0, σ_0=150kPa

Figure13a ($\sigma_1 - \sigma_3$) vs. ε_1 with m_L = 5%, t = 7 days, and different m_F and σ_0

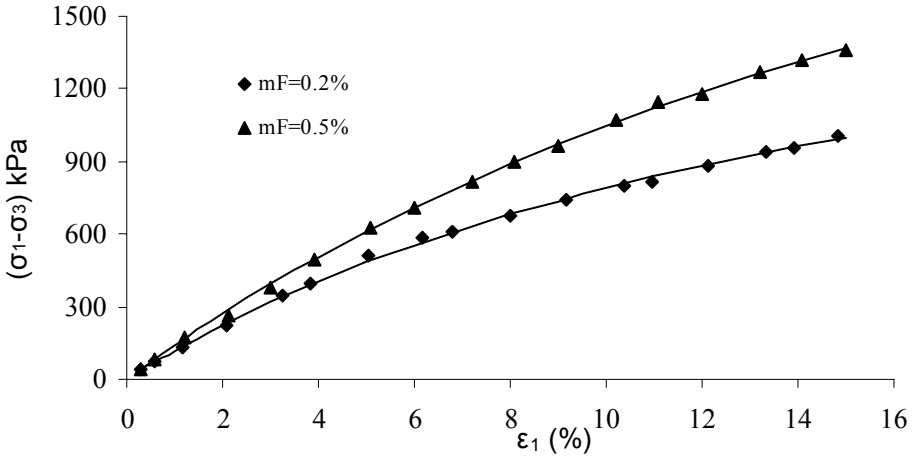

Fig.13.a.1 (σ_1-σ_3) vs. ε_1 for m_L=5%, t=7days and σ_0=50kPa

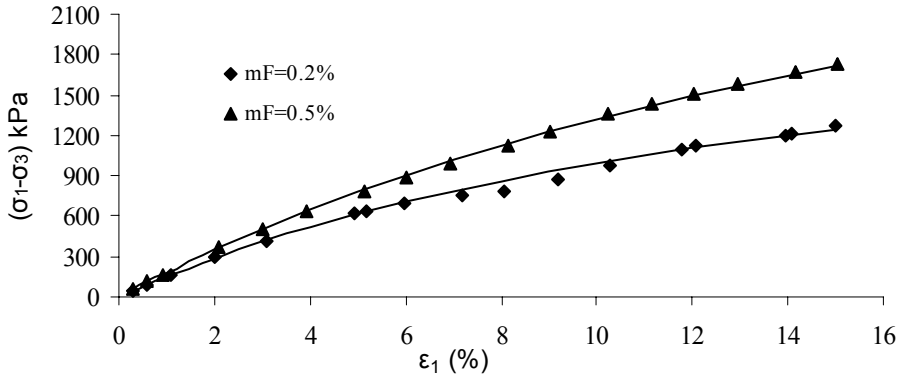

Fig.13.a.2 (σ_1-σ_3) vs. ε_1 for m_L=5%, t=7days and σ_0=100kPa

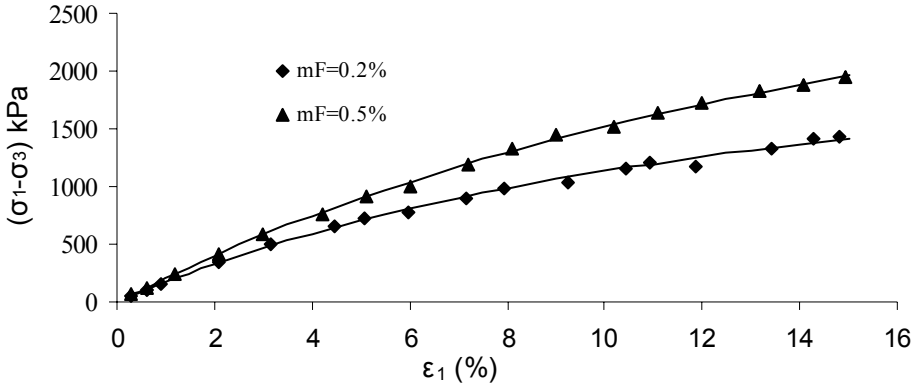

Fig.13.a.3 (σ_1-σ_3) vs. ε_1 for m_L=5%, t=7days, σ_0=150kPa

Figure13b ($\sigma_1 - \sigma_3$) vs. ε_1 with m_L = 5%, t = 14 days, and different m_F and σ_0

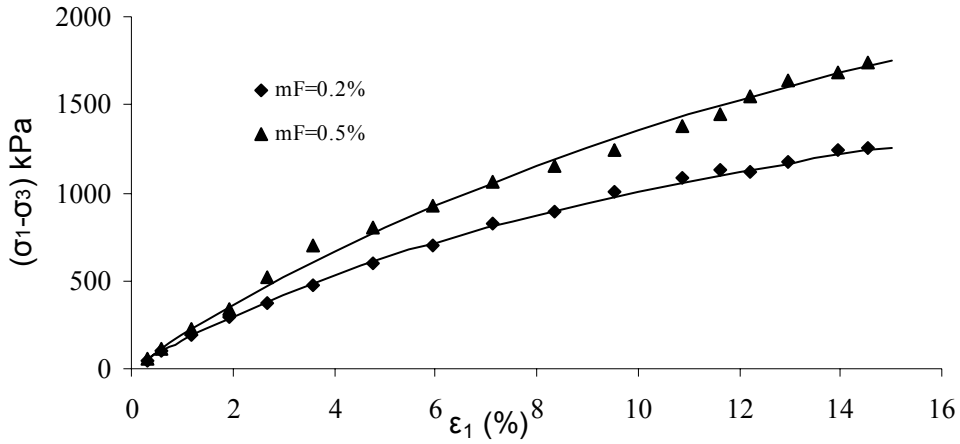

Fig.13.b.1 (σ_1-σ_3) vs. ε_1 for m_L=5%, t=7days and σ_0=50kPa

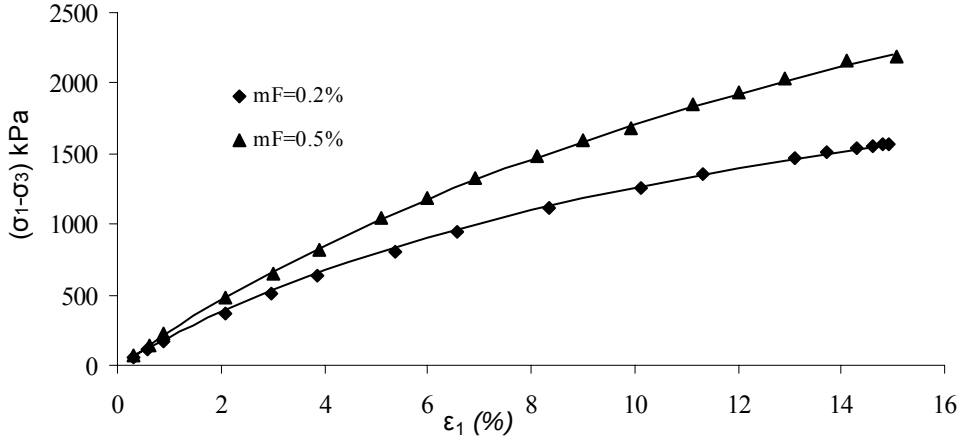

Fig.13.b.2 (σ_1-σ_3) vs. ε_1 for m_L=5%, t=14days and σ_0=100kPa

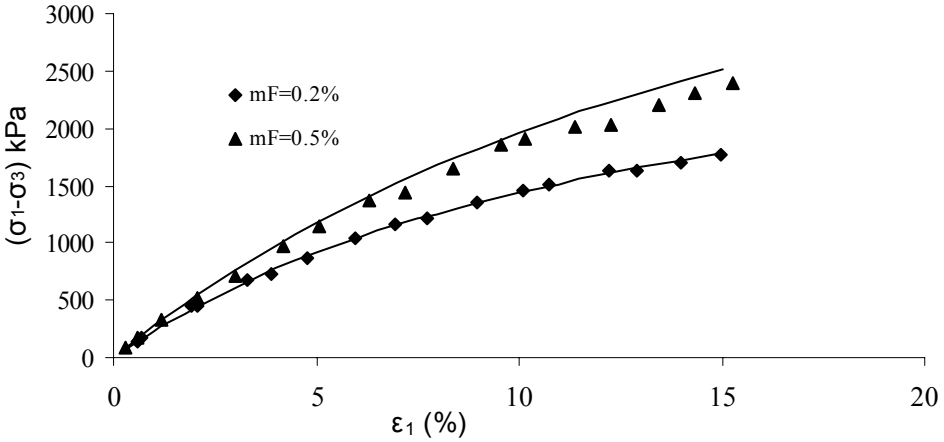

Fig.13.b.3 (σ_1-σ_3) vs. ε_1 for m_L=5%, t=14days and σ_0=150kPa

Figure13c ($\sigma_1 - \sigma_3$) vs. ε_1 with m_L = 5%, t = 28 days, and different m_F and σ_0

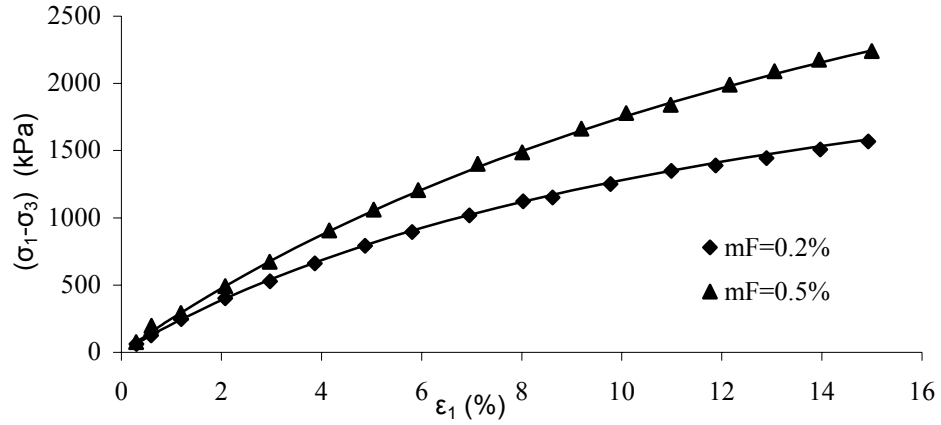

Fig.13.c.1 (σ_1-σ_3) vs. ε_1 for m_L=5%, t=28days and σ_0=50kPa

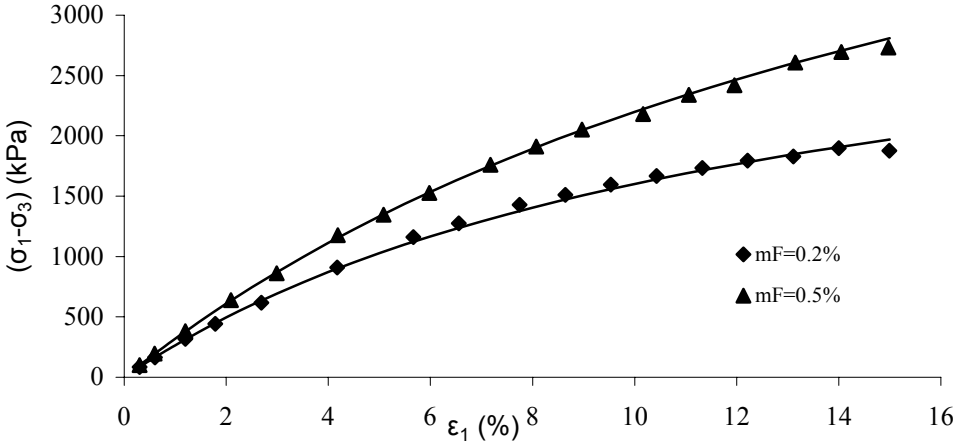

Fig.13.c.2 (σ_1-σ_3) vs. ε_1 for m_L=5%, t=28days and σ_0=100kPa

Figure14a $\varepsilon_1/(\sigma_1-\sigma_3)$ vs. ε_1 with m_L = 5%, t = 7 days, and different m_F and σ_0

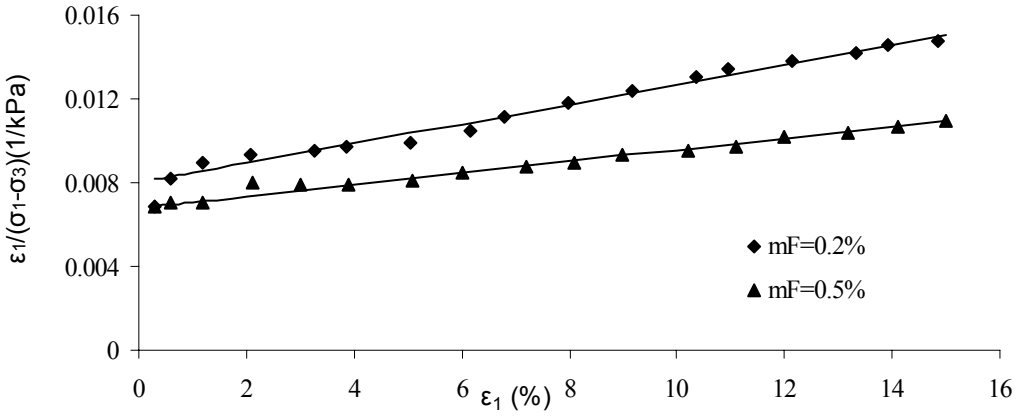

Fig.14a.1 $\varepsilon_1/(\sigma_1-\sigma_3)$ vs. ε_1 for m_L=5%, t=7days and σ_0=50kPa

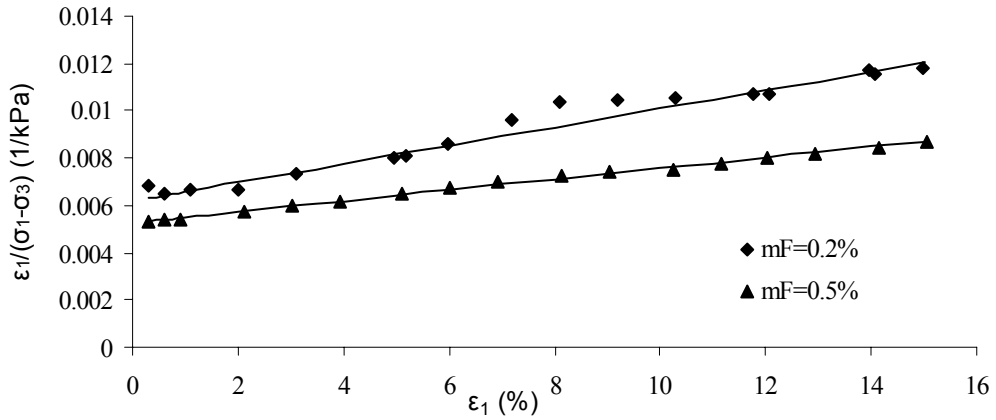

Fig.14.a2 $\varepsilon_1/(\sigma_1-\sigma_3)$ vs. ε_1 for m_L=5%, t=7days and σ_0=100kPa

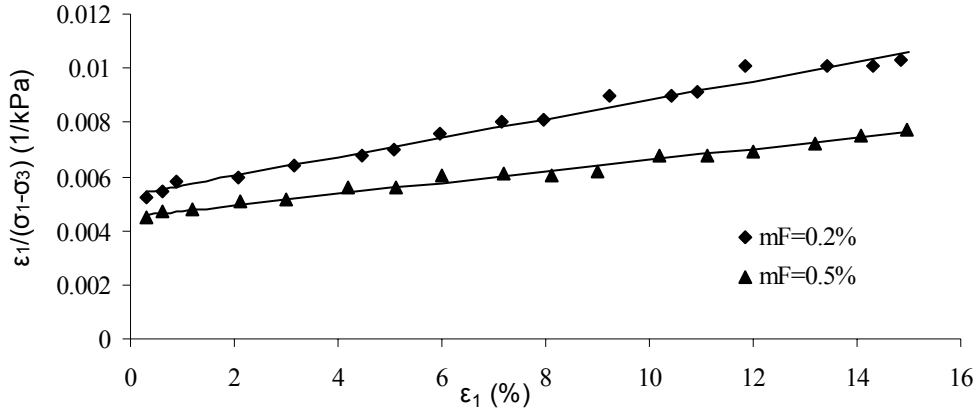

Fig.14.a3 $\varepsilon_1/(\sigma_1-\sigma_3)$ vs. ε_1 for m_L=5%, t=7days and σ_0=150kPa

Figure14b $\varepsilon_1/(\sigma_1-\sigma_3)$ vs. ε_1 with m_L = 5%, t = 14 days, and different m_F and σ_0

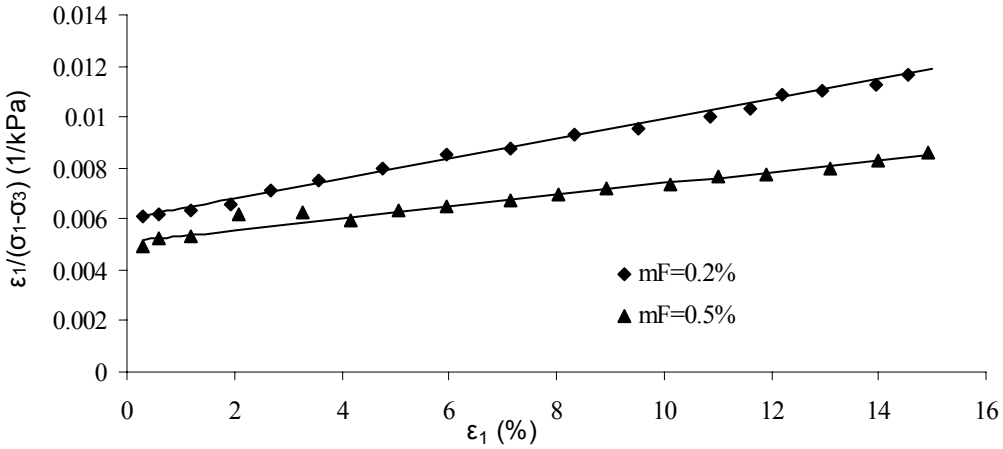

Fig14.b1 $\varepsilon_1/(\sigma_1-\sigma_3)$ vs. ε_1 for m_L=5%, t=14days and σ_0=50kPa

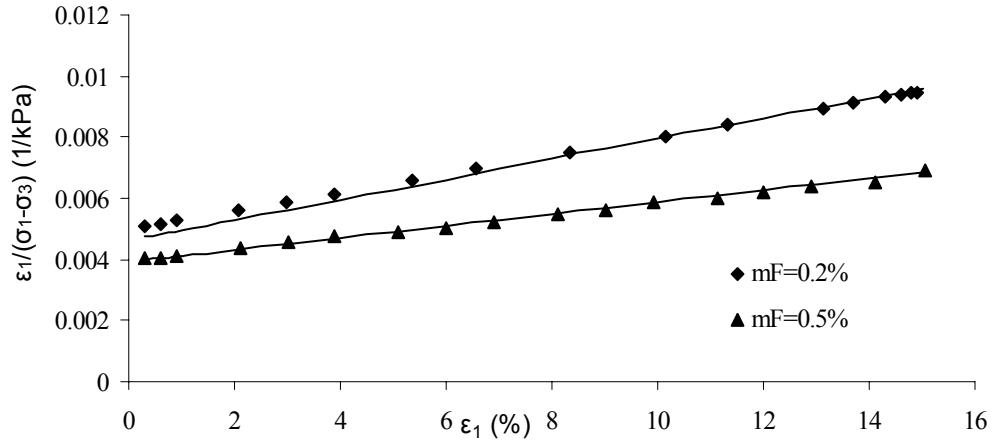

Fig.14.b2 $\varepsilon_1/(\sigma_1-\sigma_3)$ vs. ε_1 for m_L=5%, t=14days and σ_0=100kPa

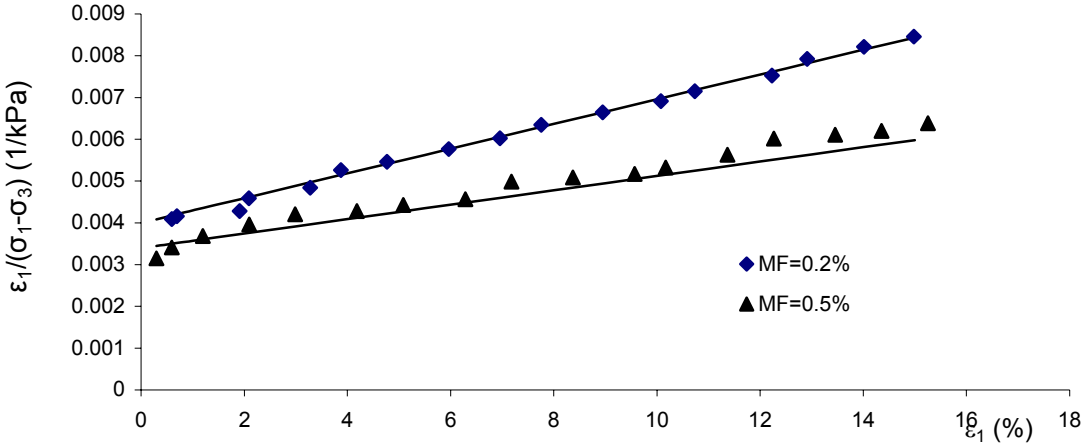

Fig.14.b3 $\varepsilon_1/(\sigma_1-\sigma_3)$ vs. ε_1 with m_L= 5%, t=14d, σ_0=150kPa

Figure14c $\varepsilon_1/(\sigma_1-\sigma_3)$ vs. ε_1 with m_L = 5%, t = 28 days, and different m_F and σ_0

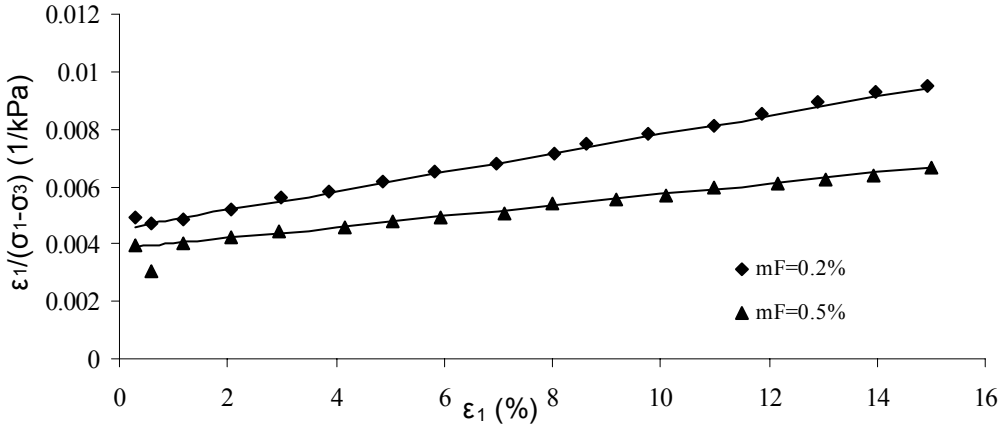

Fig.14.c.1 $\varepsilon_1/(\sigma_1-\sigma_3)$ vs. ε_1 for m_L=5%, t=7days and σ_0=50kPa

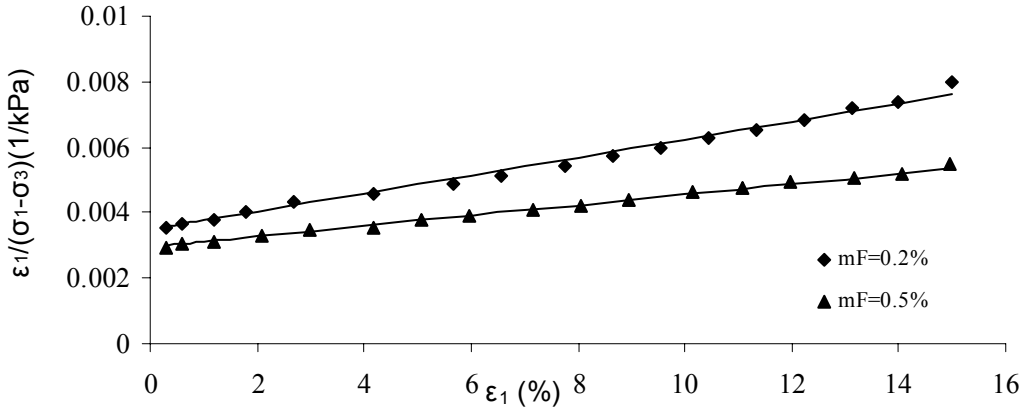

Fig.14.c.2 $\varepsilon_1/(\sigma_1-\sigma_3)$ vs. ε_1 for m_L=5%, t=28days and σ_0=100kPa

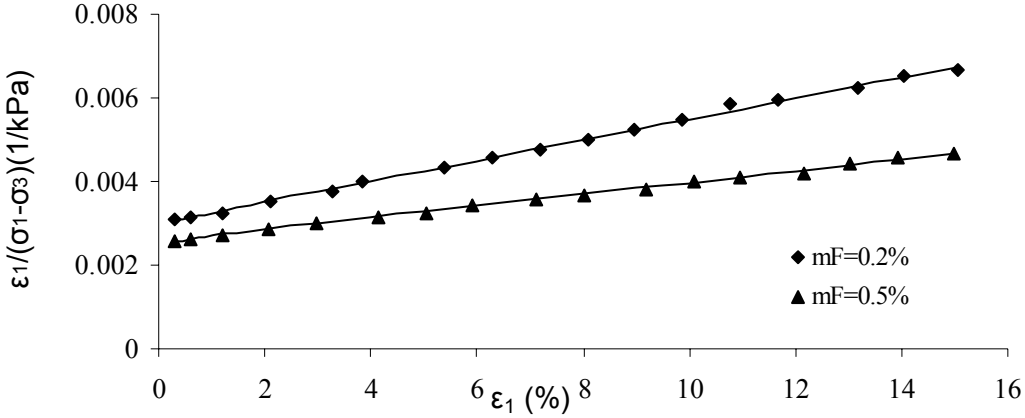

Fig.14.c.3 $\varepsilon_1/(\sigma_1-\sigma_3)$ vs. ε_1 for m_L=5%, t=28days and σ_0=150kPa

Figure 15 Mohr's circles with m_L = 0% and different m_F

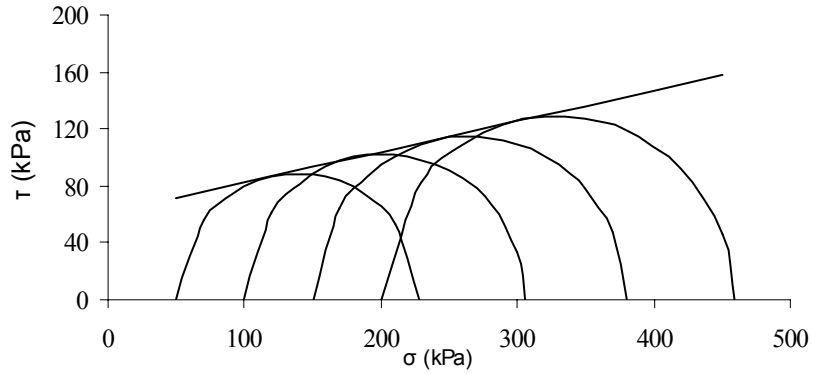

Fig. 15a τ vs. σ for m_F=0% and m_L=0%

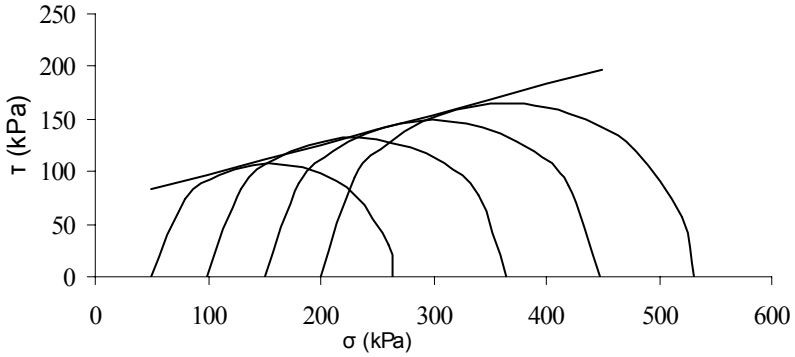

Fig.15b τ vs. σ for m_L=0% and m_F=0.2%

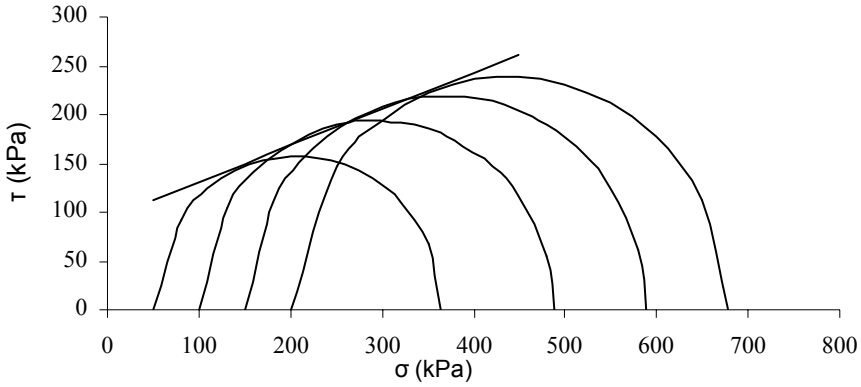

Fig.15c τ vs. σ for m_L=0% and m_F=0.5%

Figure 16 Mohr's circles with m_L = 5% and m_F= 0.2% and different t

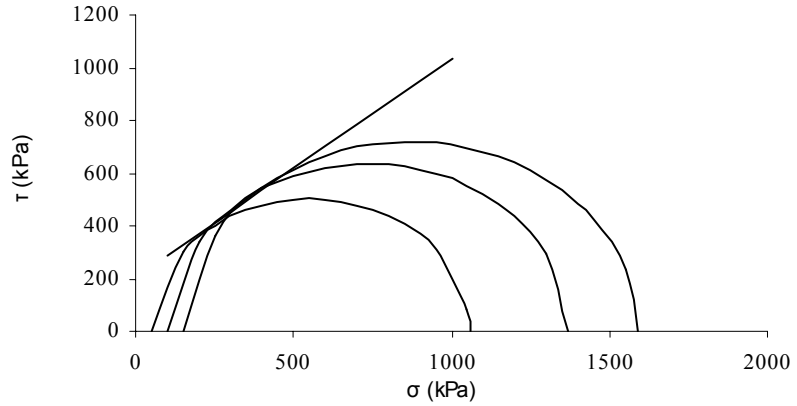

Fig. 16a τ vs. σ for m_L=5%, m_F=0.2%, and t=7days

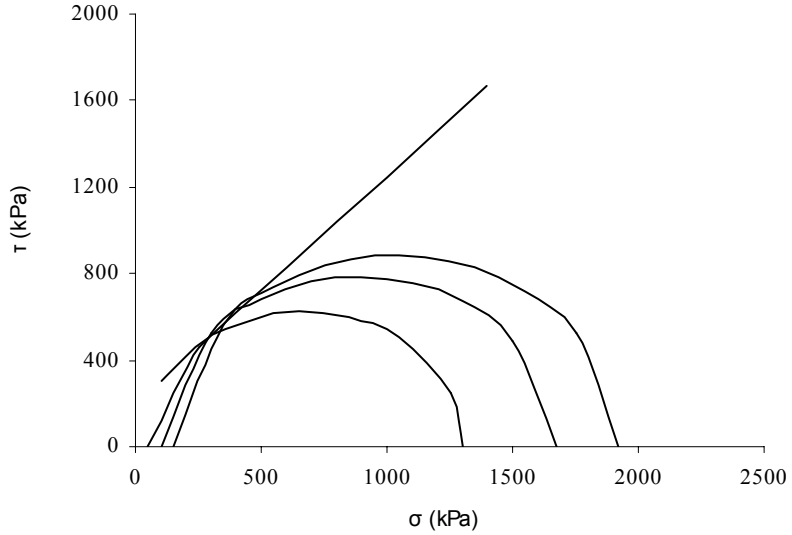

Fig. 16b τ vs. σ for m_L=5%, m_F=0.2% and t=14days

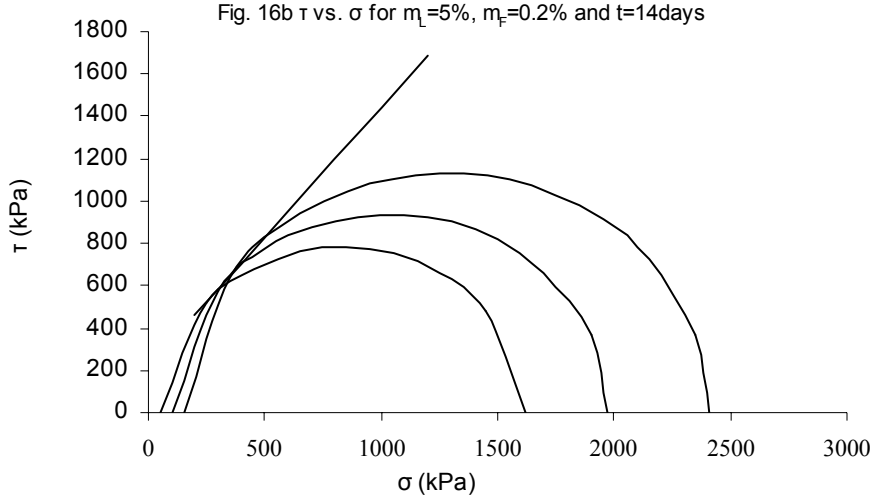

Fig. 16c τ vs. σ for m_L=5%, m_F=0.2% and t=28days

Figure 17 Mohr's circles with m_L = 5%, m_F = 0.5% and different t

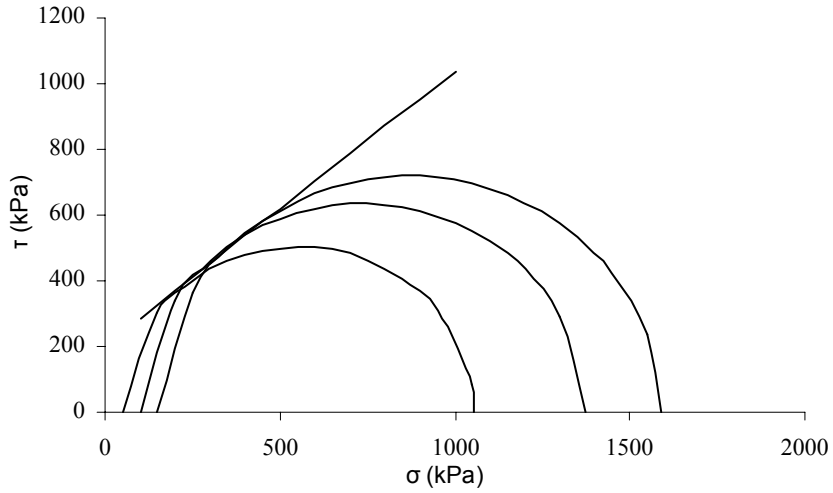

Fig. 16a τ vs. σ for m_L=5%, m_F=0.2%, and t=7days

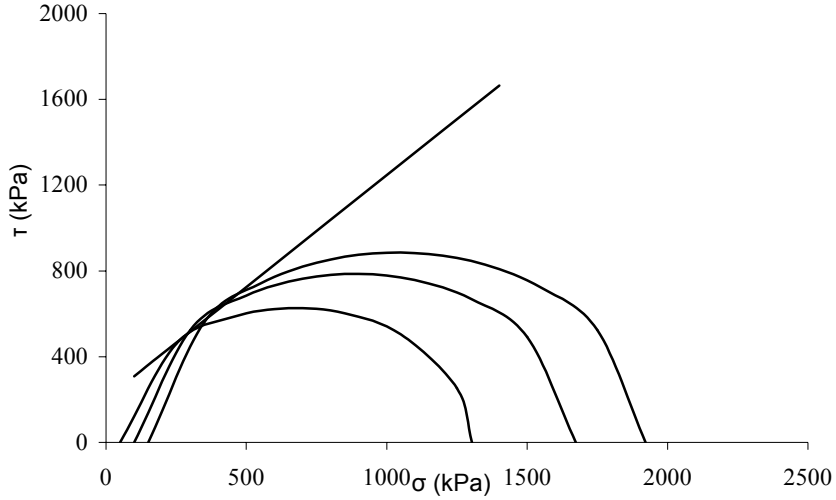

Fig. 16b τ vs. σ for m_L=5%, m_F=0.2% and t=14days

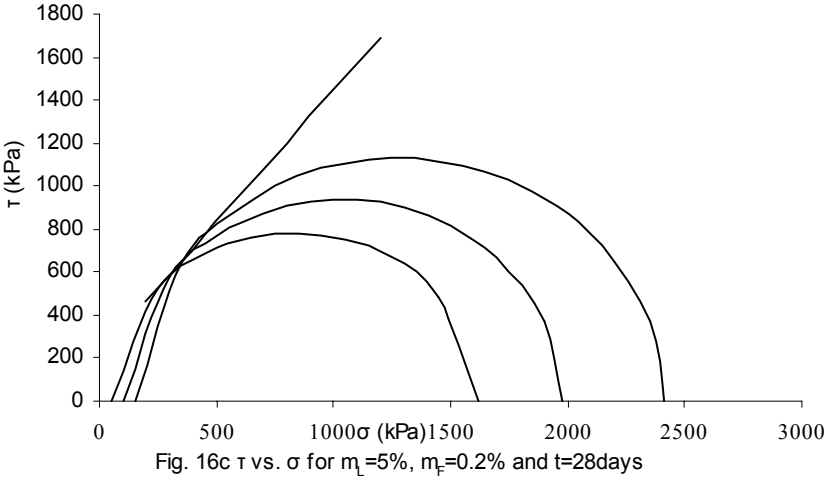

Fig. 16c τ vs. σ for m_L=5%, m_F=0.2% and t=28days

Figure 18 Cohesion c vs. fiber content m_F and curing time t

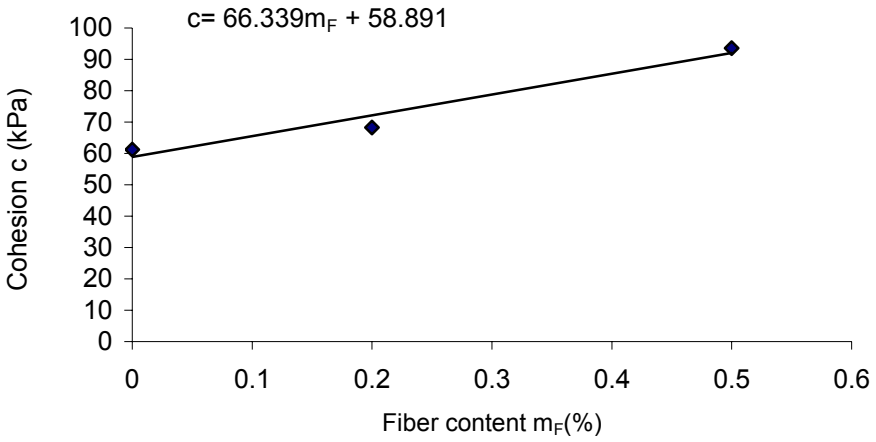

Fig.18a Cohesion vs. fiber content for m_L = 0%

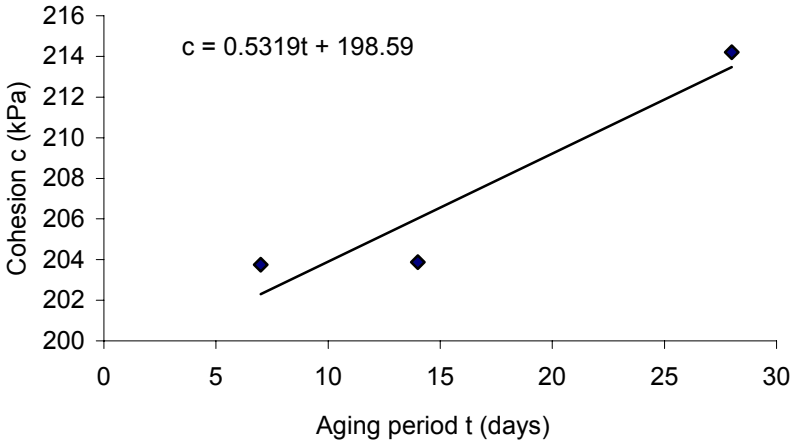

Fig.18b Cohesion vs. aging time for m_F =0.2%, m_L = 5%

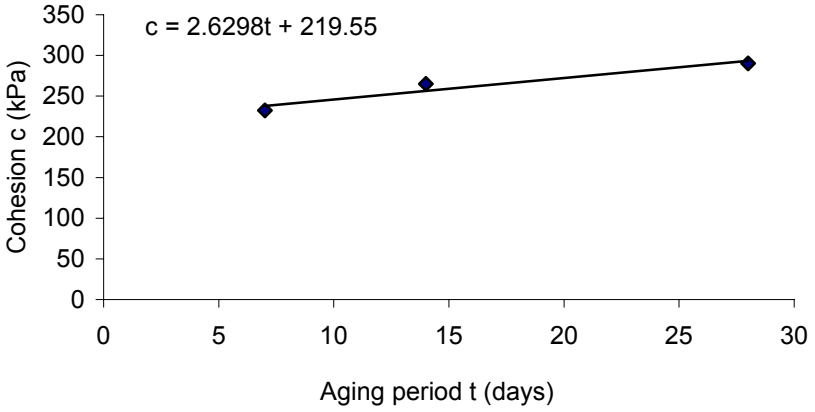

Fig. 18c Cohesion vs. aging time for m_F = 0.5%, m_L = 5%

Figure 19 Friction angle ϕ vs. fiber content m_F and curing time t

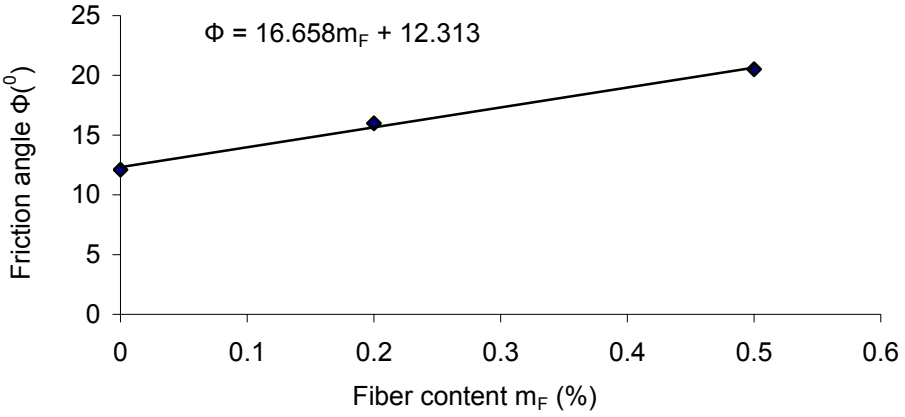

Fig. 19a Friction angle vs. fiber content for m_L = 0%

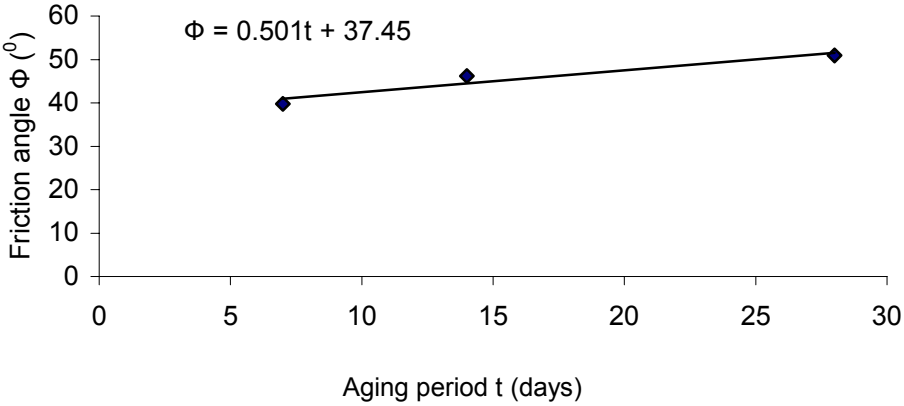

Fig. 19b Friction angle vs. aging time for m_F= 0.2%, m_L = 5%

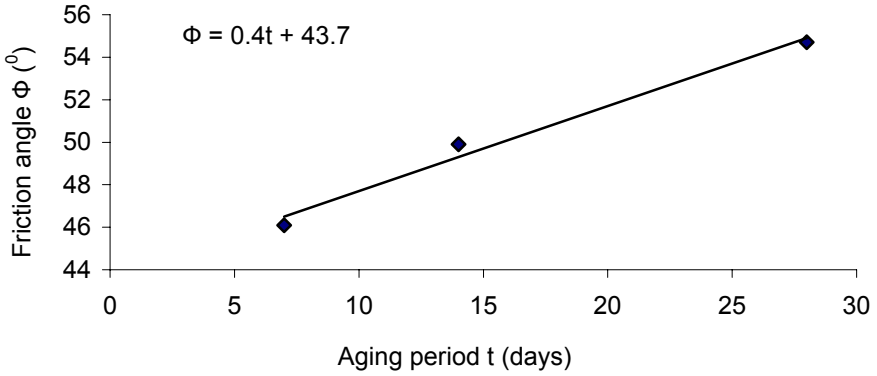

Fig. 19c Friction angle vs. aging time for m_F= 0.5%, m_L= 5%

Figure 20 σ_d ~ε_d with m_L=2%, m_F= 0.2%, t =7 days, and different σ_0 and N

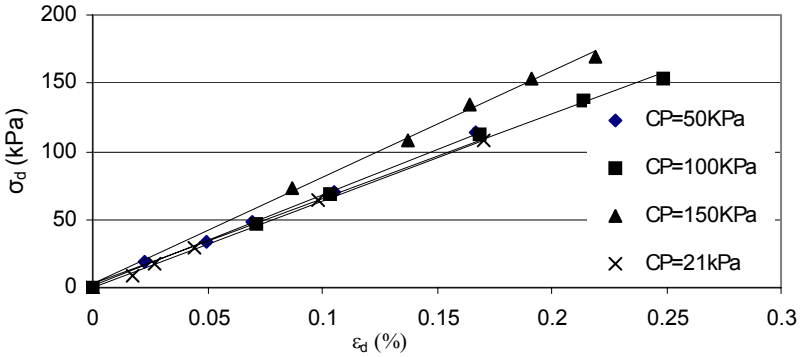

a. N=50, t =7days, m_L=2% and m_F=0.2%

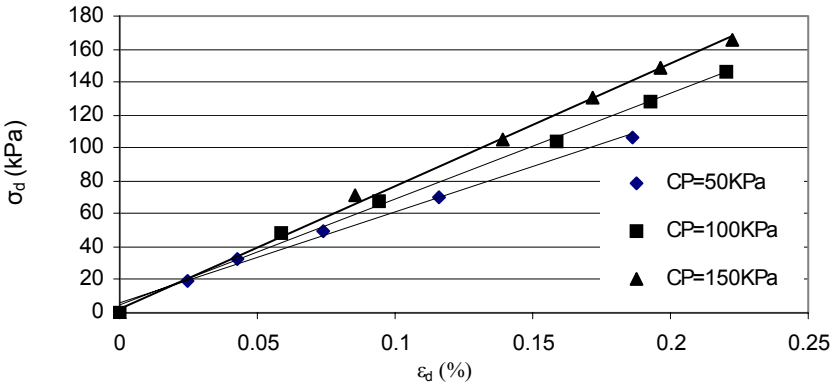

b. N=100, t =7days, m_L=2% and m_F=0.2%

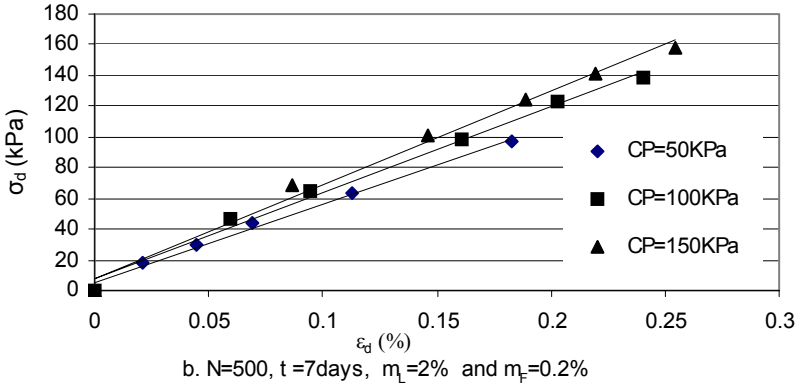

b. N=500, t =7days, m_L=2% and m_F=0.2%

Figure 21 σ_d ~ε_d with m_L=5%, m_F= 0.2%, t =7 days, and different σ_0 and N

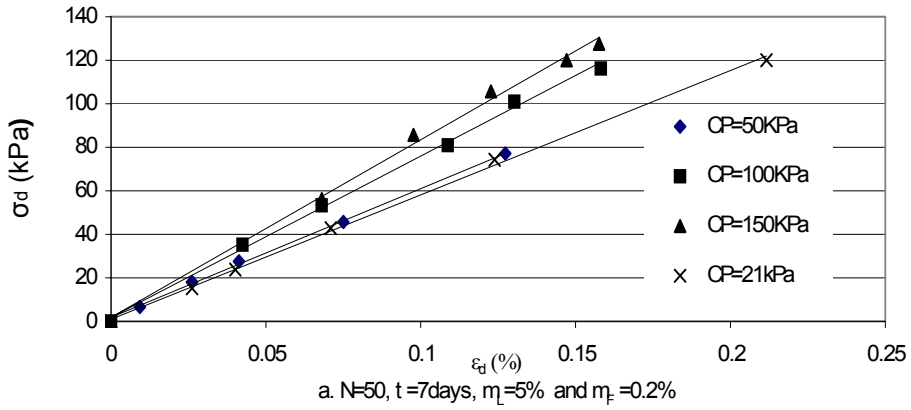

a. N=50, t =7days, m_L=5% and m_F =0.2%

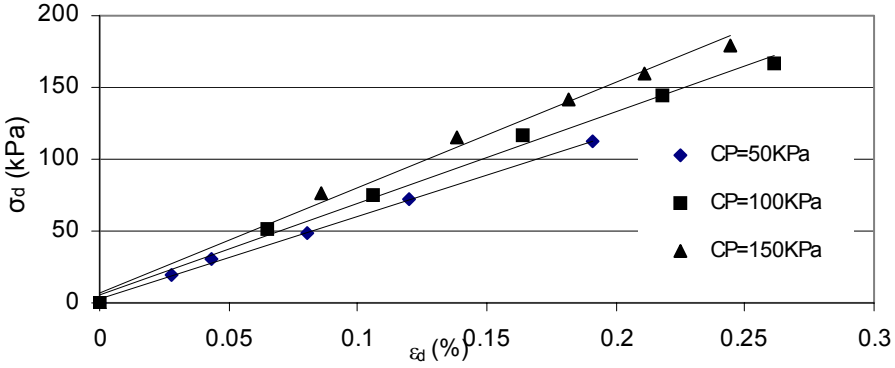

b. N=100, t =7days, m_L=5% and m_F=0.2%

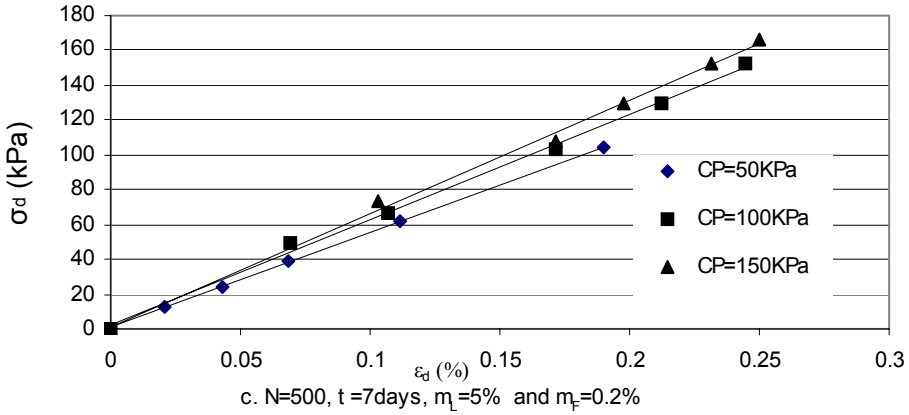

c. N=500, t =7days, m_L=5% and m_F=0.2%

Figure 22 σ_d ~ε_d with m_L=5%, m_F= 0%, t =7 days, and different σ_0 and N

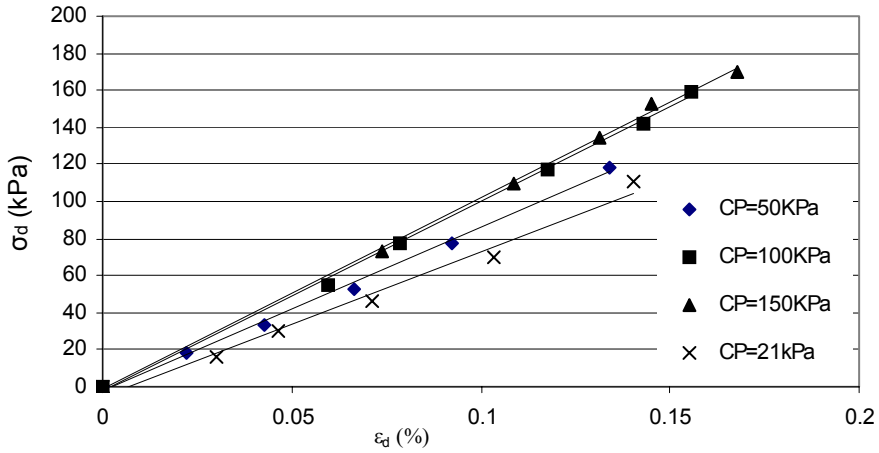

a. N=50, t =7days, m_L=5% and m_F=0%

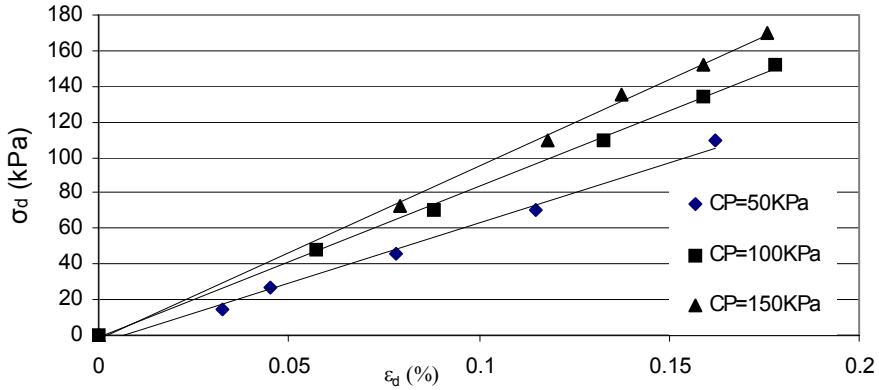

b. N=100, t =7days, m_L=5% and m_F=0%

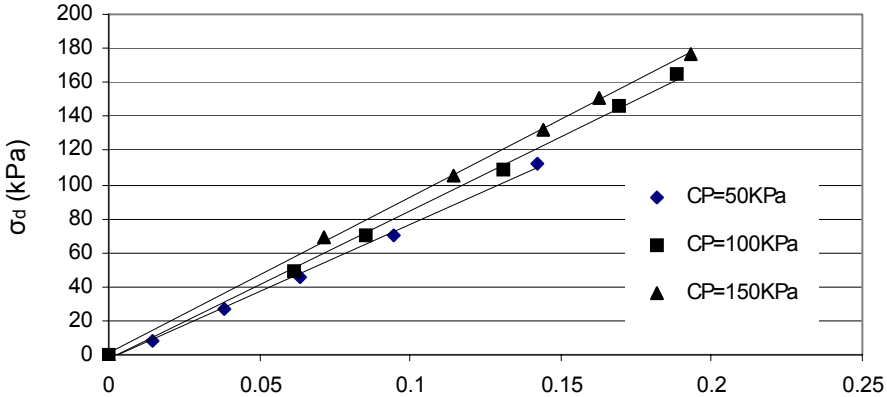

c. N=500, t =7days, m_L=5% and m_F =0%

Figure 23 σ_d ~ε_d with m_L=2%, m_F= 0.5%, t =7 days, and different σ_0 and N

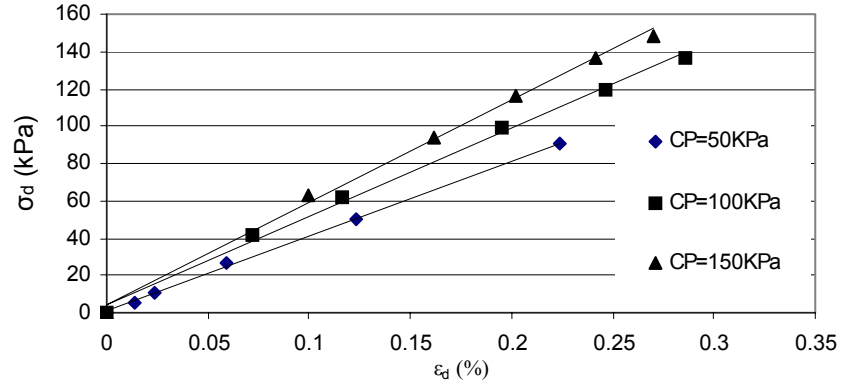

a. N=50, t 7days, m_L=2% and m_F =0.5%

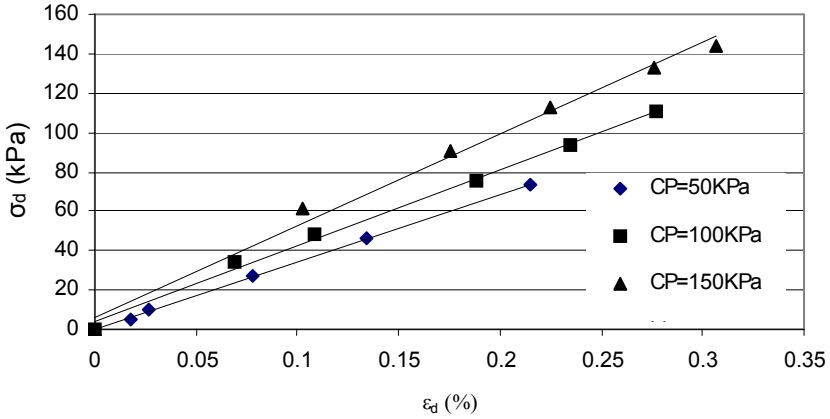

b. N=100, t =7days, m_L=2% and m_F=0.5%

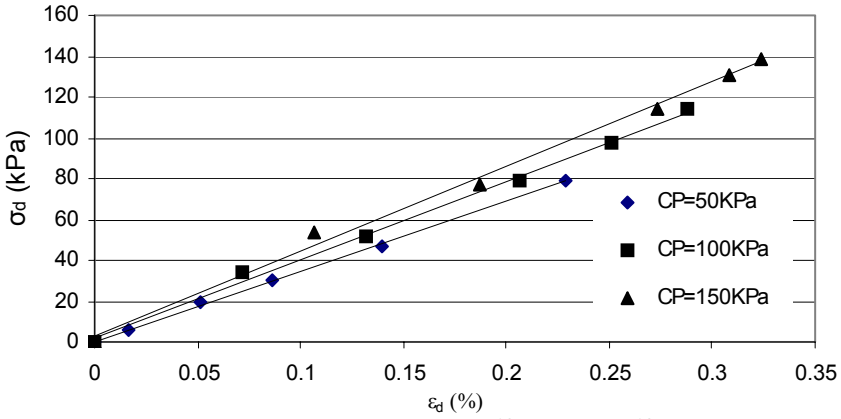

c. N=500, t =7days, m_L=2% and m_F=0.5%

Figure 24 σ_d ~ε_d with m_L=2%, m_F= 0.2%, t=7 days, and different σ_0 and N

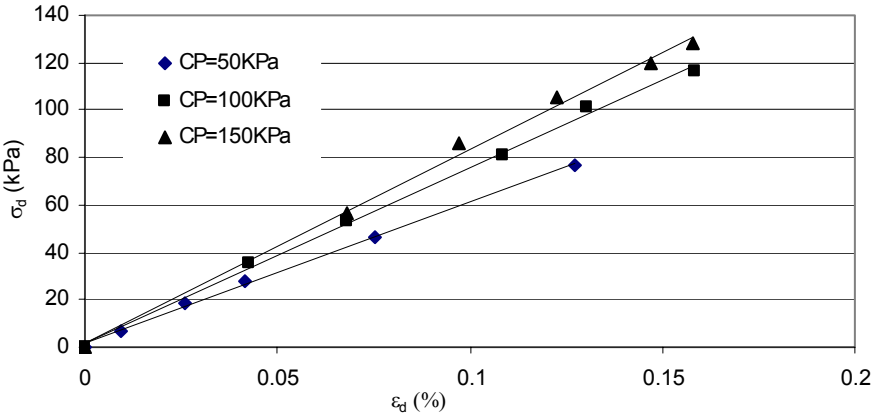

a. N=50, t =7days, m_L=5% and m_F=0.2%

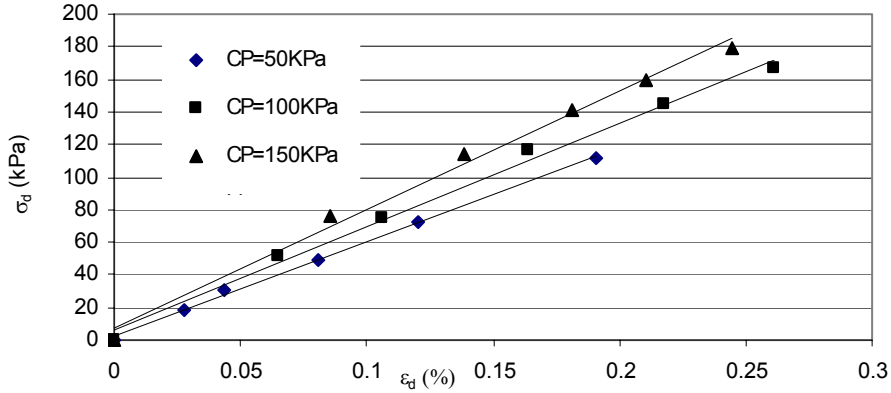

b. N=100, t =7days, m_L=5% and m_F=0.2%

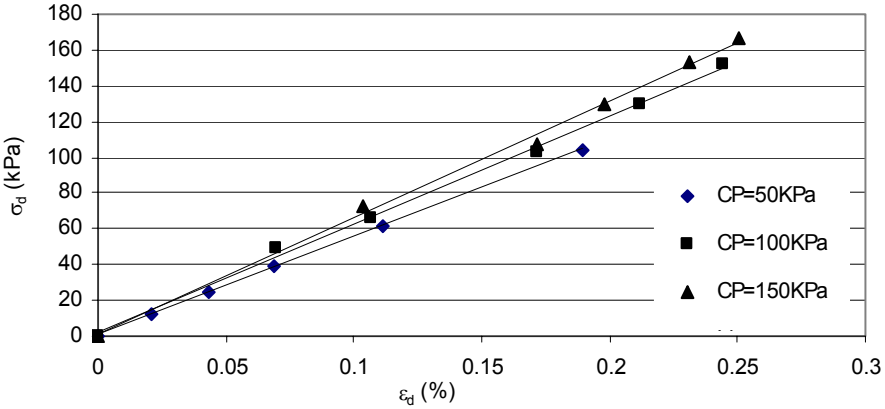

c. N=500, t =7 days, m_L =5% and m_F = 0.2%

Figure 25 σ_d ~ε_d with m_L=5%, m_F= 0.5%, t =7 days, and different σ_0 and N

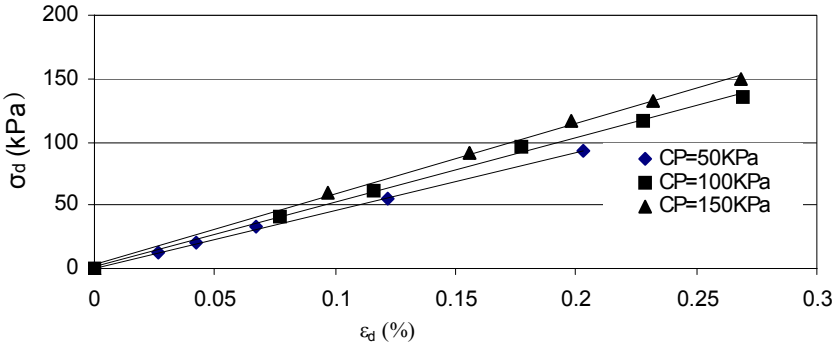

a. N = 50, t =7 days, m_L = 5% and m_F = 0.5%

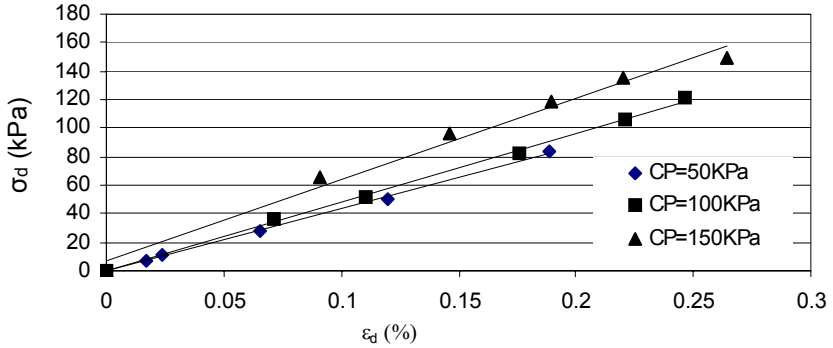

b. N = 100, t = 7 days, m_L = 5% and m_F = 0.5%

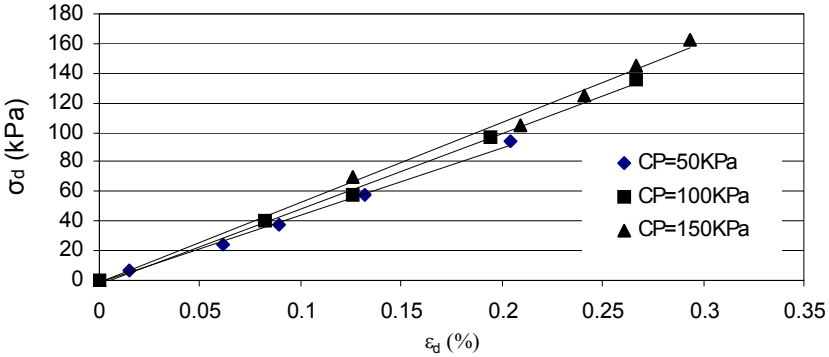

c. N = 500, t = 7 days, m_L = 5% and m_F = 0.5%

Figure 26 σ_d ~ε_d with m_L=2%, m_F= 0%, t =14 days, and different σ_0 and N

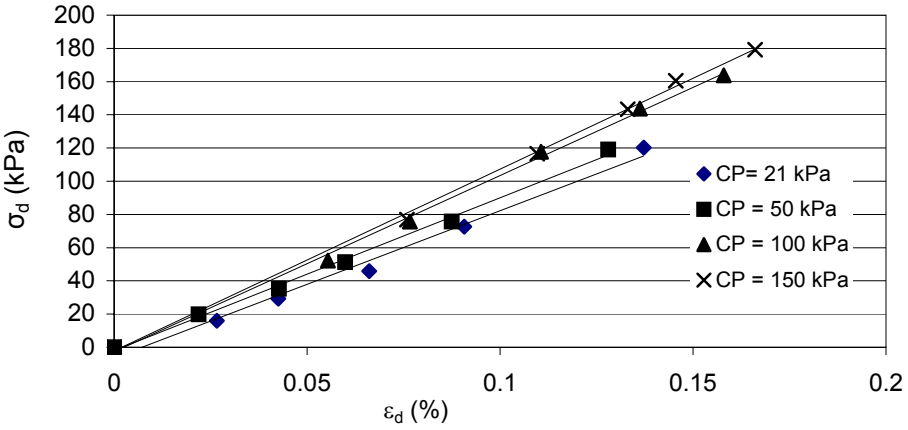

a. N = 50, t =14, m_L= 2% and m_F = 0%

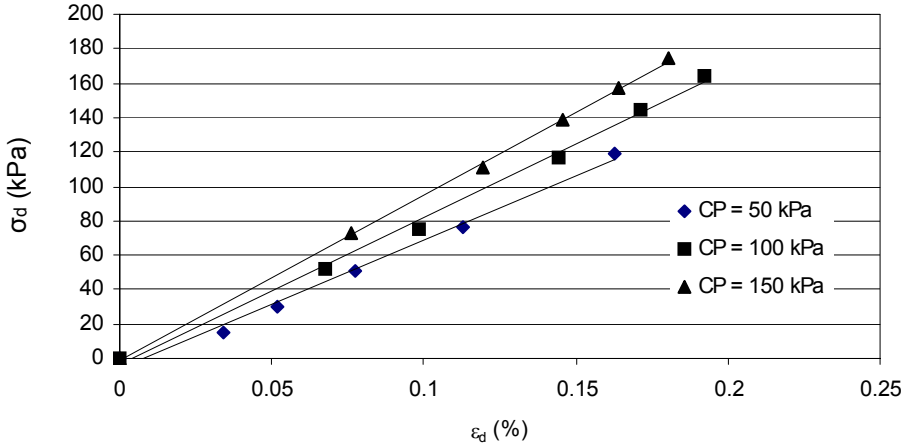

b. N = 100, t = 14 days, m_L = 2 % and m_F = 0 %

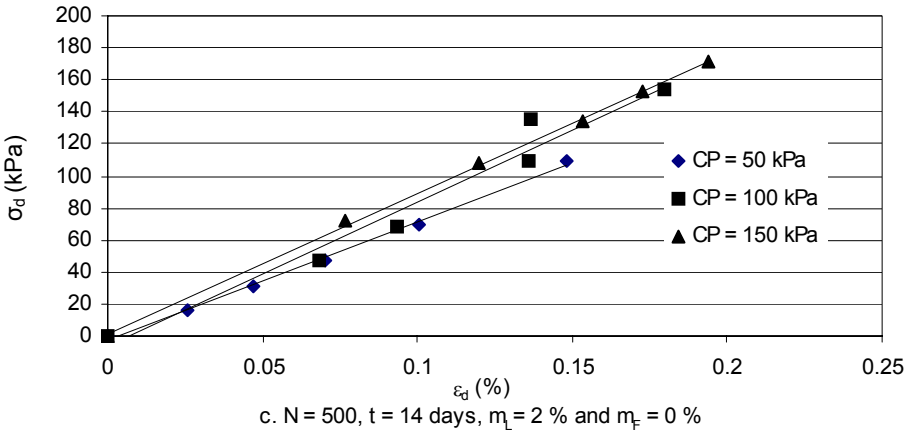

c. N = 500, t = 14 days, m_L= 2 % and m_F = 0 %

Figure 27 σ_d ~ε_d with m_L=2%, m_F= 0.2%, t =14 days, and different σ_0 and N

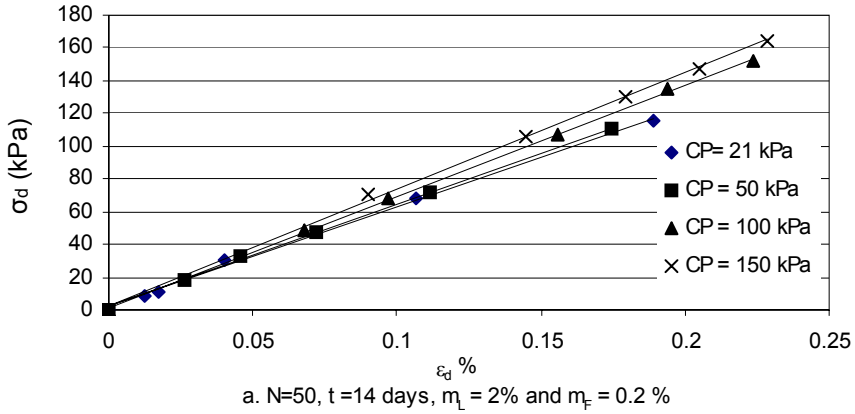

a. N=50, t =14 days, m_L = 2% and m_F = 0.2 %

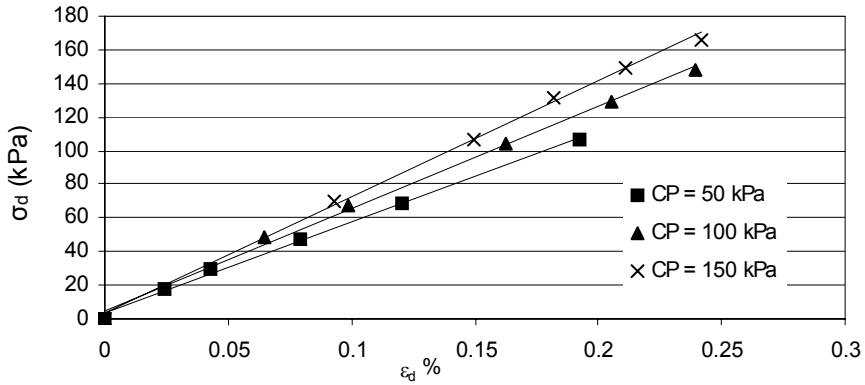

b. N=100, t =14 days, m_L = 2% and m_F= 0.2 %

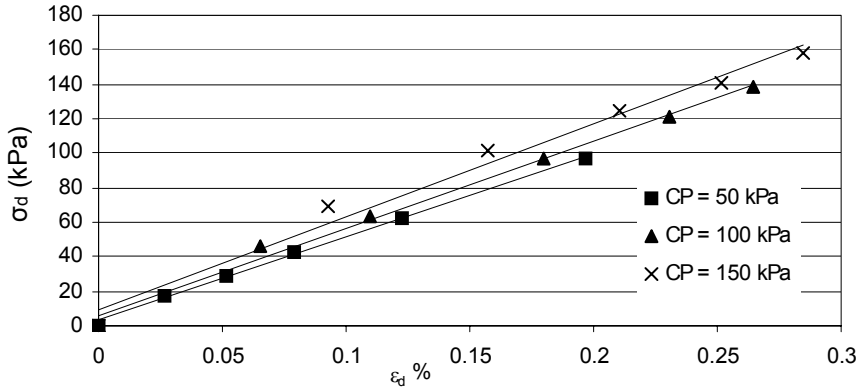

c. N=500, t =14 days, m_L= 2% and m_F = 0.2 %

Figure 28 σ_d ~ε_d with m_L=5%, m_F= 0.2%, t =14 days, and different σ_0 and N

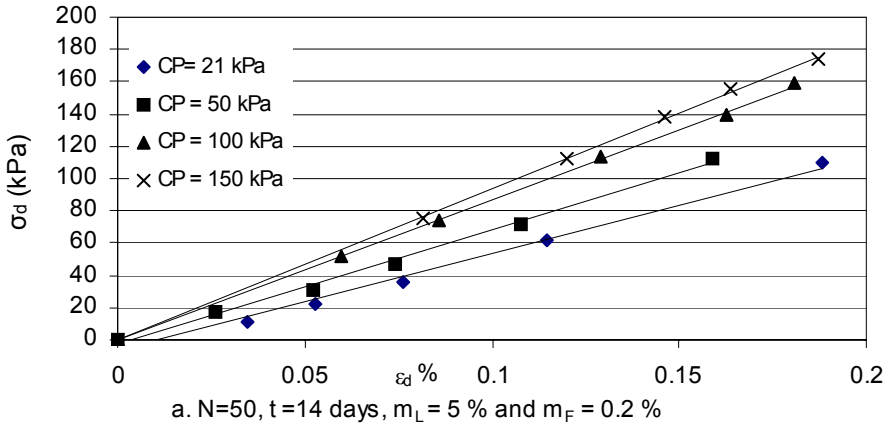

a. N=50, t =14 days, m_L = 5 % and m_F = 0.2 %

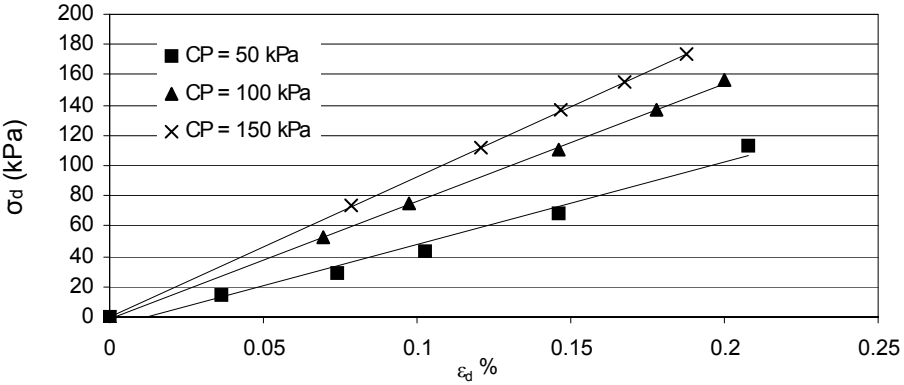

b. N=100, t =14 days, m_L = 5 % and m_F= 0.2 %

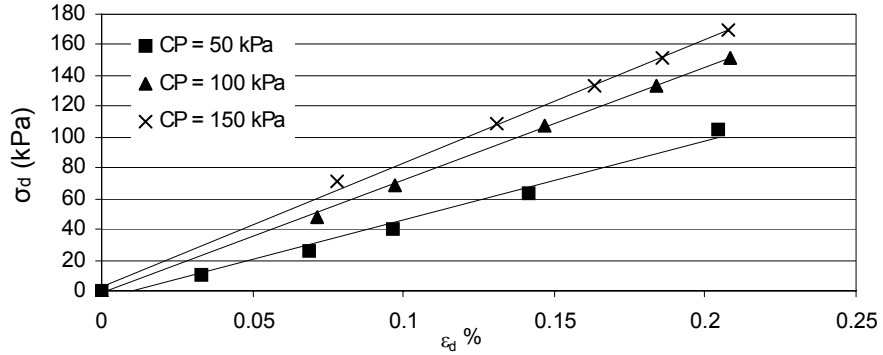

c. N=500, t =14 days, m_L = 5 % and m_F = 0.2 %

Figure 29 σ_d ~ε_d with m_L=2%, m_F= 0.5%, t =14 days, and different σ_0 and N

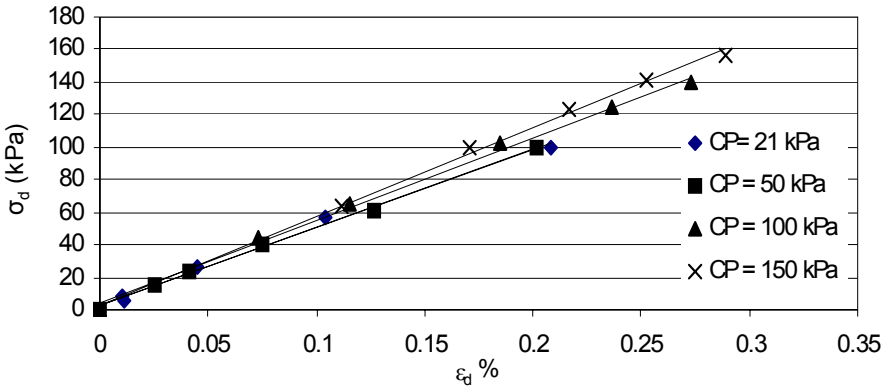

a. N=50, t =14 days, m_L = 2 % and m_F= 0.5 %

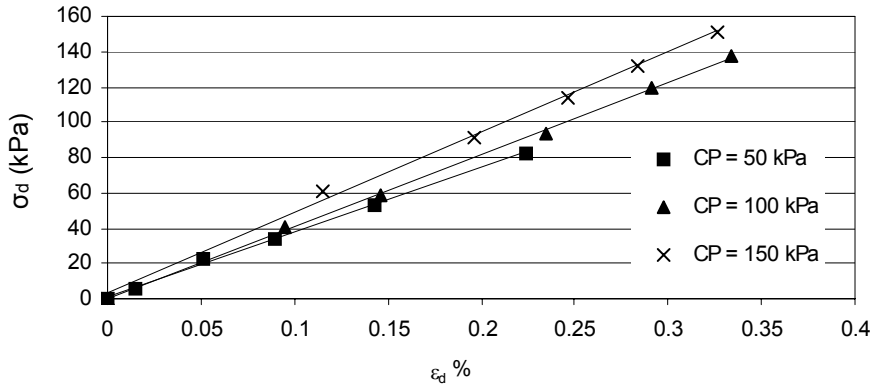

b. N=100, t =14 days, m_L = 2 % and m_F= 0.5 %

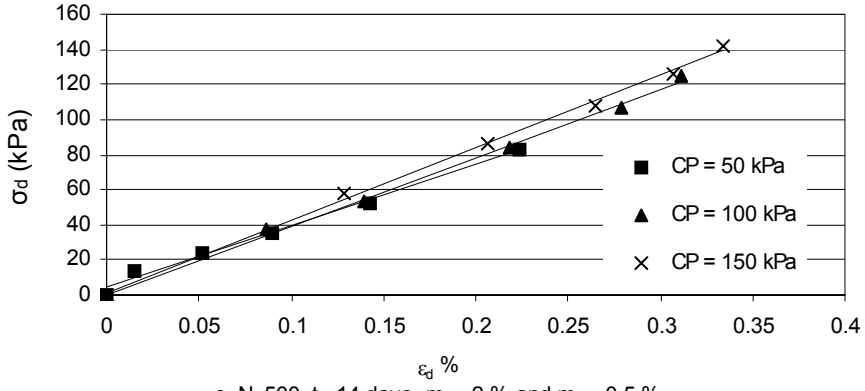

c. N=500, t =14 days, m_L = 2 % and m_F = 0.5 %

Figure 30 σ_d ~ε_d with m_L=5%, m_F= 0.5%, t =14 days, and different σ_0 and N

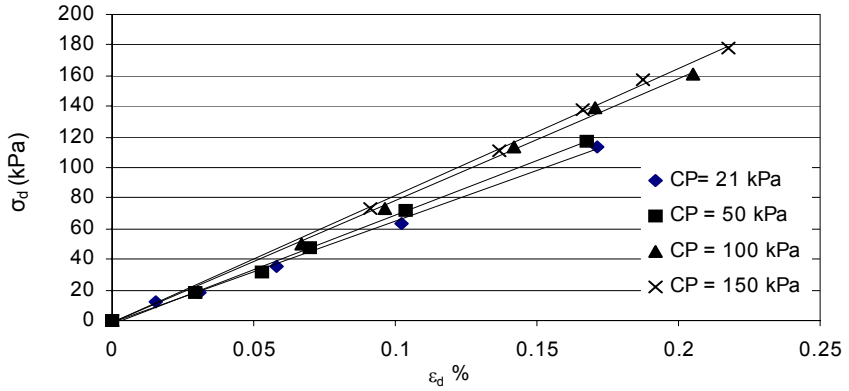

a. N=50, t =14 days, m_L = 5 % and m_F = 0.5 %

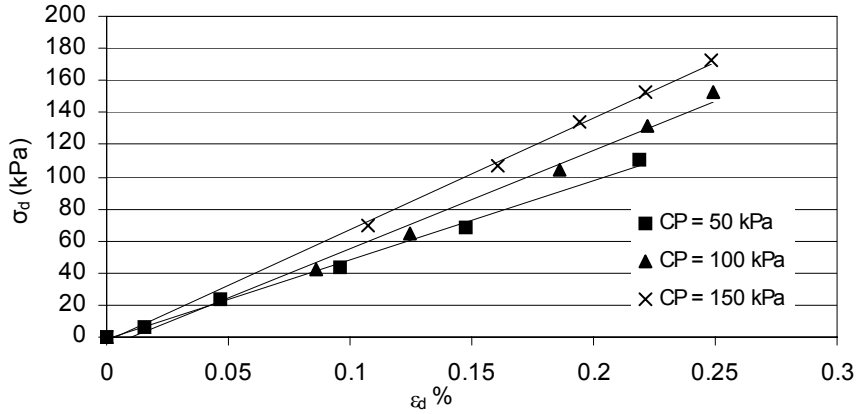

b. N=100, t =14 days, m_L= 5 % and m_F = 0.5 %

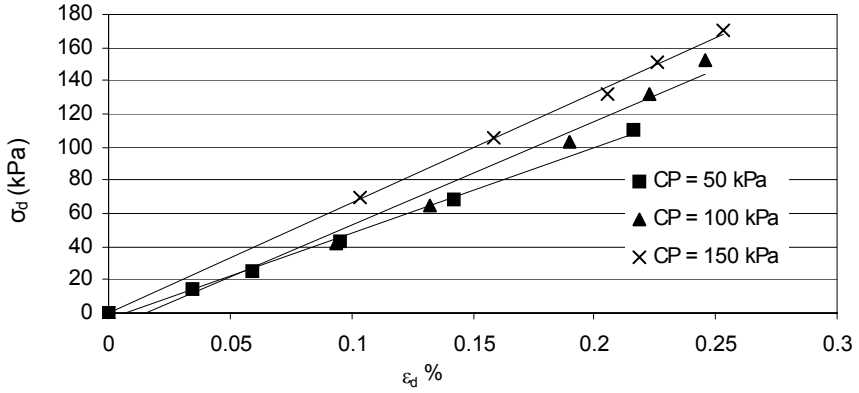

c. N=500, t =14 days, m_L = 5 % and m_F= 0.5 %

Figure 31 σ_d ~ε_d with m_L=2%, m_F= 0%, t =28 days, and different σ_0 and N

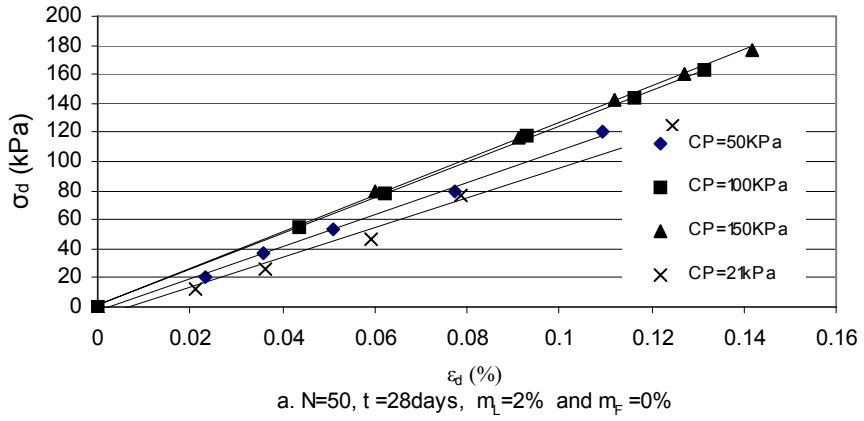

a. N=50, t =28days, m_L=2% and m_F =0%

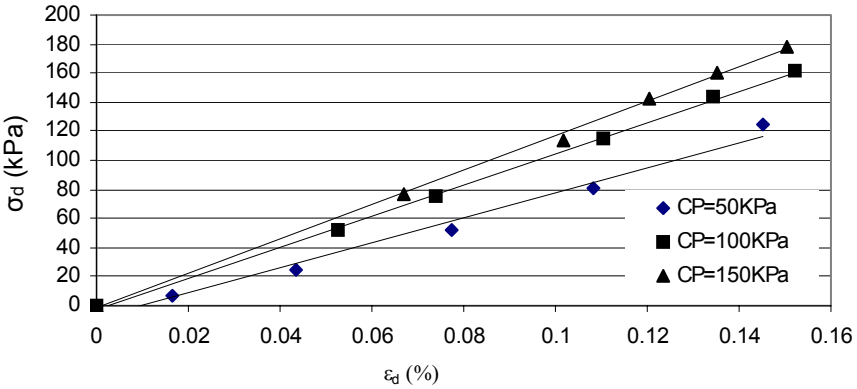

b. N=100, t =28days, m_L=2% and m_F=0%

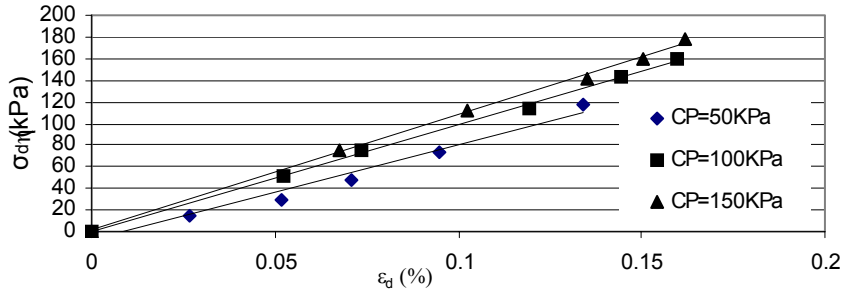

c. N=150, t =28 days, m_L=2% and m_F=0%

Figure 32 σ_d ~ε_d with m_L=2%, m_F= 0.2%, t =28 days, and different σ_0 and N

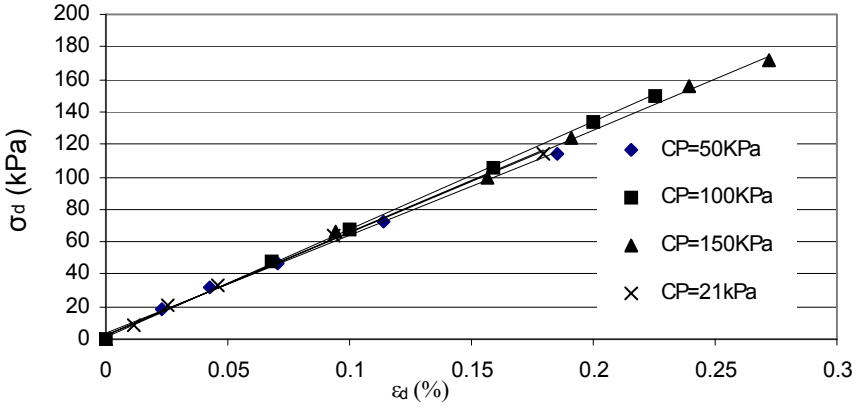

a. N=50, t =28days, m_l=2% and m_f =0.2%

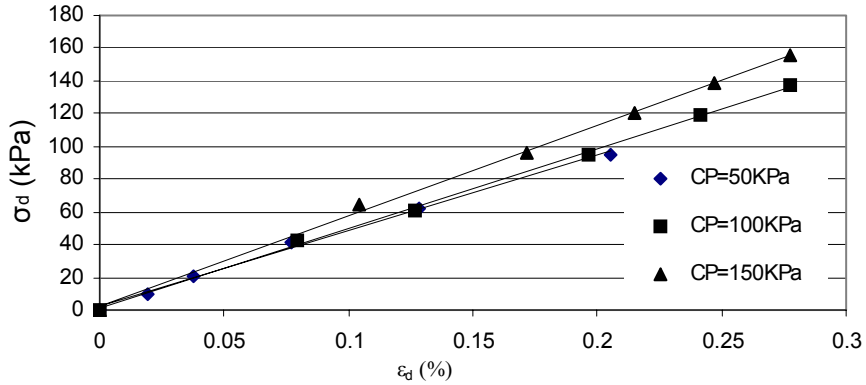

b. N=100, t =28days, m_L=2% and m_F=0.2%

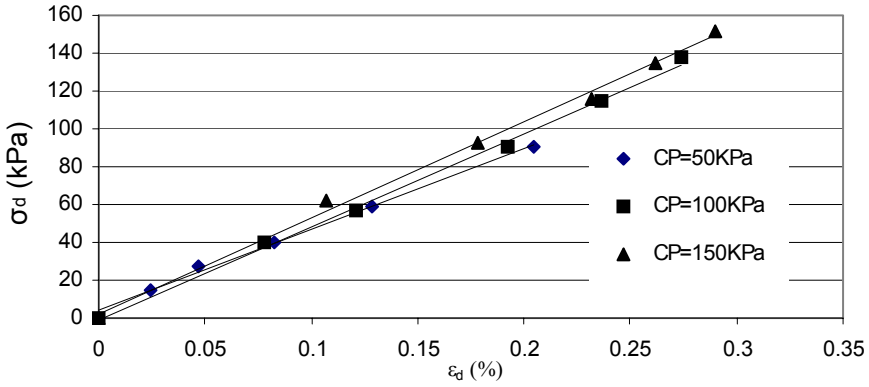

c. N=500, t =28days, m_L=2% and m_F =0.2%

Figure 33 σ_d ~ε_d with m_L=5%, m_F= 0.2%, t =28 days, and different σ_0 and N

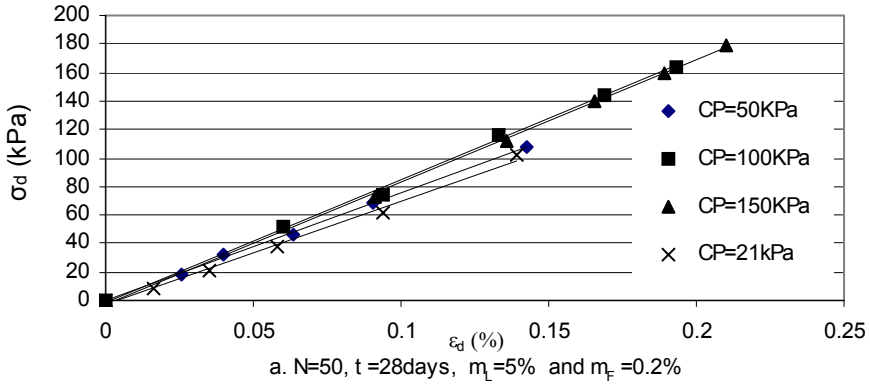

a. N=50, t =28days, m_L=5% and m_F =0.2%

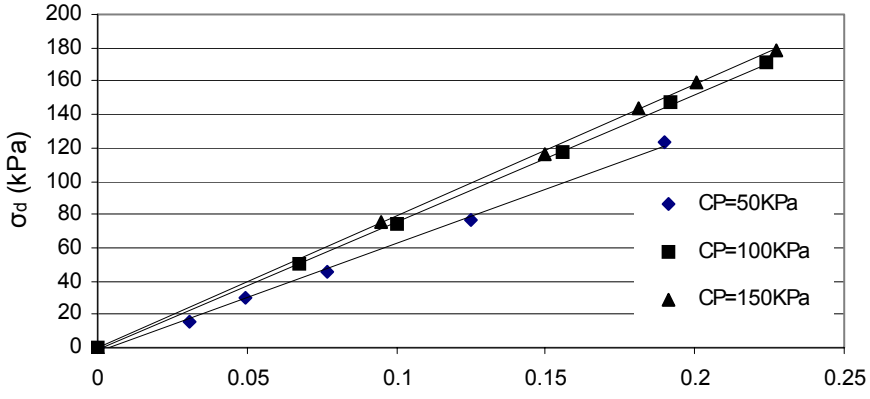

b. N=100, t =28days, m_L=5% and m_F =0.2%

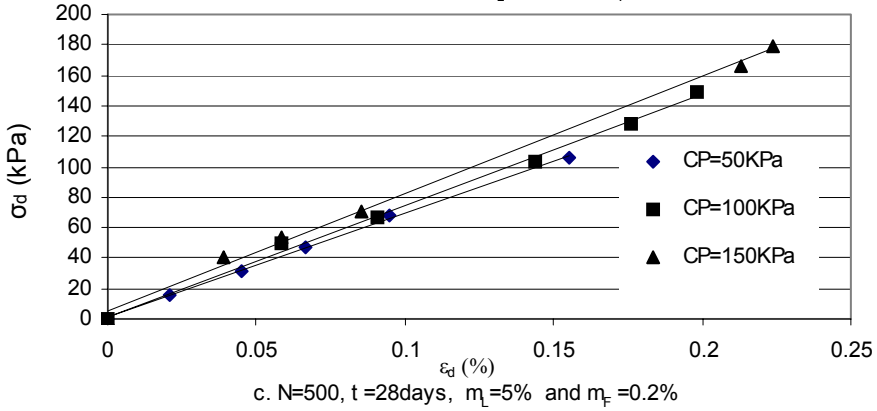

c. N=500, t =28days, m_L=5% and m_F =0.2%

Figure 34 σ_d ~ε_d with m_L=0%, m_F= 0.2%, t =28 days, and different σ_0 and N

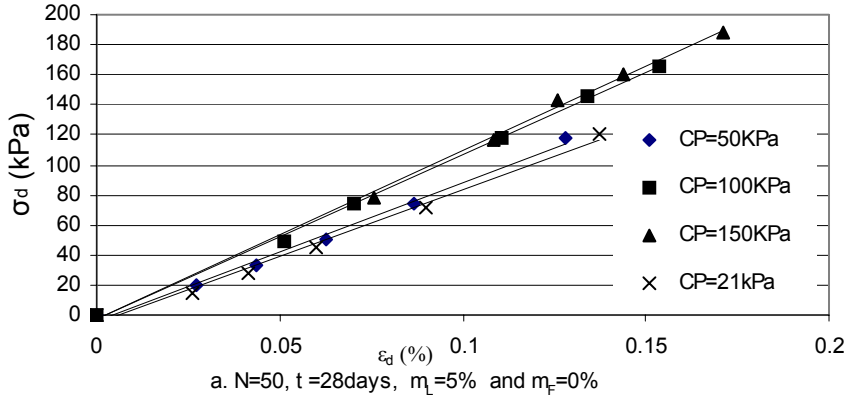

a. N=50, t =28days, m_L=5% and m_F=0%

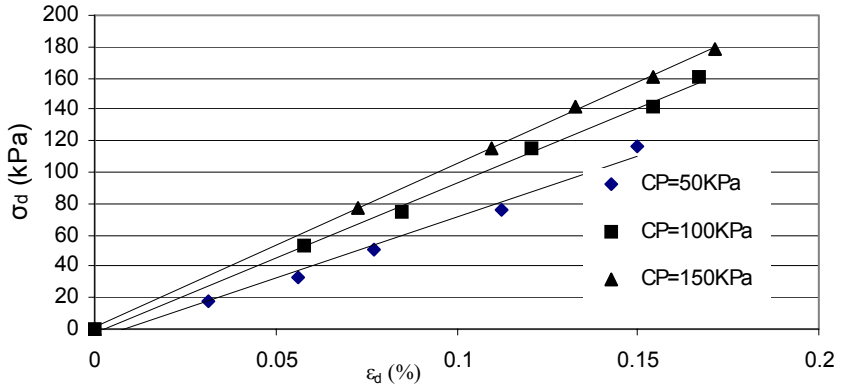

b. N=100, t =28days, m_L=5% and m_F =0%

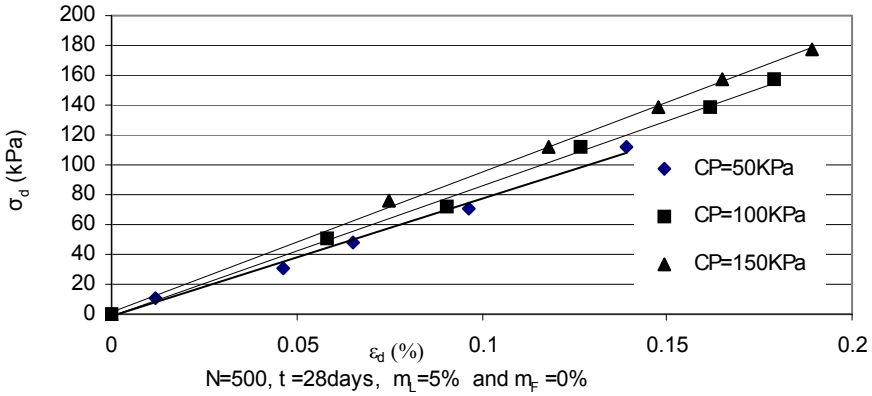

N=500, t =28days, m_L=5% and m_F =0%

Figure 35 σ_d ~ε_d with m_L=2%, m_F= 0.5%, t =28 days, and different σ_0 and N

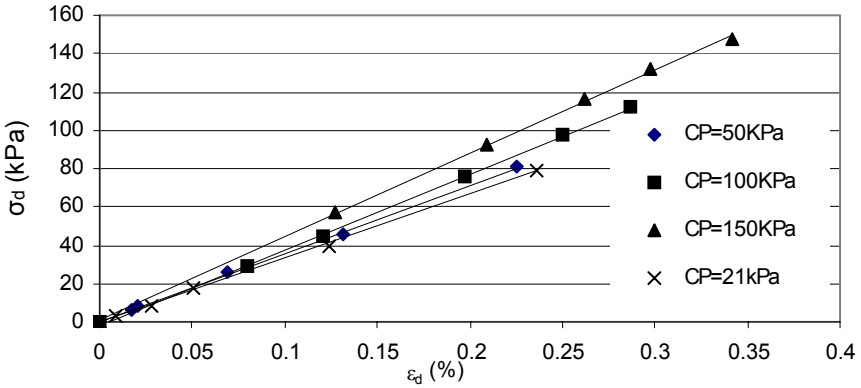

a. N=50, t =28days, m_L=2% and m_F=0.5%

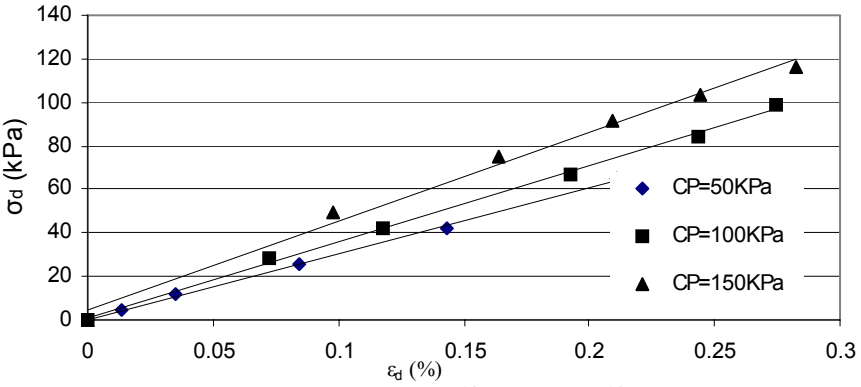

b. N=100, t =28days, m_L=2% and m_F =0.5%

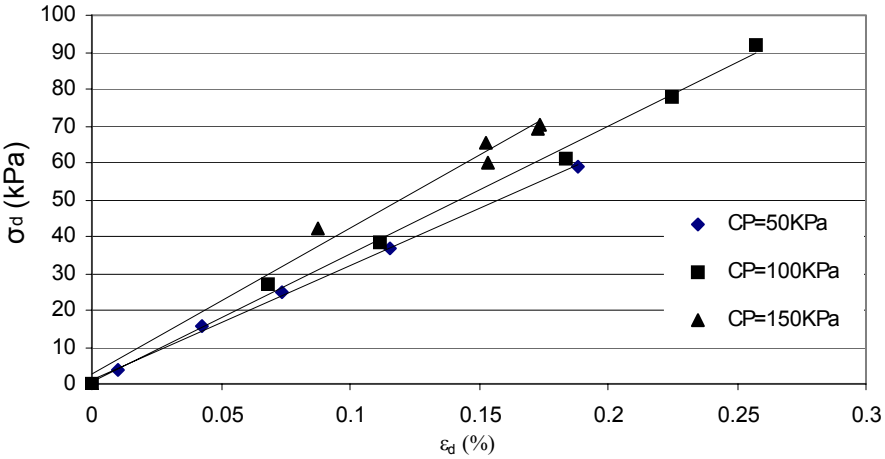

c. N=500, t =28days, m_L=2% and m_F =0.5%

Figure 36 σ_d ~ε_d with m_L=5%, m_F= 0.5%, t =28 days, and different σ_0 and N

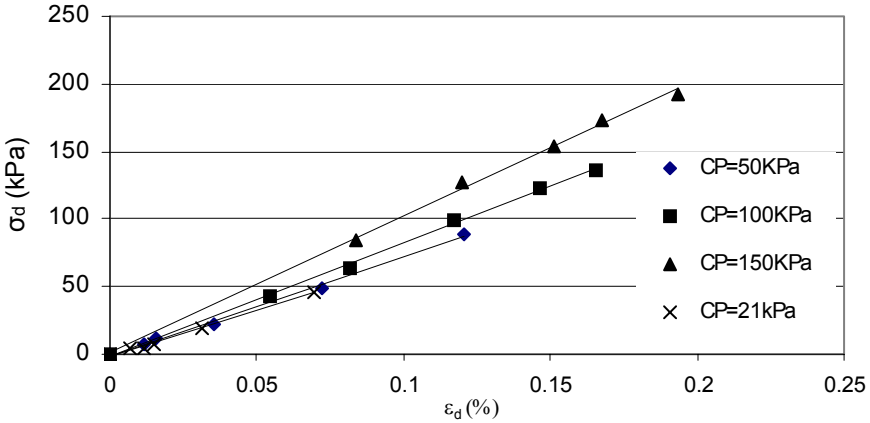

a. N = 50, t = 28 days, m_L = 5% and m_F = 0.5%

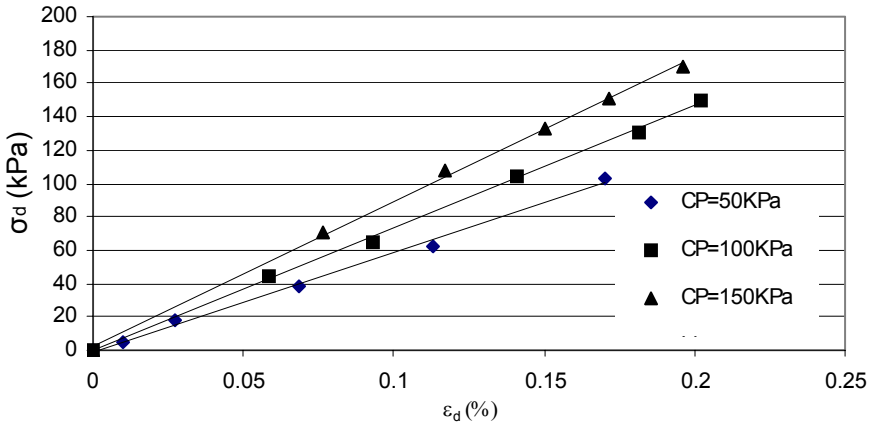

b. N = 100, t = 28 days, m_L = 5% and m_F = 0.5%

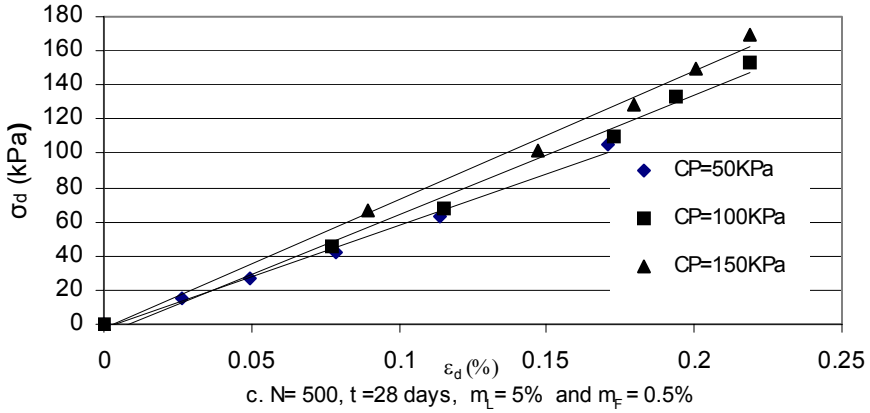

c. N= 500, t =28 days, m_L = 5% and m_F = 0.5%

Figure 37 G vs. N, m_L, m_F, t and σ_0

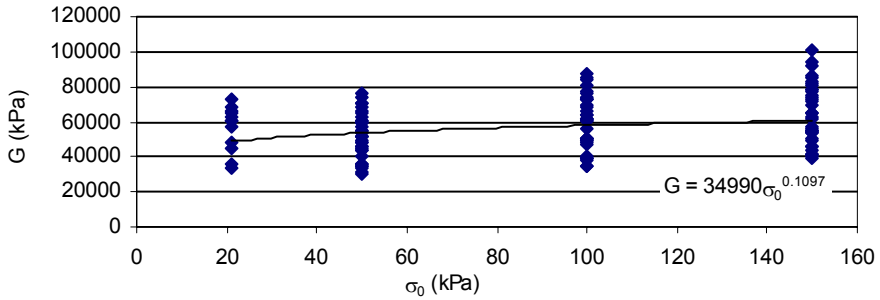

a G vs. σ_0 with different m_L, m_F, t and N

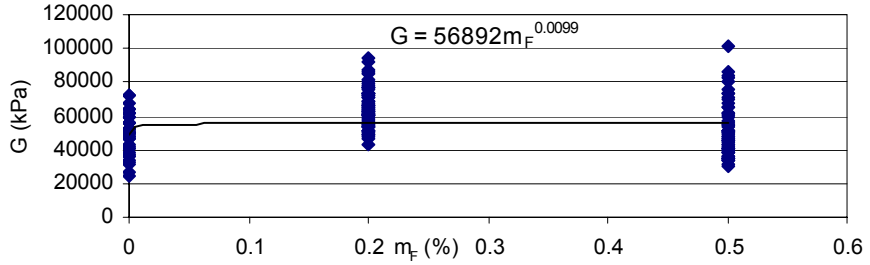

b. G vs. m_F with different m_F, t, N and σ_0

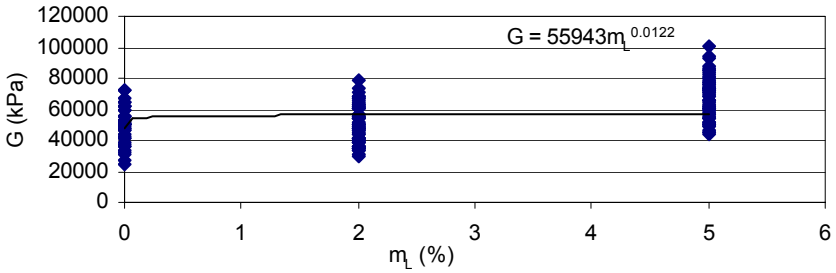

c G vs. m_L with different m_F, t, N and σ_0

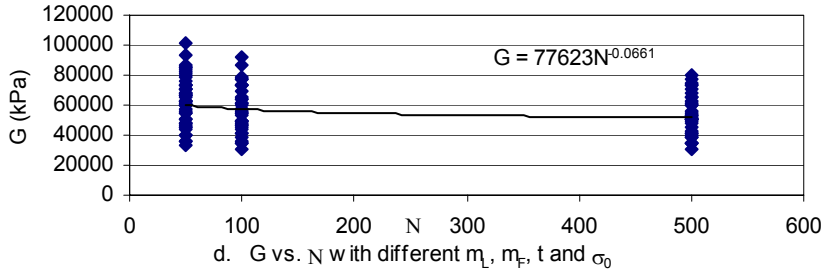

d. G vs. N with different m_L, m_F, t and σ_0

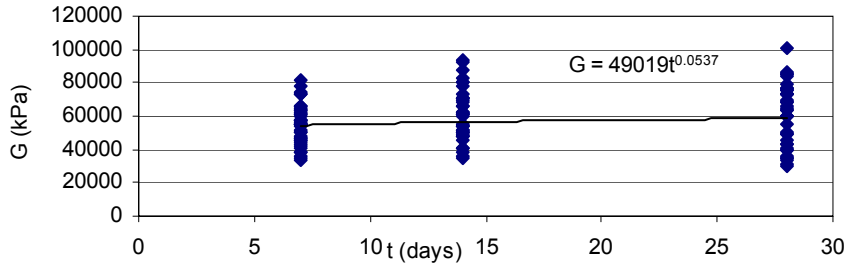

e. G vs. t with different m_L, m_F, N and σ_0

Figure 38 Mr ~σ_m with t =7 days and different m_F, m_L and N

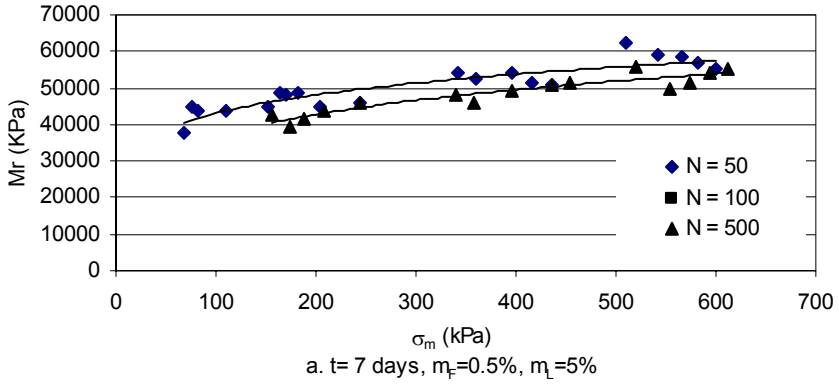

a. t= 7 days, m_F=0.5%, m_L=5%

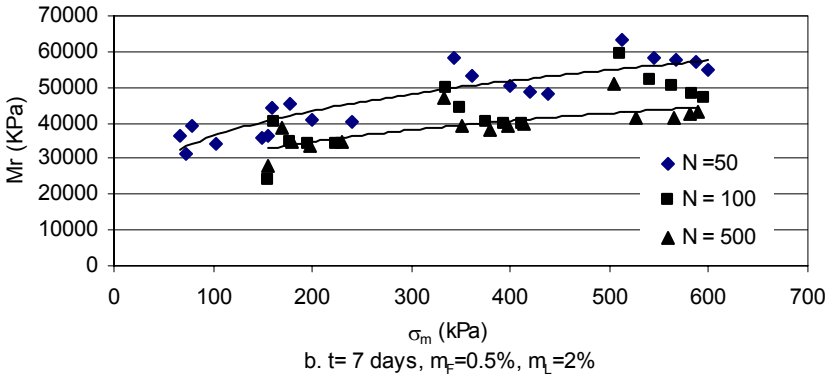

b. t= 7 days, m_F=0.5%, m_L=2%

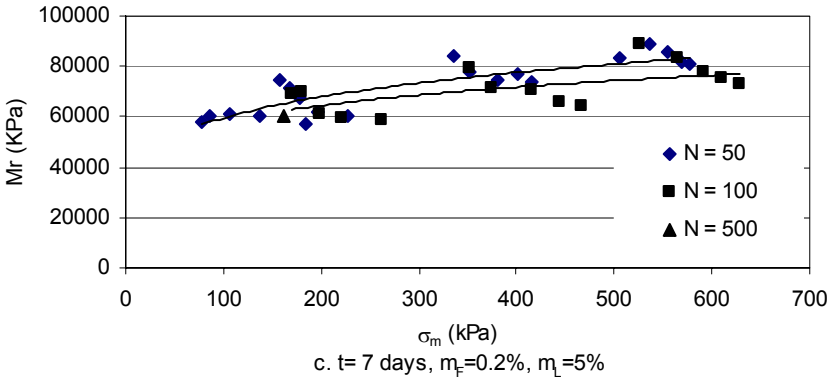

c. t= 7 days, m_F=0.2%, m_L=5%

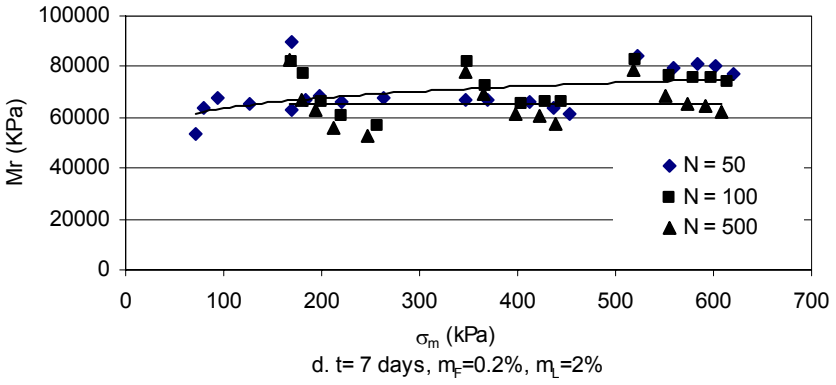

d. t= 7 days, m_F=0.2%, m_L=2%

Figure 39 Mr ~σ_m with t =14 days and different m_F, m_L and N

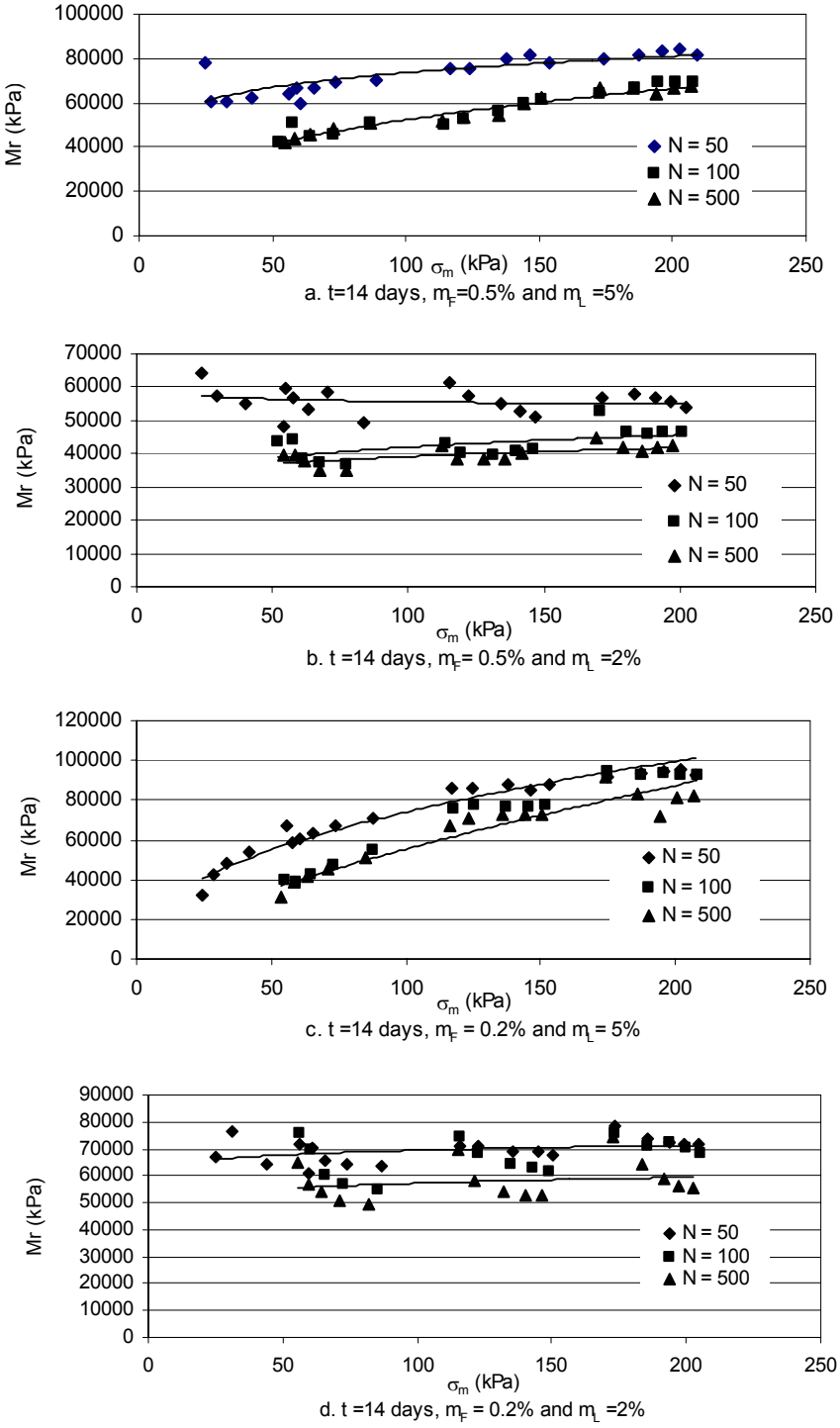

Figure 40 Mr ~σ_m with t =28 days and different m_F, m_L and N

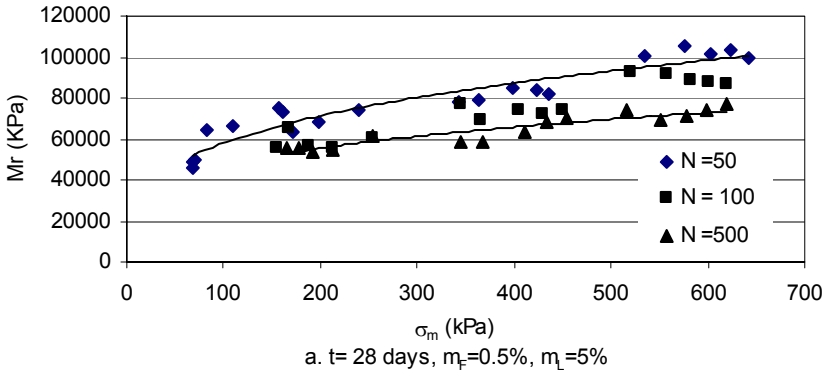

a. t= 28 days, m_F=0.5%, m_L=5%

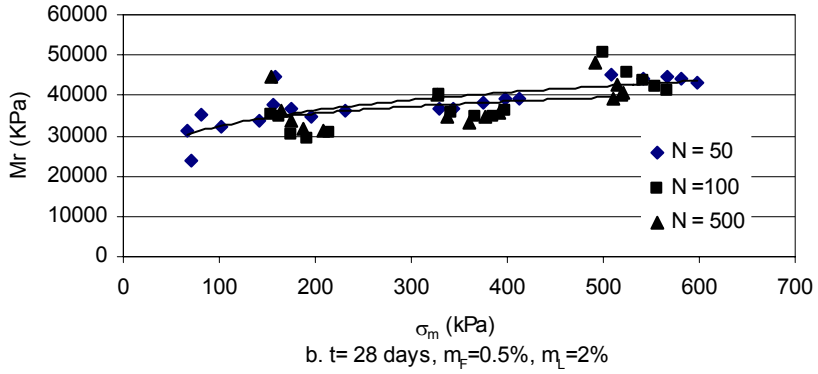

b. t= 28 days, m_F=0.5%, m_L=2%

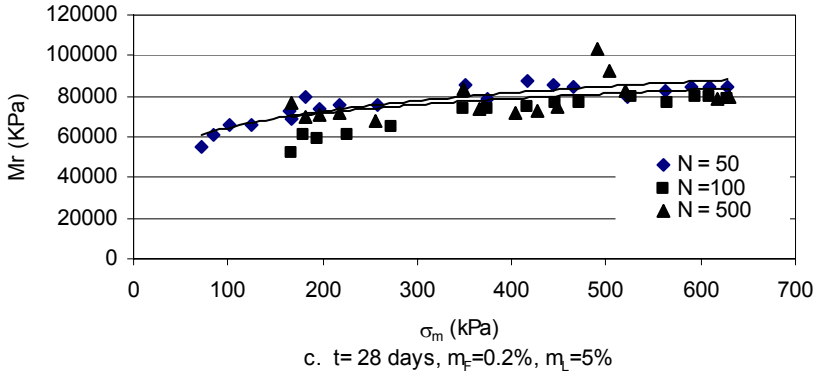

c. t= 28 days, m_F=0.2%, m_L=5%

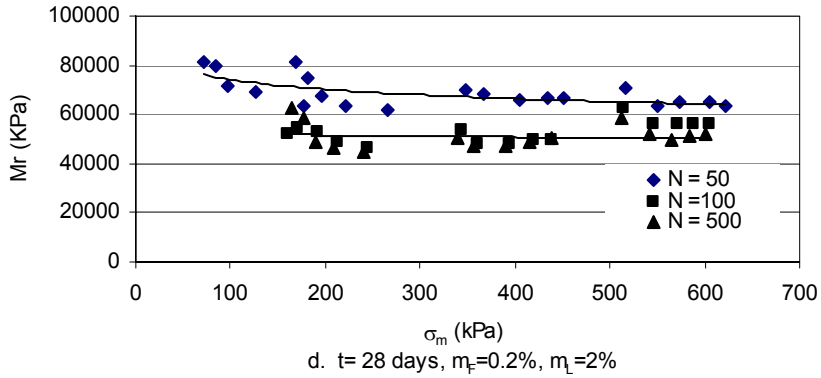

d. t= 28 days, m_F=0.2%, m_L=2%

THE LIST OF TABLES

Table 1 Specimens for static tests with fiber and without lime

Group Number	Specimen Number	Fiber Content m_F	Lime Content m_L	Cell Pressure σ_0
		(%)	(%)	(kPa)
1	S11	0	0	50
	S12	0	0	100
	S13	0	0	150
	S14	0	0	200
2	F5	0.2	0	50
	F6	0.2	0	100
	F7	0.2	0	150
	F8	0.2	0	200
3	F5-5	0.5	0	50
	F5-6	0.5	0	100
	F5-7	0.5	0	150
	F5-8	0.5	0	200

Table 2 Specimens for static tests with fiber and lime

Group Number	Specimen Number	Fiber Content m_F	Lime Content m_L	Cell Pressure σ_0	Aging Periods
		(%)	(%)	(kPa)	(day)
4	Slf2	0.2	5	0	7
	Slf1, 11, 9	0.2	5	50	7
	Slf6, 17	0.2	5	100	7
	Slf3, 15	0.2	5	150	7
5	Slf5, 12, 16	0.2	5	50	14
	Slf4	0.2	5	100	14
	Slf7, 8	0.2	5	150	14
6	Slf14	0.2	5	50	28
	Slf13	0.2	5	100	28
	Slf18, 19, 20	0.2	5	150	28
7	Slf5-9	0.5	5	0	7
	Slf5-1	0.5	5	50	7
	Slf5-2	0.5	5	100	7
	Slf5-4, 5-10	0.5	5	150	7
	Slf5-6, 5-12	0.5	5	200	7
8	Slf5-3	0.5	5	50	14
	Slf5-5	0.5	5	100	14
	Slf5-7, 5-11	0.5	5	150	14
	Slf5-8	0.5	5	200	14
9	Slf5-16	0.5	5	50	28
	Slf5-13	0.5	5	100	28
	Slf5-14	0.5	5	150	28
	Slf5-15	0.5	5	200	28

Table 3 Specimens for dynamic tests with m_F = 0% and m_L = 2%

Group Number	Specimen Number	Fiber Content m_F	Lime Content m_L	Cell Pressure σ_0	Aging Time t	Repetition Number N	Dry Unit Weight γ_d
		(%)	(%)	(kPa)	(day)		(g/cm^3)
1	21002050	0	2	21	7	50	1.88
	A0002050			50			
	B0002050			100			
	C0002050			150			
2	A0002100			50		100	
	B0002100			100			
	C0002100			150			
3	A0002500			50		500	
	B0002500			100			
	C0002500			150			
4	21142050	0	2	21	14	50	1.82
	A1402050			50			
	B1402050			100			
	C1402050			150			
5	A1402100			50		100	
	B1402100			100			
	C1402100			150			
6	A1402500			50		500	
	B1402500			100			
	C1402500			150			
7	21282050	0	2	21	28	50	1.84
	A2802050			50			
	B2802050			100			
	C2802050			150			
8	A2802100			50		100	
	B2802100			100			
	C2802100			150			
9	A2802500			50		500	
	B2802500			100			
	C2802500			150			

Table 4 Specimens for dynamic tests with m_F = 0% and m_L = 5%

Group Number	Specimen Number	Fiber Content m_F	Lime Content m_L	Cell Pressure σ_0	Aging Time t	Repetition Number N	Dry Unit Weight γ_d
		(%)	(%)	(kPa)	(day)		(g/cm^3)
10	21000550	0	5	21	7	50	1.82
	A0005050			50			
	B0005050			100			
	C0005050			150			
11	A0005100			50		100	
	B0005100			100			
	C0005100			150			
12	A0005500			50		500	
	B0005500			100			
	C0005500			150			
13	21145050	0	5	21	14	50	1.79
	A0145050			50			
	B0145050			100			
	C0145050			150			
14	A0145100			50		100	
	B0145100			100			
	C0145100			150			
15	A0145500			50		500	
	B0145500			100			
	C0145500			150			
16	21285050	0	5	21	28	50	1.8
	A0285050			50			
	B0285050			100			
	C0285050			150			
17	A0285100			50		100	
	B0285100			100			
	C0285100			150			
18	A0285500			50		500	
	B0285500			100			
	C0285500			150			

Table 5 Specimens for dynamic tests with m_L = 0%, and m_F = 0.2 & 0.5%

Group Number	Specimen Number	Fiber Content m_F	Lime Content m_l	Cell Pressure σ_0	Aging Time t	Repetition Number N	Dry Unit Weight γ_d
		(%)	(%)	(kPa)	(day)		(g/cm^3)
19	21002050	0.2	0	21	0	50	1.94
	A0020050			50			
	B0020050			100			
	C0020050			150			
20	A0020100			50		100	
	B0020100			100			
	C0020100			150			
21	A0020500			50		500	
	B0020500			100			
	C0020500			150			
22	21005050	0.5	0	21	0	50	1.9
	A0050050			50			
	B0050050			100			
	C0050050			150			
23	A0050100			50		100	
	B0050100			100			
	C0050100			150			
24	21005050	0.5	0	21	0	50	1.94
	A0050050			50			
	B0050050			100			
	C0050050			150			
25	A0050100			50		100	
	B0050100			100			
	C0050100			150			
26	A0050500			50		500	
	B0050500			100			
	C0050500			150			

Table 6 Specimens for dynamic tests with m_F = 0.2% and m_L = 2%

Group Number	Specimen Number	Fiber Content m_F	Lime Content m_L	Cell Pressure σ_0	Aging Time t	Repetition Number. N	Dry Unit Weight γ_d
		(%)	(%)	(kPa)	(day)		(g/cm^3)
27	21072250	0.2	2	21	7	50	1.86
	A0722050			50			
	B0722050			100			
	C0722050			150			
28	A0722100			50		100	
	B0722100			100			
	C0722100			150			
29	A0722500			50		500	
	B0722500			100			
	C0722500			150			
30	21142250	0.2	2	21	14	50	1.86
	A1422050			50			
	B1422050			100			
	C1422050			150			
31	A1422100			50		100	
	B1422100			100			
	C1422100			150			
32	A1422500			50		500	
	B1422500			100			
	C1422500			150			
33	21282250	0.2	2	21	28	50	1.85
	A2822050			50			
	B2822050			100			
	C2822050			150			
34	A2822100			50	28	100	
	B2822100			100			
	C2822100			150			
35	A2822500			50	28	500	
	B2822500			100			
	C2822500			150			

Table 7 Specimens for dynamic tests with m_F = 0.5% and m_L = 5%

Group Number	Specimen Number	Fiber Content m_F	Lime Content m_L	Cell Pressure σ_0	Aging Time t	Repetition Number. N	Dry Unit Weight γ_d
		(%)	(%)	(kPa)	(day)		(g/cm^3)
36	21075550	0.5	5	21	7	50	1.8
	A0755050			50			
	B0755050			100			
	C0755050			150			
37	A0755100			50		100	
	B0755100			100			
	C0755100			150			
38	A0755500			50		500	
	B0755500			100			
	C0755500			150			
39	21145550	0.5	5	21	14		1.82
	A1455050			50		50	
	B1455050			100			
	C1455050			150			
40	A1455100			50		100	
	B1455100			100			
	C1455100			150			
41	A1455500			50		500	
	B1455500			100			
	C1455500			150			
42	21285550	0.5	5	21	28	50	1.81
	A2855050			50			
	B2855050			100			
	C2855050			150			
43	A2855100			50		100	
	B2855100			100			
	C2855100			150			
44	A2855500			50		500	
	B2855500			100			
	C2855500			150			

Table 8 Specimens for dynamic tests with m_F = 0.2% and m_L = 5%

Group Number	Specimen Number	Fiber Content m_F	Lime Content m_L	Cell Pressure σ_0	Aging Time t	Repetition Number. N	Dry Unit Weight γ_d
		(%)	(%)	(kPa)	(day)		(g/cm^3)
45	21072550	0.2	5	21	7	50	1.83
	A0725050			50			
	B0725050			100			
	C0725050			150			
46	A0725100			50		100	
	B0725100			100			
	C0725100			150			
47	A0725500			50		500	
	B0725500			100			
	C0725500			150			
48	21020550	0.2	5	21	14	50	1.84
	A1425050			50			
	B1425050			100			
	C1425050			150			
49	A1425100			50		100	
	B1425100			100			
	C1425100			150			
50	A1425500			50		500	
	B1425500			100			
	C1425500			150			
51	21282550	0.2	5	21	28	50	1.86
	A2825050			50			
	B2825050			100			
	C2825050			150			
52	A2825100			50		100	
	B2825100			100			
	C2825100			150			
53	A2825500			50		500	
	B2825500			100			
	C2825500			150			

Table 9 Specimens for dynamic tests with m_F = 0.5% and m_L = 2%

Group Number	Specimen Number	Fiber Content m_F	Lime Content m_L	Cell Pressure σ_0	Aging Time t	Repetition Number N	Dry Unit Weight γ_d
		(%)	(%)	(kPa)	(day)		(g/cm^3)
54	21075250	0.5	2	21	7	50	1.84
	A0752050			50			
	B0752050			100			
	C0752050			150			
55	A0752100			50		100	
	B0752100			100			
	C0752100			150			
56	A0752500			50		500	
	B0752500			100			
	C0752500			150			
57	21145250	0.5	2	21	14	50	1.86
	A1452050			50			
	B1452050			100			
	C1452050			150			
58	A1452100			50		100	
	B1452100			100			
	C1452100			150			
59	A1452500			50		500	
	B1452500			100			
	C1452500			150			
60	21285250	0.5	2	21	28	50	1.88
	A2852050			50			
	B2852050			100			
	C2852050			150			
61	A2852100			50		100	
	B2852100			100			
	C2852100			150			
62	A2852500			50		500	
	B2852500			100			
	C2852500			150			

Table 10 A and B values from static shear tests

Table 10a A and B values for m_L = 0% and t = 1 day

σ_3 (kPa)	Log(σ_3/p_0)	m_F (%)	Log(1+m_F)	Log(1+m_L)	Log(t/t_1)	A (1/kPa)	Log(A)	B (1/kPa)	Log(B)
50	1.699	0	0	1	0	0.034	-1.47	0.0036	-2.444
100	2.000					0.027	-1.575	0.003	-2.523
150	2.176					0.022	-1.65	0.0028	-2.553
200	2.301					0.020	-1.699	0.0026	-2.585
50	1.699	0.2	0.000868			0.031	-1.509	0.0023	-2.638
100	2.000					0.023	-1.633	0.0022	-2.658
150	2.176					0.021	-1.688	0.0019	-2.721
200	2.301					0.018	-1.742	0.0018	-2.745
50	1.699	0.5	0.002167			0.026	-1.592	0.0015	-2.824
100	2.000					0.020	-1.706	0.0013	-2.886
150	2.176					0.017	-1.770	0.0011	-2.959
200	2.301					0.016	-1.807	0.001	-3

Table 10b A and B values for m_F = 0.2% and m_L = 5%

σ_3 (kPa)	Log(σ_3/p_0)	Log(1+m_F)	Log(1+m_L)	t (day)	Log(t/t_1)	A (1/kPa)	Log(A)	B (1/kPa)	Log(B)
50	1.699	0.000868	0.02111	7	0.845	0.008	-2.108	0.0005	-3.301
100	2.000					0.006	-2.194	0.0004	-3.398
150	2.176					0.005	-2.276	0.0004	-3.398
200	2.301					0.004	-2.367	0.0004	-3.398
50	1.699			14	1.146	0.006	-2.222	0.0004	-3.398
100	2.000					0.005	-2.301	0.0003	-3.523
150	2.176					0.004	-2.409	0.0003	-3.523
50	1.699			28	1.447	0.005	-2.337	0.0003	-3.523
100	2.000					0.003	-2.469	0.0003	-3.523
150	2.176					0.003	-2.523	0.0002	-3.699

Table 10c A and B values for m_F = 0.5% and m_L = 5%

σ_3 (kPa)	Log(σ_3/p_0)	Log(1+m_F)	Log(1+m_L)	t (day)	Log(t/t_1)	A (1/kPa)	Log(A)	B (1/kPa)	Log(B)
50	1.699	0.00212	0.0212	7	0.845	0.0069	-2.161	0.0003	-3.523
100	2.000					0.0053	-2.276	0.0002	-3.699
150	2.176					0.0046	-2.337	0.0002	-3.699
200	2.301					0.0041	-2.387	0.0002	-3.699
50	1.699			14	1.146	0.0052	-2.284	0.0002	-3.699
100	2.000					0.004	-2.398	0.0002	-3.699
150	2.176					0.0034	-2.469	0.0002	-3.699
200	2.301					0.0029	-2.538	0.0002	-3.699
50	1.699			28	1.447	0.0037	-2.432	0.0002	-3.699
100	2.000					0.0029	-2.538	0.0002	-3.699
150	2.176					0.0025	-2.602	0.0001	-4.000
200	2.301					0.0023	-2.638	0.0001	-4.000

Table 11 Calibration of parameters and coefficients a_i, b_i and c_i

11a. Calibration of constitutive parameters a_i and b_i ($i = 0…4$) in the nonlinear model

a_0 (1/kPa)	a_1	a_2	a_3	a_4
0.15	-0.38	-54.29	-10.76	-0.42
b_0 (1/kPa)	b_1	b_2	b_3	b_4
0.01	-0.17	-167.25	-25.81	-0.21

11b. Calibration of constitutive parameters c_i ($i = 0…5$) in the linear model

c_0 (kPa)	c_1	c_2	c_3	c_4	c_5
40684	0.11	0.01	0.012	-0.066	0.054

Table 12 Strength indices c and ϕ with different m_F, m_L and t

Table 12a Strength indices c and ϕ changing with m_F, m_L and t

Fiber Content m_F (%)	Lime Content m_L(%)	Aging period (days)	Cohesion c (kPa)	Internal friction angle ϕ (degree)
0	0	1	61.23	12.1
0.2	0	1	68.26	16.0
0.5	0	1	93.62	20.5
0.2	5	7	203.75	39.8
		14	203.87	46.2
		28	214.20	50.9
0.5	5	7	232.23	46.1
		14	264.96	49.9
		28	290.32	54.7

Table 12b Calibration of parameters from linear regression for c and ϕ

Linear functions	a	b	R^2	m_F	m_L
$c = a + bm_F$	58.9 (kPa)	66.3 (kPa)	0.96	N/A	0%
$c = a + bt$	198.6 (kPa)	0.53 (kPa/day)	0.90	0.2%	5%
$c = a + bt$	219.6 (kPa)	2.63 (kPa/day)	0.93	0.5%	5%
$\phi = a + bm_F$	12.3 (^{o})	16.7 (^{o})	0.99	N/A	0%
$\phi = a + bt$	37.5 (^{o})	0.5 (^{o}/day)	0.93	0.2%	5%
$\phi = a + bt$	43.7 (^{o})	0.4 (^{o}/day)	0.99	0.5%	5%

Table 12c Found coefficients k_i and n_i (i = 0…3) for the strength indices

k_0 (kPa)	k_1 (kPa)	k_2 (kPa)	k_3 (kPa/days))
12.31	16.68 - 20.83	6.65	0.4
n_0 (^{o})	n_1 (^{o})	n_2 (^{o})	n_3 (^{o} /days)
58.89	66.39 - 69.87	25.14	2.63

Table 13 Shear modulus G with m_F = 0%, m_L = 5%, different σ_0, N and t

	Elastic Modulus		Cell Pressure	Fiber Content	Lime Content	Repetition Number	Sample Curing Time
Specimen Number	G (kPa) x10^2	log(G/G_0) +2	log(σ_0/p_0)	log(1+m_F)	log(1+m_L)	logN	log(t/t_1)
21005050	779.87	2.89202221	1.32221929	0	0.021189	1.69897	0.84509804
A0705050	882.43	2.94568026	1.69897	0	0.021189	1.69897	0.84509804
B0705050	1021.8	3.0093659	2	0	0.021189	2	0.84509804
C0705050	1030.9	3.01321654	2.17609126	0	0.021189	2.69897	0.84509804
A0705100	679.92	2.83245782	1.69897	0	0.021189	1.69897	0.84509804
B0705100	850.34	2.92959261	2	0	0.021189	2	0.84509804
C0705100	971.16	2.98729079	2.17609126	0	0.021189	2.69897	0.84509804
A0705500	793.8	2.89971109	1.69897	0	0.021189	1.69897	0.84509804
B0705500	875.2	2.94210731	2	0	0.021189	2	0.84509804
C0705500	914.88	2.96136413	2.17609126	0	0.021189	2.17609126	0.84509804
21140550	971.12	2.9872729	1.32221929	0	0.021189	1.69897	1.14612804
A1405050	1031.3	3.01338502	1.69897	0	0.021189	1.69897	1.14612804
B1405050	1043.8	3.01861729	2	0	0.021189	2	1.14612804
C1405050	1155	3.06258198	2.17609126	0	0.021189	2.69897	1.14612804
A1405100	937.1	2.97178594	1.69897	0	0.021189	1.69897	1.14612804
B1405100	1039.5	3.01682449	2	0	0.021189	2	1.14612804
C1405100	1104.4	3.0431264	2.17609126	0	0.021189	2.69897	1.14612804
A1405500	878.88	2.94392958	1.69897	0	0.021189	1.69897	1.14612804
B1405500	923.79	2.96557326	2	0	0.021189	2	1.14612804
C1405500	993.33	2.99709355	2.17609126	0	0.021189	2.69897	1.14612804
21280550	889.36	2.94907759	1.32221929	0	0.021189	1.69897	1.44715803
A2805050	926.13	2.96667195	1.69897	0	0.021189	1.69897	1.44715803
B2805050	1093.5	3.03881879	2	0	0.021189	2	1.44715803
C2805050	1118	3.0484418	2.17609126	0	0.021189	2.69897	1.44715803
A2805100	771.58	2.88738096	1.69897	0	0.021189	1.69897	1.44715803
B2805100	954.12	2.979603	2	0	0.021189	2	1.44715803
C2805100	1043.9	3.0186589	2.17609126	0	0.021189	2.69897	1.44715803
A2805500	790.29	2.89778649	1.69897	0	0.021189	1.69897	1.44715803
B2805500	877.2	2.94309862	2	0	0.021189	2	1.44715803
C2805500	933.25	2.969998	2.17609126	0	0.021189	2.69897	1.44715803

Table 14 Shear modulus G with m_F = 0.2%, m_L = 2%, different σ_0, N and t

	Elastic Modulus		Cell Pressure	Fiber Content	Lime Content	Repetition Number	Sample Curing Time
Specimen Number	G (kPa) x10^2	log(G/G_0) +2	log(σ_0/p_0)	log(1+m_F)	log(1+m_L)	logN	log(t/t_1)
21072250	665.01	2.8228	1.322219	0.000868	0.0086	1.69897	0.8451
A0722050	665.01	2.8228	1.69897	0.000868	0.0086	1.69897	0.8451
B0722050	640.69	2.8066	2	0.000868	0.0086	1.69897	0.8451
C0722050	780.95	2.8926	2.176091	0.000868	0.0086	1.69897	0.8451
A0722100	552.74	2.7425	1.69897	0.000868	0.0086	2	0.8451
B0722100	619.96	2.7924	2	0.000868	0.0086	2	0.8451
C0722100	738.53	2.8684	2.176091	0.000868	0.0086	2	0.8451
A0722500	512.42	2.7096	1.69897	0.000868	0.0086	2.69897	0.8451
B0722500	563.73	2.7511	2	0.000868	0.0086	2.69897	0.8451
C0722500	612.23	2.7869	2.176091	0.000868	0.0086	2.69897	0.8451
21142250	606.39	2.7828	1.322219	0.000868	0.0086	1.69897	1.14613
A1422050	625.43	2.7962	1.69897	0.000868	0.0086	1.69897	1.14613
B1422050	679.57	2.8322	2	0.000868	0.0086	1.69897	1.14613
C1422050	712.26	2.8526	2.176091	0.000868	0.0086	1.69897	1.14613
A1422100	536.82	2.7298	1.69897	0.000868	0.0086	2	1.14613
B1422100	607.07	2.7832	2	0.000868	0.0086	2	1.14613
C1422100	690.29	2.839	2.176091	0.000868	0.0086	2	1.14613
A1422500	481.46	2.6826	1.322219	0.000868	0.0086	2.69897	1.14613
B1422500	506.32	2.7044	1.69897	0.000868	0.0086	2.69897	1.14613
C1422500	537.38	2.7303	2	0.000868	0.0086	2.69897	1.14613
21282250	632.75	2.8012	2.176091	0.000868	0.0086	1.69897	1.44716
A2822050	605.1	2.7818	1.69897	0.000868	0.0086	1.69897	1.44716
B2822050	661.5	2.8205	2	0.000868	0.0086	1.69897	1.44716
C2822050	632.13	2.8008	2.176091	0.000868	0.0086	1.69897	1.44716
A2822100	461.58	2.6642	1.69897	0.000868	0.0086	2	1.44716
B2822100	489.76	2.69	2	0.000868	0.0086	2	1.44716
C2822100	553.78	2.7433	2.176091	0.000868	0.0086	2	1.44716
A2822500	432.34	2.6358	1.69897	0.000868	0.0086	2.69897	1.44716
B2822500	493.74	2.6935	2	0.000868	0.0086	2.69897	1.44716
C2822500	508.03	2.7059	2.176091	0.000868	0.0086	2.69897	1.44716

Table 15 Shear modulus G with m_F = 0.5%, m_L = 5%, different σ_0, N and t

	Elastic Modulus		Cell Pressure	Fiber Content	Lime Content	Repetition No.
Specimen Number.	G (kPa) x10^2	log(G/G_0) +2	log(σ_0/p_0)	log(1+m_F)	log(1+m_L)	logN
21075550	447.66	2.6509	1.322219	0.002166	0.021189	1.69897
A0755050	453.48	2.6566	1.69897	0.002166	0.021189	1.69897
B0755050	507.73	2.7056	2	0.002166	0.021189	1.69897
C0755050	556.4	2.7454	2.176091	0.002166	0.021189	1.69897
A0755100	436.13	2.6396	1.69897	0.002166	0.021189	2
B0755100	484.02	2.6849	2	0.002166	0.021189	2
C0755100	570.17	2.756	2.176091	0.002166	0.021189	2
A0755500	458.14	2.661	1.69897	0.002166	0.021189	2.69897
B0755500	508.28	2.7061	2	0.002166	0.021189	2.69897
C0755500	537.52	2.7304	2.176091	0.002166	0.021189	2.69897
21145550	656.05	2.8169	1.322219	0.002166	0.021189	1.69897
A1455050	707.93	2.85	1.69897	0.002166	0.021189	1.69897
B1455050	803.22	2.9048	2	0.002166	0.021189	1.69897
C1455050	830.73	2.9195	2.176091	0.002166	0.021189	1.69897
A1455100	496.29	2.6957	1.69897	0.002166	0.021189	2
B1455100	614.28	2.7884	2	0.002166	0.021189	2
C1455100	798.08	2.902	2.176091	0.002166	0.021189	2
A1455500	511.9	2.7092	1.322219	0.002166	0.021189	2.69897
B1455500	620.89	2.793	1.69897	0.002166	0.021189	2.69897
C1455500	655.19	2.8164	2	0.002166	0.021189	2.69897
21285550	678.53	2.8316	2.176091	0.002166	0.021189	1.69897
A2855050	735.16	2.8664	1.69897	0.002166	0.021189	1.69897
B2855050	839.13	2.9238	2	0.002166	0.021189	1.69897
C2855050	1010.4	3.0045	2.176091	0.002166	0.021189	1.69897
A2855100	594.3	2.774	1.69897	0.002166	0.021189	2
B2855100	731.81	2.8644	2	0.002166	0.021189	2
C2855100	865.43	2.9372	2.176091	0.002166	0.021189	2
A2855500	604.18	2.7812	1.69897	0.002166	0.021189	2.69897
B2855500	700.89	2.8456	2	0.002166	0.021189	2.69897
C2855500	752.17	2.8763	2.176091	0.002166	0.021189	2.69897

Table 16 Shear modulus G with m_F = 0.2%, m_L = 5%, different σ_0, N and t

	Elastic Modulus		Cell Pressure	Fiber Content	Lime Content	Repetition Number.	Sample Curing Time
Specimen Number	G (kPa) x10^2	log(G/G_0) +2	log(σ_0/p_0)	log(1+m_F)	log(1+m_L)	logN	log(t/t_1)
21072550	571.92	2.7573	1.322219	0.000868	0.021189	1.69897	0.8451
A0725050	596.33	2.7755	1.69897	0.000868	0.021189	1.69897	0.8451
B0725050	736.16	2.867	2	0.000868	0.021189	1.69897	0.8451
C0725050	818.22	2.9129	2.176091	0.000868	0.021189	1.69897	0.8451
A0725100	577.32	2.7614	1.69897	0.000868	0.021189	2	0.8451
B0725100	635.39	2.803	2	0.000868	0.021189	2	0.8451
C0725100	728.52	2.8624	2.176091	0.000868	0.021189	2	0.8451
A0725500	547.23	2.7382	1.69897	0.000868	0.021189	2.69897	0.8451
B0725500	606.09	2.7825	2	0.000868	0.021189	2.69897	0.8451
C0725500	653.64	2.8153	2.176091	0.000868	0.021189	2.69897	0.8451
21020550	601.9	2.7795	1.322219	0.000868	0.021189	1.69897	1.14613
A1425050	709.2	2.8508	1.69897	0.000868	0.021189	1.69897	1.14613
B1425050	871.89	2.9405	2	0.000868	0.021189	1.69897	1.14613
C1425050	939.82	2.973	2.176091	0.000868	0.021189	1.69897	1.14613
A1425100	540.49	2.7328	1.69897	0.000868	0.021189	2	1.14613
B1425100	774.75	2.8892	2	0.000868	0.021189	2	1.14613
C1425100	923.85	2.9656	2.176091	0.000868	0.021189	2	1.14613
A1425500	514.22	2.7111	1.322219	0.000868	0.021189	2.69897	1.14613
B1425500	733.95	2.8657	1.69897	0.000868	0.021189	2.69897	1.14613
C1425500	805.68	2.9062	2	0.000868	0.021189	2.69897	1.14613
21282550	727.98	2.8621	2.176091	0.000868	0.021189	1.69897	1.44716
A2825050	759	2.8802	1.69897	0.000868	0.021189	1.69897	1.44716
B2825050	855.51	2.9322	2	0.000868	0.021189	1.69897	1.44716
C2825050	857.49	2.9332	2.176091	0.000868	0.021189	1.69897	1.44716
A2825100	650.96	2.8136	1.69897	0.000868	0.021189	2	1.44716
B2825100	767.05	2.8848	2	0.000868	0.021189	2	1.44716
C2825100	787.23	2.8961	2.176091	0.000868	0.021189	2	1.44716
A2825500	681.82	2.8337	1.69897	0.000868	0.021189	2.69897	1.44716
B2825500	726.97	2.8615	2	0.000868	0.021189	2.69897	1.44716
C2825500	769.98	2.8865	2.176091	0.000868	0.021189	2.69897	1.44716

Table 17 Shear modulus G with m_F = 0.5%, m_L = 2%, different σ_0, N and t

	Elastic modulus		Cell Pressure	Fiber Content	Lime Content	Repetition No.	Curing time
Specimen Number.	G (kPa) x10^2	log(G/G_0) +2	log(σ_0/p_0)	log(1+m_F)	log(1+m_L)	logN	log(t/t_1)
21075250	355.88	2.5513	1.322219	0.002166	0.0086	1.69897	0.8451
A0752050	403.05	2.6054	1.69897	0.002166	0.0086	1.69897	0.8451
B0752050	471.25	2.6733	2	0.002166	0.0086	1.69897	0.8451
C0752050	548.13	2.7389	2.176091	0.002166	0.0086	1.69897	0.8451
A0752100	341.29	2.5331	1.69897	0.002166	0.0086	2	0.8451
B0752100	387.39	2.5881	2	0.002166	0.0086	2	0.8451
C0752100	463.71	2.6662	2.176091	0.002166	0.0086	2	0.8451
A0752500	342.60	2.5348	1.69897	0.002166	0.0086	2.69897	0.8451
B0752500	385.00	2.5855	2	0.002166	0.0086	2.69897	0.8451
C0752500	414.74	2.6178	2.176091	0.002166	0.0086	2.69897	0.8451
21145250	482.38	2.6834	1.322219	0.002166	0.0086	1.69897	1.14613
A1452050	483.31	2.6842	1.69897	0.002166	0.0086	1.69897	1.14613
B1452050	508.64	2.7064	2	0.002166	0.0086	1.69897	1.14613
C1452050	547.96	2.7387	2.176091	0.002166	0.0086	1.69897	1.14613
A1452100	364.22	2.5614	1.69897	0.002166	0.0086	2	1.14613
B1452100	408.56	2.6113	2	0.002166	0.0086	2	1.14613
C1452100	455.41	2.6584	2.176091	0.002166	0.0086	2	1.14613
A1452500	347.53	2.541	1.322219	0.002166	0.0086	2.69897	1.14613
B1452500	389.49	2.5905	1.69897	0.002166	0.0086	2.69897	1.14613
C1452500	412.52	2.6154	2	0.002166	0.0086	2.69897	1.14613
21285250	334.54	2.5244	2.176091	0.002166	0.0086	1.69897	1.44716
A2852050	355.29	2.5506	1.69897	0.002166	0.0086	1.69897	1.44716
B2852050	393.96	2.5955	2	0.002166	0.0086	1.69897	1.44716
C2852050	434.82	2.6383	2.176091	0.002166	0.0086	1.69897	1.44716
A2852100	301.06	2.4787	1.69897	0.002166	0.0086	2	1.44716
B2852100	349.76	2.5438	2	0.002166	0.0086	2	1.44716
C2852100	407.16	2.6098	2.176091	0.002166	0.0086	2	1.44716
A2852500	310.83	2.4925	1.69897	0.002166	0.0086	2.69897	1.44716
B2852500	345.3	2.5382	2	0.002166	0.0086	2.69897	1.44716
C2852500	395.4	2.597	2.176091	0.002166	0.0086	2.69897	1.44716